Multiple glassy states and anomalous behavior of colloidal systems: Simulations and theory

A Thesis

Submitted For the Degree of

Doctor of Philosophy

XXVI Ciclo

in the Faculty of Science

by

Gayatri Das

Dipartimento di Fisica

La Sapienza Universita di Roma

Roma

JANUARY 2014

To My Parents and My husband

Acknowledgements

I would like to express my deep gratitude to my mentor Prof. Francesco Sciortino and Dr. Emanuela Zaccarelli for their constant guidance, concern and support. Their patience and encouragement were always source of inspiration. I really enjoyed working with them and have learnt a lot from their systematic and meticulous approach to problems. They were very patient, approachable and always had time for me. I sincerely acknowledge their various supports during my Phd program.

I would like to acknowledge Prof. Egidio Longo, Prof. Massimo Testa, Prof. Enzo Marinari and Dr. Anna De Grossi for providing an excellent research environment. I would like to thank all the faculty members, staffs and friends in Dipartimento di Fisica.

I would like to thank my collaborators Dr. Nicoletta Gnan and Dr. Matthias Sperl for their useful discussions, encouragement and guidance.

I would like to acknowledge my lab mates Dr. Nicoletta Gnan, Dr. Teun Visser, Dr. Flavio Romano, Dr. Lorenzo Rovigatti, Dr. Cristiano De Michele, Dr. Gianmarco Munao, Dr. Sandalo Roldan, Dr. Frank Smallenburg, Dr. Sofia Biagi, Francesca Bomboi, Zdenek Preisler, Nguyen Khanh Thuy and Sofia Kantorovich.

I am grateful to Comploids, 7th Frame Work Program and Marie Curie Fellowship during my Phd program. This is a very extensive European project which has helped me to come across a big environment of scientific discussions. This program gives a platform to interact with many scientists from different part of the world. I would like to acknowledge all the members in Comploids for their support, encouragement and guidance. I would like to acknowledge Prof. Christos N. Likos.

I would like to thank my friends from Comploids - Giulia Foffano, Ivna Kavre, Lamiss Zaidouny, Zdenek Preisler, Labrini Athanasopoulou, Christian Koch, Daniela Marzi, Arash Nikoubashman, Giannis Georgiou , Nicolas Bruot, Alexandra Dobrinescu, Niek Hijnen, Besira Mihiretie. I would like to acknowledge all the members in Comploids for their support, encouragement and guidance.

Specially, I would like to acknowledge my husband Subhendu for being a strong support.

I would like to thank Sara for helping me to resolve any computational proble and Raffella Mazzarelli for helping me to resolve the problems with administration.

I would like to thank Moumita didi, Shibuda, Vishwas, Shiladitya for their constant help though out my research period and for their wonderful and valuable suggestions.

I would like to acknowledge my friends Prabhat, Hima, Aparna, Gaurav, Vijay, Shankar Newal, Prafulla Katkar, Shivangi, Smita, Payal, Sasmita, Sudipta, Sarada, Sutapa, Suman, Shaista, Manpreet, Shreyoshi, Nisha, Rajnish, Neha for their useful discussions, suggestions and continuous support

during research.

I would also like to thank my friends Flavio Marques, Valeria Marques, Gaurav, Vijay, Prabhat, Nagender, Abhishek, Shivangi, Smita, Payal for helping me with my research and for making my stay in Rome very enjoyable.

I would like to acknowledge Biswajeet, Smita, Subrat, Priyaranjan, Sasmita, Chandrashekhar, Sandeep, Devanshu, Tanushree, Chandan, Gitashree, Nirmal, Maitree, Sagar and Sameer.

Last but not the least, I would like to express my deep gratitude towards my family. I am here because of the blessings of my parents and in-laws. I am eternally grateful to my family and my husband Subhendu.

List of Figures

List of Tables

Contents

Chapter 1

Introduction

1.1 What are colloids and colloidal glass transitions?

Soft matter physics is a fascinating fundamental research field with a wide range of applications. It comprises the study of liquids, colloids, polymers, foams, gels, granulars as well as biological materials. Among these materials colloids are of particular interest as they have a large variety of industrial applications [44] and great biological importance (see ref [58] and references within). Since colloids are of sizes ranging typically from 10 nm to 10 μm, they are easily accessible to experiments. Moreover with the advancement of computational power, numerical simulations of colloids have shed light on experimental observations and theoretical predictions.

For many decades, a large effort has been devoted to understand the so called "dynamical arrest" in colloidal systems, a mechanism that can be

described as follows: For the simplest case of athermal colloidal particles, such as hard-sphere (HS) colloids, the only control parameter is packing fraction ϕ. For such systems, it has been observed that at high ϕ, the viscosity increases dramatically. Since the viscosity is a measurement of the ability to flow of a fluid, a high viscosity (typical of solids) signals a slowing down of the particles dynamics. When $\phi = \phi_g$, the viscosity diverges and the system structurally looks like a fluid, but mechanically behaves like a solid; such"amorphous solid" is out of equilibrium since for $\phi \geqslant \phi_g$, the colloids are dynamically frozen and no structural relaxation occurs in the system. There is no change in the thermodynamics occur, i.e. it is a kinetic transition. We will refer to this state as a "glass".

The pioneering investigations of HS colloids by Pusey and van Megen [42, 53] have shown that the HS glass transition occurs at a colloidal packing fraction $\phi \approx 0.58$. When instead of a simple HS potentials, systems with softer potentials [33] or with short range attractive wells [37] are considered, also the temperature T and the well width Δ are the control parameters together with ϕ. For such systems a richer dynamical behavior has been found showing the presence of multiple glass transitions as described in Sec. 1.4. For all these systems the transition has been rationalized within the framework of the Mode Coupling Theory (MCT) [21]. Despite suffering of a shift of the actual glass transition value, MCT provides a good description of simulation and experimental data.

1.2 Mode Coupling Theory

MCT is a theory that describes the behavior of systems on approaching the glass transition and has been used to locate the glass transition curves in colloidal systems. The theory is able to describe the time evolution of the normalized density autocorrelation function, through a set of integro-differential equations that can be solved by knowing the static structure factors of the system, which is the only input of the theory. The mechanism of arrest is explained in terms of the so-called 'cage effect' [21, 22], where particles at high densities become trapped by their nearest neighbors for an increasingly long time. This mechanism manifests itself in the form of a two-step decay of the density auto-correlation functions approaching the liquid-glass transition.

MCT predicts the occurrence of a glass transition starting from a set of integro-differential equations for the density correlators $\Phi_q(t) = \langle \rho_{q^*}(t)\rho_q(0)\rangle/S(q)$ at different wave numbers q, where $S(q) = \langle \rho_{q^*}(0)\rho_q(0)\rangle/N$ is the static structure factor and $\rho_q(t) = \sum_{j=1}^{N_i} \exp[i\mathbf{q}\cdot\mathbf{r}_j(t)]$. The MCT equations of motions (for Newtonian Dynamics)[1] read, in the one-component case, as

$$\ddot{\Phi}_q(t) + \Omega_q^2\Phi_q(t) + \Omega_q^2 \int_0^t dt' m_q(t-t')\dot{\Phi}_q(t') = 0 \tag{1.1}$$

where $\Omega_q^2 = q^2 k_B T/mS(q)$ is a characteristic frequency and $m_q \equiv \mathcal{F}_q[\Phi_k(t)]$ is the memory kernel. The memory kernel $m_q \equiv \mathcal{F}_q[\Phi_k(t)]$ contains fluctuating stresses and plays the role of a generalized friction coefficient.

[1] The MCT equations can also be generalized to the case of Brownian Dynamics which is more realistic to describe colloidal suspensions. However, the long-time limit features and main predictions are not affected by the different microscopic dynamics.

Solving the full dynamical Eq. (1.1) close to any point on the liquid-glass transition, $\Phi_q(t)$ is found to follow a typical two-step decay. A first decay at short times corresponds to the characteristic time termed as β-relaxation that particles employ to explore the cages formed by their nearest neighbors. A second decay occurs at longer time, and is characterized by the α-relaxation time associated to the structural rearrangements necessary for restoring the ergodicity in the fluid. In between these two regimes, $\Phi_q(t)$ displays a characteristic plateau whose height is associated to the size of the cages in which particles are rattling before finally escaping. When the dynamics slows down, the correlators form a longer plateau. At the ideal glass transition, this plateau does not decay to zero. The height of the plateau is known as the non-ergodicity parameter f_q and at the transition

$$f_{ij}(q) \;=\; \lim_{t\to\infty} \Phi_{ij}(q,t) \tag{1.2}$$

Taking the long-time limit of Eq. (1.1) one obtains,

$$f_q/(1-f_q) = \mathcal{F}_q[f_k], \tag{1.3}$$

where $f_q = \lim_{t\to\infty} \Phi_q(t)$ is the so-called non-ergodicity parameter. $\mathcal{F}_q[f_k]$ is the Mode Coupling functional, which is bilinear in f_q

$$\mathcal{F}_q[f_k] = \frac{1}{2}\int \frac{d^3k}{(2\pi)^3} V_{\mathbf{q},\mathbf{k}} f_k f_{|\mathbf{q}-\mathbf{k}|}, \tag{1.4}$$

The vertices $V_{q,k}$ express the overlap of fluctuating stresses with the pair

density modes and are uniquely determined by the equilibrium structure

$$V_{\mathbf{q},\mathbf{k}} \equiv S(q)S(k)S(|\mathbf{q}-\mathbf{k}|)\frac{\rho}{q^4}[\mathbf{q}\cdot\mathbf{k}c_k + \mathbf{q}\cdot(\mathbf{q}-\mathbf{k})c_{|\mathbf{q}-\mathbf{k}|}]^2 \qquad (1.5)$$

where, $c_k = 1/[1-\rho S(k)]$ is the direct correlation function related to the static structure factor $S(k)$. Both c_k and $S(k)$ depend on thermodynamic parameters such as density or temperature.

During the transition from liquid to glassy state, the system loses ergodicity and the non-ergodicity parameter f_q jumps from zero to a finite value, i.e. there is a bifurcation of solution of MCT equation (because $f_q = 0$ is always a solution of Eq. (1.3)).

Besides the occurrence of a liquid-glass transition, under specific conditions, a system can display multiple glassy states, giving rise to the presence of glass-glass transitions in the kinetic phase diagram. These multiple glasses occur as bifurcations of the solutions of Eq. (1.3) upon variation of the control parameters. Across a glass-glass transition the non-ergodicity parameter jumps discontinuously between two non-zero values. This transition is found to terminate at an endpoint, named higher-order singularity, beyond which one can go from one glassy solution to the other continuously. The higher-order singularities can be of type A_3, when the two glasses coalesce already inside the glassy region, and of type A_4 when the two glasses merge also with the liquid solution right on top of the liquid glass line. The latter is a very special point occurring at (ϕ^*, T^*, Δ^*), which can be identified by finely tuning the value of the control parameter Δ [11, 51], and in its vicinity the form of the decay of $\Phi_q(t)$ is predicted to be unique. The singularities of

type A_l occur due to variation of $l-1$ control parameters [50]. The higher order singularity A_2 called *fold* can be identified with variation of one control parameter. Similarly, an A_3 singularity - called *cusp* - requires two control parameters and A_4 singularity - the *swallowtail* requires the variation of three parameters.

It is well-accepted that the long-time relaxation of the correlators can be described by a stretched exponential which is termed as Kohlrausch and Williams-Watts (KWW) law

$$\Phi_q(t) \sim f_q \exp^{-(t/\tau_q)^{\beta_q}} \tag{1.6}$$

where f_q, τ_q give an estimate respectively of the non-ergodicity parameter, the α-relaxation time, while β_q is the stretching exponent. While no general analytic solution of the MCT equations is provided for $\Phi_q(t)$, its asymptotic form close to the glass is known.

On approaching the liquid-glass transition, the correlators are described by the Von Schweidler power-law decay [21]

$$\Phi_q(t) = f_q - A[t/\tau(T)]^b \tag{1.7}$$

where, A and b are positive constants and τ is relaxation time. However, close to a higher order singularity, $\Phi_q(t)$ shows a peculiar logarithmic dependence:

$$\Phi_q(t) \sim f_q^c - h_q^{(1)} \ln(t/\tau_q) + h_q^{(2)} \ln^2(t/\tau_q). \tag{1.8}$$

The parameters $f_q^c, h_q^{(1)}, h_q^{(2)}$ are the critical non-ergodicity parameter and

critical amplitudes of first and second order in the expansion in $\ln(t)$ [22]. It is found that a specific value of the wave vector q^* exists, at which $h_q^{(2)}$ is zero, thus allowing for a pure logarithmic decay of the correlator to be observed. Hence, the correlators should display a characteristic concave (convex) shape for $q < q^*$ ($q > q^*$) in a logarithmic time scale.

MCT predicts that the diffusivity should go to zero at the ideal glass transition with a power-law dependence. This should apply independently on the chosen path, and hence both along an isotherm

$$D \sim \mid \phi - \phi_g(T) \mid^{\gamma(T)} \tag{1.9}$$

and along an isochore

$$D \sim \mid T - T_g(\phi) \mid^{\gamma(\phi)} . \tag{1.10}$$

Here ϕ_g and T_g are, respectively, the critical values of the packing fraction and temperature at the ideal glass transition, while γ is a non-universal exponent that is also determined by the theory in terms of the exponents a and b. The simple relation between these exponents is represented as follows

$$\gamma = \frac{1}{2a} + \frac{1}{2b} \tag{1.11}$$

All the experiments are related to the exponent parameter λ is the one which has a microscopic definition in terms of the MCT kernel. These exponents are represented via the relation

$$\lambda = \frac{\Gamma(1+b^2)}{\Gamma(1+2b)} = \frac{\Gamma(1-a^2)}{\Gamma(1-2a)} \tag{1.12}$$

The value of λ is generally $\lambda < 1$, but for higher order singularity A_3, A_4, $\lambda = 1$. By performing the power-law fits, following Eq. (2.2) and (2.3), we can then trace the locus of points in the (ϕ, T) phase diagram for which $D \to 0$. This line can be directly compared to the MCT glass line, as previously done for other systems [33, 47, 62].

1.3 Integral equations

From Eq. (1.5) it is clear that the only inputs needed to solve Eq. (1.3) are the number density ρ and the static structure factor $S(q)$ of the system. The latter can be obtained by solving the Ornstein-Zernike (OZ) equation [**?**] through the use of integral equations [8] or it can be evaluated numerically from simulations. There are a set of closures which are used to solve the OZ equation for example; Percus-Yevick (PY), Rogers-Young (RY). The first application of MCT to hard-sphere system predicted glass transition for a packing fraction $\phi_g = 0.516$ when using the PY approximation for the calculation of the static structure factor. For Square Well (SW) System, the static structure factor both from PY and the mean-spherical approximation have been used. The glass transition obtained from both the calculations show the independence from the closure relations. When we replace the attractive well with a finite repulsive step in the potential, the MCT calculations shows different results obtained from PY and RY closure relations. Now, we will describe the different closures use to solve the Ornstein-Zernike equation.

1.3.1 Percus-Yevick Approximation

The Ornstein-Zernike (OZ) equation for the pair correlation function $h(r)$ is

$$h(r) = c(r) + \rho \int dr' c(|r - r'|)h(|r'|), \tag{1.13}$$

where $g(r) = h(r) + 1$ is the radial distribution function and $c(r)$ the direct correlation function. The radial distribution function, $g(r)$, represents the probability to find an atom in a shell dr at the distance r of another atom chosen as a reference point. On expanding Eq. (1.13), the pair distribution function can be written as following

$$g(r) = exp[-\beta v(r)][1 + h(r) - c(r)] \tag{1.14}$$

This is the Percus-Yevick approximation. Another important quantity is the static structure factor S_q, which is the equal time correlation function of the density variables in wave vector space. The Fourier transform of the correlation function h_q, is related to the static structure factor by the relation $S_q = 1 + \rho h_q$. The OZ relation in the wave vector space can be defined as

$$S_q = \frac{1}{1 - \rho \hat{c_q}} \tag{1.15}$$

The OZ relation given in Eq. (1.13) is closed using PY approximation.

In order to solve OZ equation one use following PY closures for $c(r)$

$$g(r) = 0,\ r < \sigma \tag{1.16}$$

$$c(r) = g(r)[1 - e^{\beta v(r)}],\ r > \sigma \tag{1.17}$$

Using the above closure relation in Eq. (1.13), we can rewrite the OZ equation [3] in terms of the real factor function $Q(r)$, defined for $r > 0$. For $0 \leqslant r \leqslant R$, R being the range of the potential ($\sigma + \Delta$ in the present case), one has

$$rc(r) = -Q'(r) + 2\pi\rho \int_r^R ds Q'(s) Q'(s - r) \tag{1.18}$$

as well as, for $r > 0$

$$rh(r) = -Q'(r) + 2\pi\rho \int_r^R ds (r - s) h(|r - s|) Q'(s) \tag{1.19}$$

The Fourier transform of $Q(r)$ gives the static structure factor S_q

$$S_q^{-1} = \hat{Q}(q)\hat{Q}(q^*) \tag{1.20}$$

$$\hat{Q}(q) = 1 - 2\pi\rho \int_0^\infty dr e^{iqr} Q(r) \tag{1.21}$$

The PY equation is of particular interest in the theory of simple liquids because it is solvable analytically in the special case of the hard-sphere fluid and of a Baxter fluid [4]. Also it has been successful in describing systems with short-range attractions. PY suffers from the fact that it is thermodynamically inconsistent, i.e. the equations of state calculated by different routes are different.

1.3.2 Rogers-Young Approximation

In order to improve the theory of classical fluids and to impose thermodynamic consistency more refined integrals have been proposed. For example, RY is an appropriate mixture of the Percus-Yevick (PY) and hypernated chain (HNC) equation. The pair distribution function for HNC approximation is

$$g(r) = exp[-\beta v(r)][h(r) - c(r)] \tag{1.22}$$

When we mix the PY and HNC approximation, the resulting equation is

$$g(r) = exp[-\beta v(r)][1 + \frac{exp[(h(r) - c(r))f(r)] - 1}{f(r)}] \tag{1.23}$$

When $r = 0$, $f(0) = 0$, Eq. (1.23) reduces to PY approximation. As r increases, $f(r)$ approaches to unity, and Eq. (1.23) reduces to HNC approximation. The simple mixing function,

$$f(r) = 1 - exp(-\alpha r) \tag{1.24}$$

where α is the adjustable parameter used to achieve thermodynamic consistency. In addition to thermodynamic consistency, it has been shown that RY leads to accurate radial-distribution-functions for repulsive potentials [10].

1.4 Recent studies of multiple glasses in colloids

1.4.1 Attractive Colloids

When HS colloids are in solution with non-absorbing polymers, they experience an effective short-range attraction that can be used to control the phase behavior of the system [37]. In simulations, such system can be imitated by complementing the hard-core repulsion with an attractive square-well (SW [59]). The phase diagram of SW systems together with the dynamical phase diagram (in which the glass line is located) have been widely studied for different values of the well width Δ and well depth ϵ. MCT predictions [5, 11, 16] for the dynamics of the SW model at high densities revealed an intriguing behavior. Indeed, when the range of the well width Δ is reduced down to a few percent of the particle diameter, a reentrant glass line is observed in the temperature-concentration phase diagram. This results in two different kind of glasses: a first glass (named repulsive or hard-sphere glass), which is found at high temperature T, is driven by the packing of particles, while a second glass (named attractive glass) is observed at low T, when energetic effects are dominant and particles remain caged in their attractive wells. In between the two glasses, at intermediate temperatures, a reentrant liquid region occurs. Therefore at the same concentration it is possible to go from one glass to the other by lowering T and passing through a pocket of liquid states arising from the competition between energetic and entropic effects occurring at intermediate T [46]. At even higher densities, a

glass-glass line is observed, which terminates at an endpoint (A_3 singularity). Associated to these multiple glasses and reentrant melting, MCT predicts the

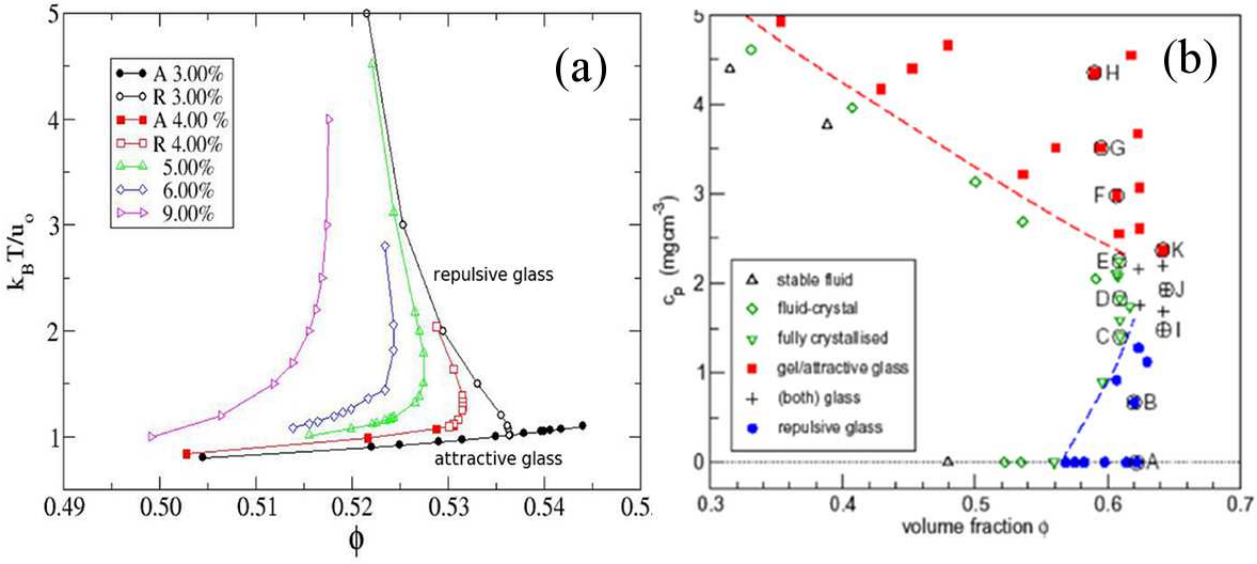

Figure 1.1: Packing fraction ϕ vs temperature T phase diagram, (a) the reentrance has been observed along the liquid-glass line predicted from MCT [11]. There are two glasses: repulsive glass and attractive glass meeting at a common point. (b) The experimental phase diagram [37] in concentration vs packing fraction plane show the same reentrant behavior.

occurrence of anomalous dynamics, which results in a logarithmic (rather than two-step) decay of the density auto-correlation functions approaching the endpoint singularity, as well as in a subdiffusive behavior of the particles mean-squared-displacement (MSD). Most of these predictions have been confirmed by several simulations [40, 59, 60] and experiments [14, 37]. In particular, in simulations, this has been possible by investigating the shape of the isodiffusivity lines i.e. lines where the self diffusion coefficient is constant [17] in the phase diagram for small diffusivity values. These lines maintain the same shape of the MCT glass line at all (sufficiently small) values of D, so

that they provide a useful reference to establish whether a reentrance (and eventually associated anomalous dynamics) is present.

1.4.2 Soft Colloids

The successful predictions of MCT for the SW system paved the way for applications of the theory in a wide variety of soft matter systems. In particular, MCT has been used to describe the arrested behavior of several, purely repulsive systems. Among these are star polymers [29], i.e. long polymer chains anchored onto a central core, where the number of chains (arms) varies the softness of the particles, bridging HS colloids (in the limit of very large arm number) to polymer chains (when the arm number is limited to 2). While one-component star polymer solutions only display a glass driven by packing of the stars [18], binary mixtures of stars of different arm numbers and sizes have been shown to display multiple glassy states through a combined effort of MCT, simulations and experiments [33].

In the kinetic phase diagram, the star polymer mixture produces three type of glasses; at low concentration of small stars, a single glass due to the arrest of large stars and a double glass due to the arrest of both large and small stars. The high concentration of small stars, brings an asymmetric glass which differs with structural and rheological properties with respect to other glasses. Despite indications that anomalous dynamics could be present in these systems [30], a clear evidence from MCT predictions has not been provided. In contrast, a recent theoretical study of binary, size-asymmetric HS mixtures has reported the occurrence of higher-order singularities and a

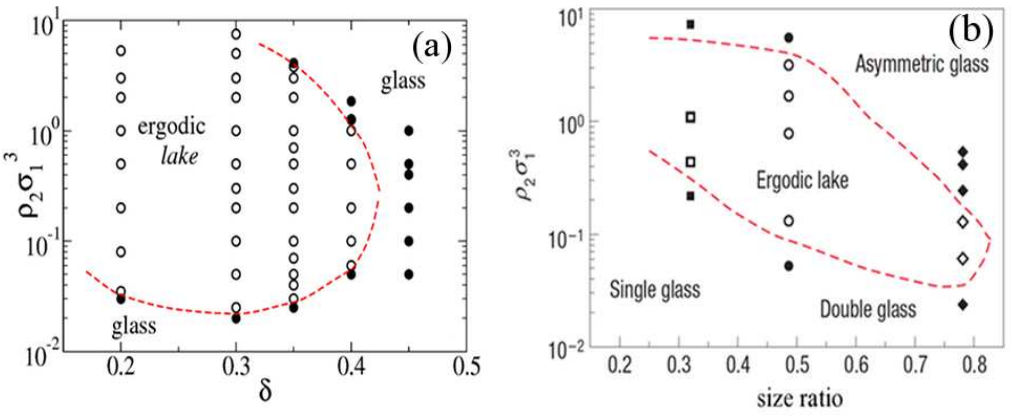

Figure 1.2: The figure represents the kinetic phase diagram in size ratio δ and number density $\rho_2\sigma_1^3$. The dashed lines are schematic curves to separate the liquid region from glassy region. (a) The MCT [33] approach predicted the multiple glass transitions. (b) The experimental [33] study for different mixture of star polymers predicted 3 different glasses: single glass, double glass and asymmetric glass.

variety of different glasses [54].

1.4.3 Purely repulsive colloids

Without necessarily turning to mixtures, it was recently realized that one-component systems with distinct length scales in the interaction potential (the so-called core softened models) are also promising candidates for detecting thermodynamic and dynamic anomalies [19,20,26,27,34,55]. Among these, the simplest model is the square shoulder (SS) model, where the hard-core is complemented by an additional repulsive corona. This model has been used to describe the behavior of some metallic glasses [57] or complex materials like micellar [35] or granular systems [13], as well as primitive models of silica [25] and water [26]. The system has three control parameters; packing

fraction ϕ, Δ and temperature T.

Recent MCT calculations reported the existence of multiple glass transitions also for the SS system both under compression and cooling [51]. The kinetic phase diagram for SS system in (ϕ, T) plane as predicted from MCT is shown in Fig. 1.3. On solving the MCT integral equations, the SS system predicts liquid-glass line for $\Delta = 0.13$. A peculiar behavior of the SS model, with no counterpart in other investigated systems, is the prediction of a disconnected glass-glass transition with two endpoint singularities. The

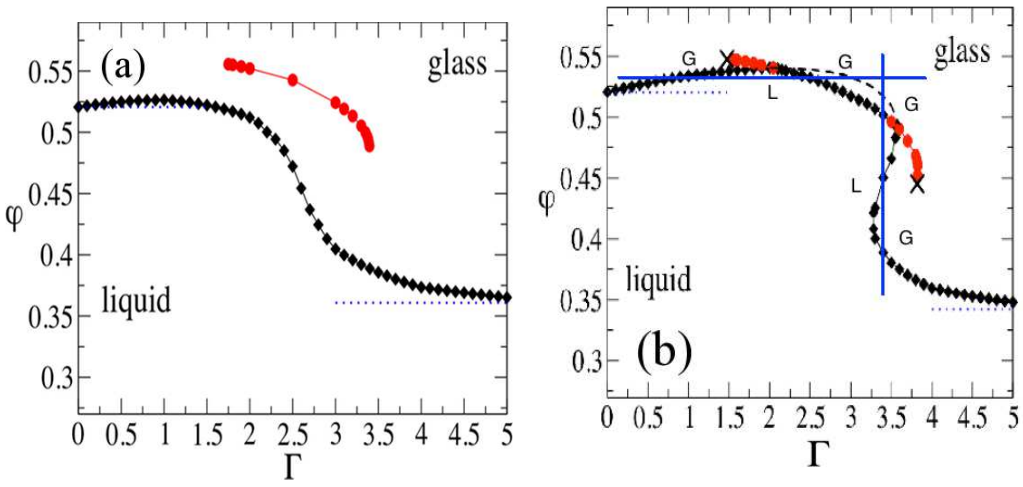

Figure 1.3: The phase diagram in the right panel and left panel have been plotted in (ϕ, Γ) plane, where $\Gamma = 1/k_B T$. The mode coupling theory (MCT) calculation for SSS using RY approximation originates (a) a disconnected glass-glass line represented by red curve for $\Delta = 0.13$ and terminated with end point singularities. (b) On increasing $\Delta = 0.15$, the glass-glass line moves and merge with liquid-glass line, gives rise to two glassy phase. Two blues horizontal and vertical schematic lines are drawn as a guideline to eye in order to observe the reentrance.

red curve in Fig. 1.3 (a) represents the glass-glass line terminating in two end point singularities. These singularities are obtained for the specific values of

the control parameters. With sufficient increase of shoulder width $\Delta = 0.15$, the disconnected glass-glass line merge with liquid-glass line giving rise to reentry phenomenon. We plot two schematic horizontal and vertical lines in Fig. 1.3 (b) as a reference. These two lines intersects the liquid-glass line into two different points and bring two glass-liquid-glass regions which underlines the melting of the glass on increasing ϕ along y-axis and the melting of the glass on decreasing T along x-axis. We will give a clear understanding of the higher order singularities and different closures used in MCT equations in Sec. 1.2.

The MCT predictions for the SS system pave the way to confirm these anomalous dynamics and to explore the kinetic phase diagram by numerical simulations. Before going into the detailed description about the numerical study and results, we describe some basic elementary techniques and properties which will be useful for understanding the thesis

1.5 Mean Square Displacement and diffusion coefficient

We previously discussed, simulations on short range attractive colloids have shown the anomalous behavior of the diffusivity. Usually, such phenomenon can be highlighted through a systematic study of quantities such as the mean square displacement (MSD), that for a system of N particles, can be defined

as

$$\langle r^2(t)\rangle = \left\langle \frac{1}{N}\sum_{i=0}^{N}(r_i(t) - r_i(0))^2 \right\rangle \tag{1.25}$$

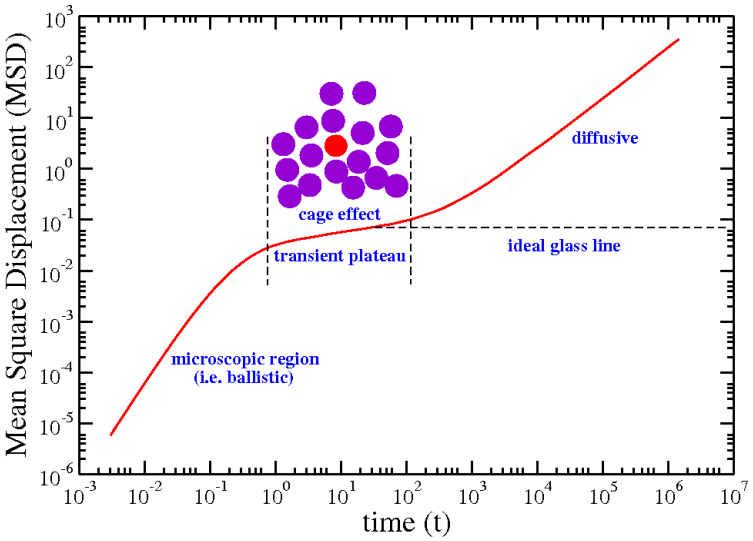

Figure 1.4: The behavior of mean square displacement is described at different time scales.

There are three regimes characterizing the motion of particles in a fluid and that can be identified in the behavior of the MSD. A first regime, occurring at short timescale, is related to the free motion of particles that do not experience any collision with their neighbors. If the system is described by Newtonian dynamics, such free motion is described by a ballistic behavior and the MSD is characterized by a quadratic dependence in time,

$$\langle r^2(t)\rangle \propto t^2 \tag{1.26}$$

The second regime, occurring at intermediate times corresponds to a situation in which diffusion is strongly limited upto the region where the particles are trapped in a"cage" formed by the neighboring particles. Due to the cage effect, each particle rattles inside the cage and the effect of this mechanism on the MSD results into a transient plateau whose height gives an estimation of the average size of the cage. After a finite period of time, particles get the way out of their own cages and start to diffuse. The recovery of the diffusion at large time scales is signaled by a linear behavior of MSD with time t.

$$\langle r^2(t)\rangle \propto t \tag{1.27}$$

The whole diffusive motion of the particle is shown in Fig. 1.4. Indeed, following the Einstein relation [24], one has that

$$\lim_{t\to\infty} \langle r^2(t)\rangle = 2dDt \tag{1.28}$$

where, d is the dimension of the system. The slope of the MSD, for the long time intervals gives the self diffusion constant D. In a three dimensional system, the self-diffusion constant is defined as

$$D = \lim_{t\to\infty} \frac{\langle r^2(t)\rangle}{6t} \tag{1.29}$$

The diffusive behavior of the particle is preserved until the dynamical arrest occurs. In fact, when the system gets more and more viscous, then particles rattle inside the cage for longer and longer time, thus forming a plateau in the MSD that extend over a several decades. In the glassy state,

the diffusive regime is never recovered and particles remain trapped in the cage forever.

1.6 Plan of the thesis

In this section, we give an outline of the thesis. In Chapter 2, building on the theoretical predictions Sperl *et al.*, we perform an extensive simulation study for SS system. We compare our simulation results with MCT predictions. The dynamical phase diagram shows the reentrance due to cooling which is observed in terms of diffusion anomaly along isochores. We also perform novel MCT calculations using as input the partial structure factors obtained within MD, confirming the simulation results. This new calculation produces liquid-glass line along with the disconnected glass-glass line terminating with two A_3 higher order singularities. These singularities generate a logarithmic dependence of the density correlators as well as a subdiffusive behavior of the mean squared displacement. The presence of these singularities is detected indirectly as the glass-glass line buried inside the glassy regime. This work has been published as [10].

In Chapter 3, we reported the MD simulation results for $\Delta = 0.17$. We redraw the dynamical phase diagram which produces the reentrance due to cooling but not upon isothermal compression. The diffusion anomaly is only observed along isochores. The MCT calculations using as input the simulation partial structure factors produce the liquid-glass line along with the glass-glass line terminating with A_3 and A_4 higher order singularities. In the present study for $\Delta = 0.17$, we locate A_4 singularity in the liquid

phase. During a precise analysis for A_4 singularity we unveil a novel invariant dynamics close to the glass line. The dynamics are indistinguishable along the invariant line.

In Chapter 4, we make a detailed investigation for $\Delta = 0.15$ and explore the low ϕ and T region of the phase diagram. The presence of the repulsive length scale in the potential generates the activated process which allow us to achieve the glass transition in low density region for $T \to 0$. We study the temperature dependence of diffusivity and observe the Arrhenius behavior. We evaluate the Stokes-Einstein relation, finding a clear breakdown. In low density region of the phase diagram, the system shows a transition from fragile to strong behavior.

Chapter 2

Complex glassy dynamics in Square Shoulder (SS) system: simulations and theory

2.1 Introduction

The Mode Coupling Theory (MCT) has predicted a rich phenomenology for square shoulder (SS) system where the system shows diffusion anomalies and reentrant behavior. Numerical simulations are aiming to confirm these complex behaviors which have not been performed so far. In this work we provide an extensive and systematic characterization of the SS model by means of event-driven molecular dynamics (MD) simulations in order to describe its dynamical behaviour. We examine the one-component system as well as a suitably chosen binary mixture which is considered in order to avoid crystallization at high densities and low temperatures, and to probe a sufficiently

slow dynamics. The Chapter is organized as follows. In Section 2.2 we describe the simulation methods and provide a summary of MCT. Then in Section 2.3 we report our main results in four different subsections: in 2.3.1 we discuss the behaviour of the self-diffusion coefficient calculated from the simulations and extract an ideal glass line using power-law fits of the data; in 2.3.3 we compare with existing MCT results and perform new calculations for the binary mixture currently under study to closely compare the theoretical results with the simulations; in 2.3.4 we then search for the existence of the predicted MCT higher order singularities; finally in 2.3.5 we report results for the non-ergodicity parameters obtained from theory and simulations to assess the types of the glasses that the system forms at various packing fractions and temperatures. Finally in Section 4.5 we discuss our findings and provide some conclusions and perspectives.

2.2 Methods: Simulations and Theory

We study a $50 : 50$ mixture of $N = 2000$ particles of species A and B interacting via pairwise SS potential

$$V_{ij}(r) = \begin{cases} \infty, & r < \sigma_{ij} \\ u_0, & \sigma_{ij} \leq r < (1+\Delta)\sigma_{ij} \\ 0, & r \geq (1+\Delta)\sigma_{ij}, \end{cases} \tag{2.1}$$

where $i, j = A, B$, σ_{AA} and σ_{BB} are the particles diameters (and $\sigma_{AB} = (\sigma_{AA} + \sigma_{BB})/2$), $\Delta\sigma_{ij} = 0.15\sigma_{ij}$ are the shoulder widths, and $u_0 = 1$ is the

shoulder height. The mass m of both particles is chosen as unit mass, while σ_{BB} and u_0 are the units of length and energy respectively. T is measured in units of energy (i.e. k_B=1).

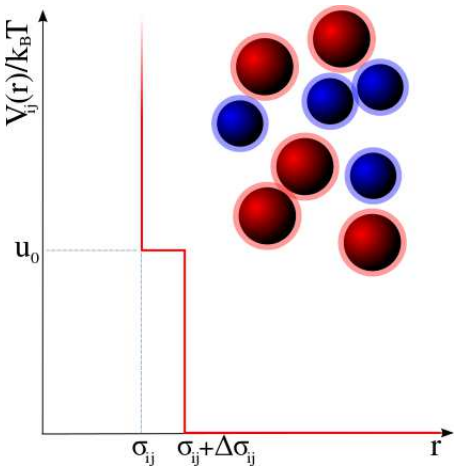

Figure 2.1: Square shoulder potential for a generic additive binary mixture of species i, j. Here $\sigma_{ij} = (1/2)(\sigma_i + \sigma_j)$ are the hard-cores, $\Delta\sigma_{ij}$ are the shoulder widths and $u_0 = 1$ is the shoulder height.

The size ratio between the two species is $\sigma_{AA}/\sigma_{BB} = 1.2$. We also study the simple monodisperse version of the SS system with the same width. However, the one-component system crystallizes before it has actually entered a sufficiently slowed-down regime of dynamics, similarly to what generally observed for one-component glass-formers. The introduction of a small difference in the species size allows to extend the non-crystallizing region of the phase diagram and to explore liquid states with very low diffusivity. In this way, we get as close as possible to the ideal glass line, which is defined as the locus of points in the packing fraction-temperature state diagram having diffusivity $D \to 0$.

We perform event-driven MD simulations of the system as a function of T

and packing fraction, defined as $\phi = (\pi/6)(\rho_A\sigma_A^3 + \rho_B\sigma_B^3)$, being $\rho_i = N_i/L$, L the edge of the cubic simulation box and N_i the number of particles for each species. Simulations are performed in the canonical and microcanonical ensemble. For the desired packing fraction an initial configuration is generated randomly and the particles velocities are extracted from a Maxwell-Boltzmann distribution corresponding to the desired T. Then, the system is equilibrated by performing MD simulations in the canonical ensemble with appropriate rescaling of particle velocities. After the equilibration, for each state point investigated, NVE simulations are performed for times ranging from $t = 10^2$ for the highly diffusive state points, to $t = 10^6$ for the most viscous state points. For all the simulations t is measured in units of $\sigma_{BB}(m/u_0)^{1/2}$. A detail understanding of the Event-driven MD simulation can be found in Appendix.

A first comparison with MCT results is possible by the calculation of iso-diffusivity lines, which typically preserve the shape of the ideal liquid-glass line. These lines, along which the self-diffusion coefficient D is constant, are evaluated by using the Einstein relation given in Eq. (1.29). Then we identify state points with the same D and connect them by iso-D lines. Repeating this procedure for lower and lower values of D, typically covering a few orders of magnitude in D, we can extrapolate the $D = 0$-ideal glass line.

As we have already discussed in Chapter 1, at the ideal glass transition the diffusivity D obeys powerlaw behavior along an isotherm

$$D \sim \mid \phi - \phi_g(T) \mid^{\gamma(T)} \tag{2.2}$$

and along an isochore

$$D \sim \mid T - T_g(\phi) \mid^{\gamma(\phi)} . \tag{2.3}$$

We can extrapolate the arrested temperature T_g and arrested packing fraction ϕ_g following the Eqs. (2.2) and (2.3) respectively. This line can be directly compared to the MCT glass line, as previously done for other systems [33, 47, 62]. Indeed, MCT usually overestimates the tendency to form a glass, so that the two lines (numerical and theoretical) are always shifted by a certain amount in both T and ϕ. However, the shape of the two lines has been found, for all previously investigated systems, to be identical: this makes possible to establish an effective bilinear mapping between the two curves so that they scale on top of each other, as it has been done for the SW model [48]. In the presence of singular state points, such as the MCT higher order singularities [50], the mapping procedure allows to estimate their exact location on the numerical phase diagram. Indeed, for the SW system, it was shown [47] that one of such singularities does exist by performing ad-hoc simulations near this particular state point. In the present work, we aim to carry out a similar, detailed investigation for the SS system.

For the SW system, higher-order singularities have been predicted and observed by numerical simulations and experiments. In particular, it was shown [11, 12] that MCT predictions in this case are robust upon the use of different closure relations such as mean spherical approximation (MSA) or Percus-Yevick (PY). Different closures only produce a shift of the glass transition lines with respect to each other.

For the SS system the situation appears to be more complex. Recent

theoretical studies [49,51] have shown that for the same value of the shoulder width, the use of two different closures, namely PY and Rogers-Young (RY), as input to the theory (from now on denoted as RY-MCT and PY-MCT respectively), provide qualitatively different results. While the liquid-glass line obtained within RY-MCT displays two reentrances (and hence diffusion minima and maxima) associated both to cooling (as in the SW system) and to compression, no reentrance is observed using PY-MCT. In the latter case, there is also no evidence of a glass-glass transition, while RY-MCT predicts two glass-glass lines each terminating in a higher order singularity. However, for the SS system at the investigated Δ, RY is expected to be superior to PY in the description of its structural and thermodynamic properties. Therefore, one of the aims of this work will be also to assess the validity of PY-MCT or RY-MCT predictions in order to establish the correct scenario for the SS system while approaching the glass transition.

2.3 Results for $\Delta = 0.15$

2.3.1 Iso-diffusivity lines and ideal liquid-glass line from simulations

We start by reporting the behavior of D along isothermal and isochoric cuts in the (ϕ,T) phase diagram in order to assess the presence of diffusion anomalies, perhaps like the ones observed in other core-softened potentials [19, 27, 43], conceptually similar to the SS system. In order to observe the diffusion anomalies in the system, we look at the dependency of the diffusion coefficient

on packing fraction ϕ and T. We remark that all shown data points do not crystallize and have reached a diffusive behaviour at long times, a condition necessary in order to extract D. In the following, we report results only for A particles, because the behaviour of the B particles is qualitatively the same due to the quasi-one-component nature of the mixture.

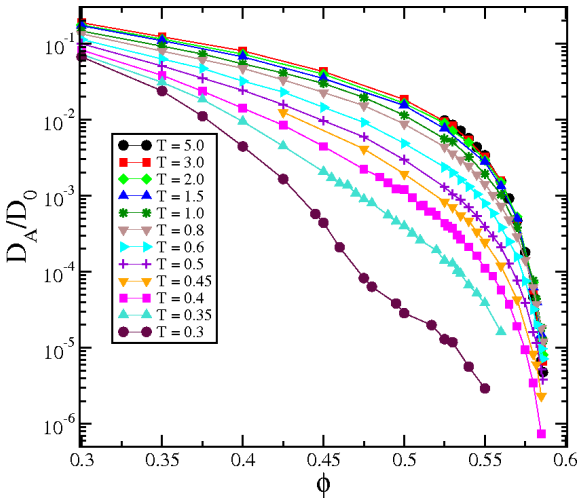

Figure 2.2: Normalized diffusion coefficient D_A/D_0 as a function of (a) ϕ for several isotherms, as reported in the labels. At all investigated T data show a monotonic decrease with increasing ϕ, which clearly indicates the absence of diffusion anomalies associated to compression/expansion.

Fig. 2.2(a) shows the normalized self-diffusion coefficient of A particles D_A/D_0 as function of ϕ for several isotherms, varying from $T = 5.0$ (close to the HS regime) to $T = 0.3$ (where the shoulder effect becomes prominent). The normalization factor $D_0 = \sigma_{BB}\sqrt{T/m}$ is introduced to account for the T dependence of the particles average velocities. The behavior of D_A with ϕ is similar along all studied isotherms: from the dilute limit D_A decreases monotonically at all T. For not too low T, the decrease becomes faster with increasing ϕ and is compatible with a power-law decay, as discussed below.

Notable exceptions are data points for $T \lesssim 0.35$: in these cases, a robust power-law dependence is not observed with decreasing T. Indeed, at $T = 0.3$ the data show a much wider range of decay. For a deeper investigation we have performed simulations for $T \leq 0.3$ and many adjacent ϕ with mesh 0.05 in the range $0.40 \leq \phi \leq 0.53$. This has allowed us to carefully check that the behavior of D_A is strictly monotonic within numerical error at the studied Δ value of the SS model. However, despite the absence of a diffusivity maximum, we are tempted to speculate that at these low T the observed slower decrease of D_A seems to be an effect of the competition between the two length scales in the potential. Indeed, at low enough ϕ the system behaves as being composed of effective HS particles of diameter $\sigma + \Delta$, while with increasing ϕ the bare hard-core at σ becomes dominant, thereby providing an intermediate non-trivial ϕ-dependence of D_A. Such scenario does not exclude the presence of a non-monotonic behavior for different values of Δ, that will be investigated in future studies. The studied normalized diffusivity varies between 10^{-2} to 10^{-6} in our numerical simulations. The highest packing fraction ϕ we could access in our numerical accuracy is $\phi = 0.59$ as the system becomes extremely slower to equilibrate.

The monotonic behavior of diffusivity is understood by looking at MSD. We monitor isotherm $T = 0.4$ and plotted MSD for several isochores as shown in Fig. 2.3. In the short time limit MSD shows a ballistic regime. At the intermediate time scale the particle get caged by it's neighboring particles and rattle inside the cage for a finite period of time. In the long time limit particle escape from the cage and starts to diffuse. At low packing fraction $\phi < 0.50$, the particle diffuses faster and then the diffusive motion of the particle slows

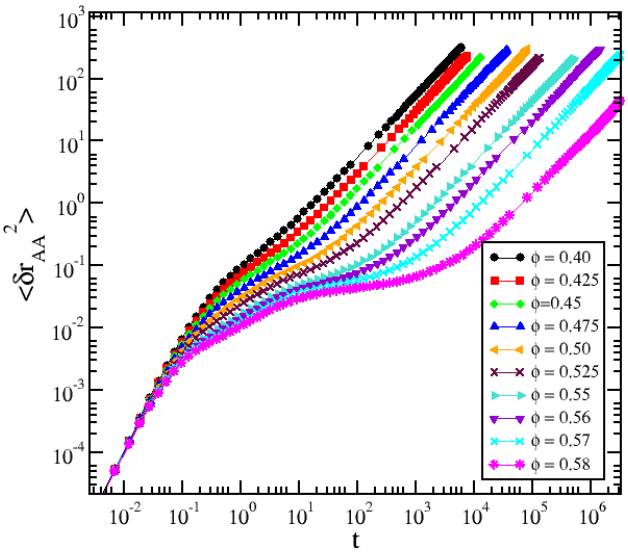

Figure 2.3: Mean Square Displacement along isotherm $T = 0.4$ for a set of packing fraction ϕ. The particle diffuses slowly in a monotonic way with increasing ϕ indicates the absence of diffusion anomaly due to compression/expansion.

down with increasing ϕ. The monotonic diffusive behavior of particle in MSD clarify the absence of diffusion anomaly due to compression/expansion.

Next, we investigate the behavior of D_A/D_0 with T along several different isochores, ranging between $\phi = 0.40$ and $\phi = 0.59$. This is reported in Fig. 2.4. At lower ϕ the system does not reach a glass transition even for very low temperatures. Indeed, in this limit, it can be considered as an effective hard sphere of diameter $\sigma + \Delta$. Since hard spheres are expected to undergo a glass transition at $\phi_g^{HS} \sim 0.58$, we expect for the low-T limit that the system becomes glassy for $\phi_g^{HS}[1/(\sigma + \Delta)^3] \sim 0.381$, in agreement with our simulations.

For packing fractions $0.40 \leq \phi \leq 0.56$ the diffusion coefficient decreases monotonically with T. For $\phi \geq 0.57$, D_A/D_0 becomes non-monotonic: from

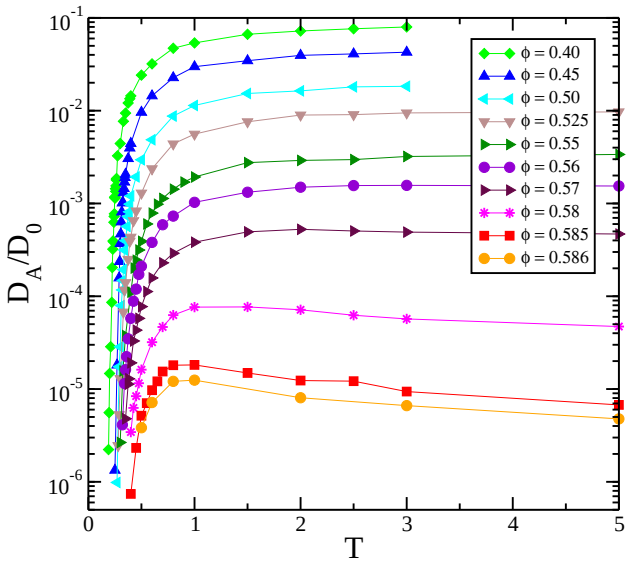

Figure 2.4: Normalized diffusion coefficient D_A/D_0 as a function of T for several isochores, as reported in the labels. The increase in the height of the peak for $\phi > 0.57$ show a non-monotonic behavior with decreasing T which can be clearly observed in terms of a crossing of the data at high ϕ in Fig. 2.2. This non-monotonicity in normalized diffusivity signals the presence of a diffusivity maximum associated to cooling.

the high T limit, it initially increases and then decreases, giving rise to the presence of a diffusivity (local) maximum at intermediate T. When we plot MSD for a fixed $\phi = 0.585$ and vary the temperature, we observe a peculiar dynamics in long time limit as shown in Fig. 2.5 (a). The diffusivity first decreases with increasing T and then, at $T = 1.5$, the diffusivity increases upto $T = 1.0$ and decreases again on lowering T. This fluctuation of the particle dynamics in the long time limit of MSD can clearly observed in the zoomed part as shown in Fig. 2.5 (b). The increase in the height of the peak with increasing ϕ gives rise to the non-monotonic behavior of diffusivity. This is also visible from the crossing of the high-T data (at large ϕ) in Fig. 2.2(a).

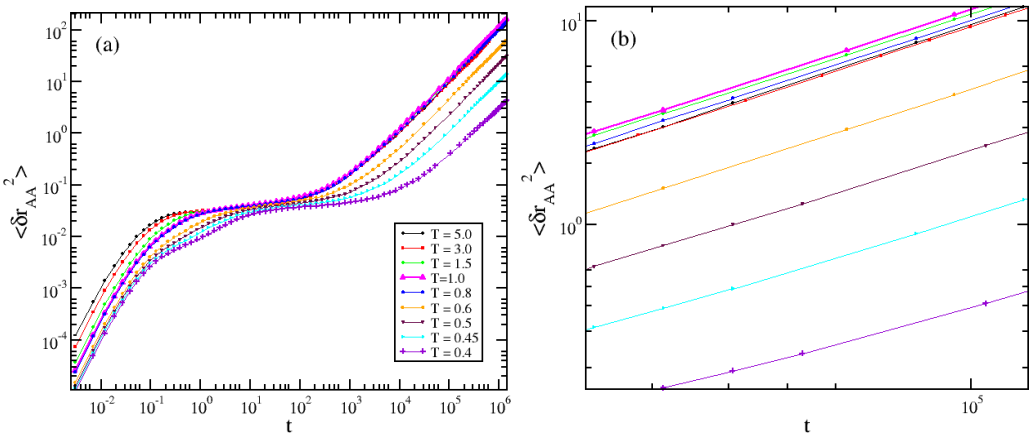

Figure 2.5: Mean Square Displacement of particle has been plotted at a fixed $\phi = 0.585$ with varying T. (a) On lowering T particle dynamics slows down and a nonmonotonic behavior of diffusivity has been observed at intermediate $1.5 \leq T \leq 0.6$. (b) On magnifying the long-time limit of MSD, we could observe that the diffusivity decreases and then increases again on lowering T. This non-monotonicity in dynamics satisfies the anomalous behavior of diffusivity along isochore as shown in Fig. 2.4.

The anomalous behavior of D_A upon cooling is similar to that observed for the SW system at high enough packing fractions when the width of the well is of few percent of the particle size [59]. When we look at the long time limit of MSD, the particle.

Compiling all data from Fig. 2.2 and Fig. 2.4 we are able to trace isodiffusivity lines in the phase diagram to be compared with the MCT glass lines. The monotonic (non-monotonic) behavior of D_A is reflected in the absence (presence) of a reentrance in the iso-D_A lines.

Fig. 2.6(a), shows the iso-diffusivity curves for three fixed values of normalized diffusion coefficients: $D_A/D_0 = 1.0 \times 10^{-3}, 1.0 \times 10^{-4}$ and 1.1×10^{-5}. Each curve is obtained by extrapolating from Fig. 2.2 and Fig. 2.4 a set of i states (ϕ_i, T_i) having the same value of D_A/D_0. As discussed above, we do

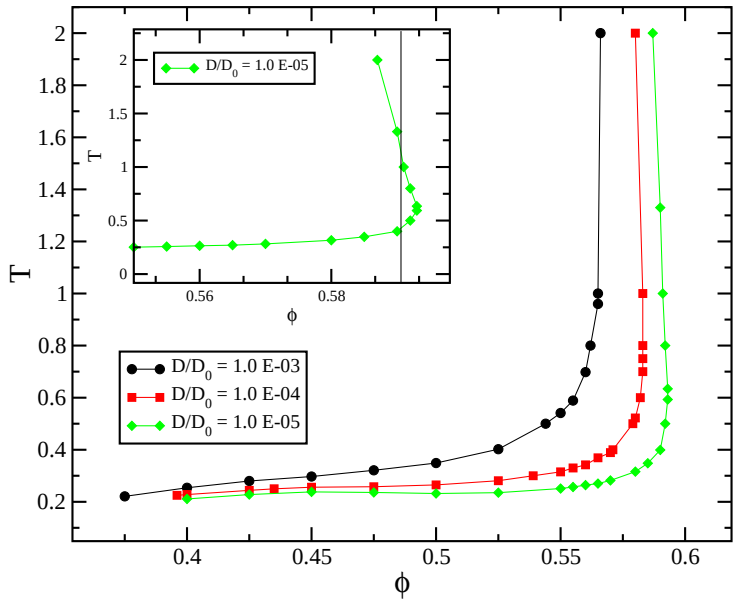

Figure 2.6: Isodiffusivity lines for $D_A/D_0 = 1.0 \times 10^{-3}, 1.0 \times 10^{-4}$ and 1.1×10^{-5}, are extrapolated from the diffusivity plots in Fig. 2.2 and Fig. 2.4 along isotherms and isochores. The data display a reentrance in T (inset), while no reentrance in ϕ is observed.

not observe a reentrant behaviour along ϕ even if we consider very low values of D_A/D_0. On the other hand, for $D_A/D_0 \sim 10^{-5}$ a reentrance is observed along T, as highlighted in the inset of Fig. 2.6(a). This is in agreement with the presence of a diffusivity maximum at high enough ϕ (Fig. 2.4).

From this analysis we conclude that the liquid-glass line shows only a reentrance along T. While the glass at high T corresponds to a HS glass, the low-T glass could have a different nature and its properties will be elucidated in the following.

As said above, the iso-D_A lines are precursors of the ideal liquid-glass line, where $D_A \to 0$. We can extrapolate this line where the simulated system

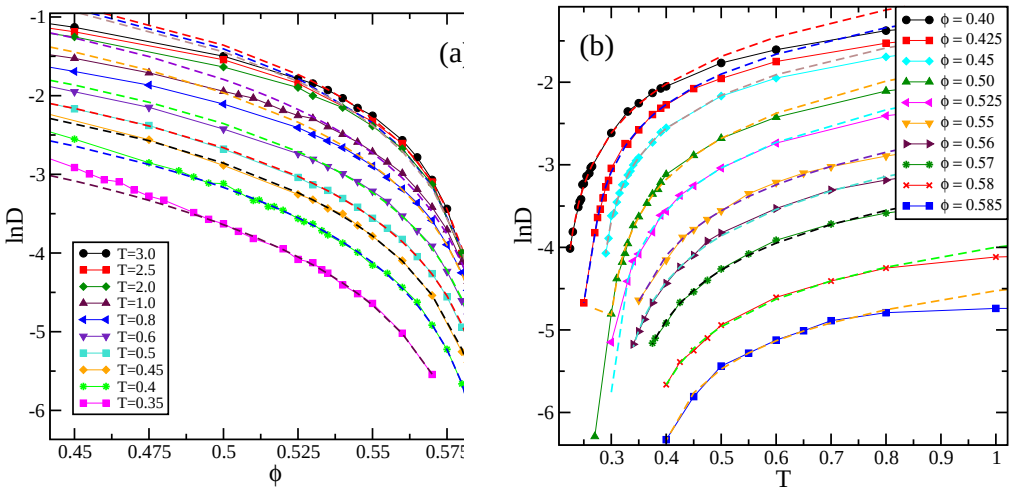

Figure 2.7: We have shown the power-law fits of diffusivity with respect to (a) ϕ and (b) T in semi-log scale within a fixed range of diffusivity.

should undergo dynamical arrest by performing power-law fits of the diffusivity both along isochores and along isotherms, following the MCT equations given by Eq. (2.2) and Eq. (2.3). We do the power-law fit of bare diffusion coefficient D as a function of ϕ and T in log scale. and extracted the arrested temperature T_g and packing fraction ϕ_g with the corresponding γ.

We put all the fits together both along isotherms and isochores which are shown in Fig. 2.8. In this way, we can extract both the transition values ϕ_g and T_g where the system arrests and the associated power-law exponents γ. These values are reported in Table 4.1. Note that no fits are performed for $T < 0.35$ due to the fact that the data do not show a clear power-law behaviour. Also for low values of ϕ some deviations from power-law dependence are observed at low T.

The resulting ideal glass line is presented in Fig. 2.9 together with isodiffusivity lines. As expected the two branches, extrapolated by the different

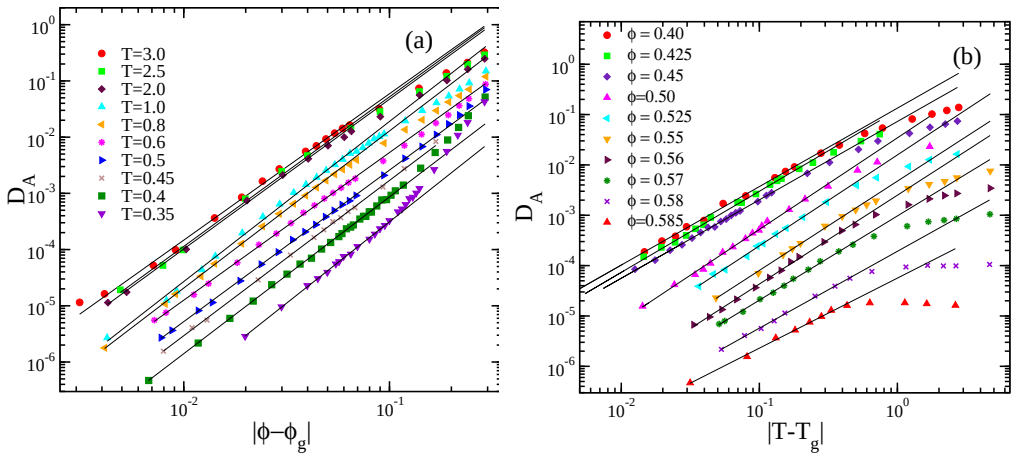

Figure 2.8: The power-law fits of diffusivity in log-log scale (a) along isotherms with the formula $D_A\ |\phi - \phi_g(T)|^{\gamma(T)}$, and (b) along isochores with the formula $D_A\ |T - T_g(\phi)|^{\gamma(\phi)}$.

paths, merge continuously in the high-ϕ, low-T region of the phase diagram and confirm the shape of the isodiffusivity lines. We note that the power-law exponents obtained along each isotherm are consistent with previous estimates for HS or SW systems. On the other hand, for the fits along isochores the γ exponents are systematically lower, at times going below the lowest limit predicted by MCT [21]. However, the values of γ obtained from the fits should be taken with caution due to the significant variation of results upon change of the chosen fit interval and relative distance to the transition. Nonetheless, the values of ϕ_g and T_g extracted in the same way show only little changes (of the order of a few percent), and hence they are robust.

We note that power-law fits along isochores could not be performed in most systems with isotropic potentials, where the exploration of the low-T region is preempted by intervening phase separation. For systems with

T	$\gamma(T)$	ϕ_g		ϕ	$\gamma(\phi)$	T_g
3.0	2.6	0.589		0.40	1.56	0.221
2.5	2.66	0.589		0.425	1.61	0.255
2.0	2.66	0.59		0.45	1.56	0.277
1.0	2.84	0.594		0.50	1.81	0.285
0.8	2.79	0.594		0.525	1.81	0.293
0.6	2.62	0.593		0.55	1.77	0.301
0.5	2.69	0.593		0.56	1.76	0.306
0.45	2.76	0.592		0.57	1.67	0.323
0.4	2.78	0.591		0.58	1.52	0.346
0.35	2.89	0.589		0.585	1.39	0.368

Table 2.1: Extrapolated values of $\gamma(T)$, ϕ_g, $\gamma(\phi)$ and T_g obtained from fitting data of Fig. 2.6 (a) and (b) with MCT predictions of Eqs. (2.2,2.3) for the diffusion coefficient D_A. Error bars of the fit parameters typically amount to a few percent for the values of ϕ_g and T_g, while the γ exponents can vary systematically over different fit intervals, so they should be taken with caution.

directional interactions where phase separation is suppressed by using a limited valence [31, 61], at low T bonding is the dominant mechanism of arrest so that the dynamics is dominated by an Arrhenius (strong) behaviour [7]. Here, however, we do not find evidence of an Arrhenius dependence even at very low T in the investigated window of densities, suggesting that the system remains power-law (fragile). Indeed, in the SS system temperature does not induce bonding, but rather has an effect on the excluded volume of particles by changing the effective diameter. In this sense, the arrest at low T remains of the same kind of the HS glass, so that a similar behaviour (fragile) is then expected throughout the phase diagram. However, it is then legitimate to ask, given that the nature of the glass transition remains the same, whether a simple competition between two length scales is capable to generate higher-order singularities as those predicted by MCT and related

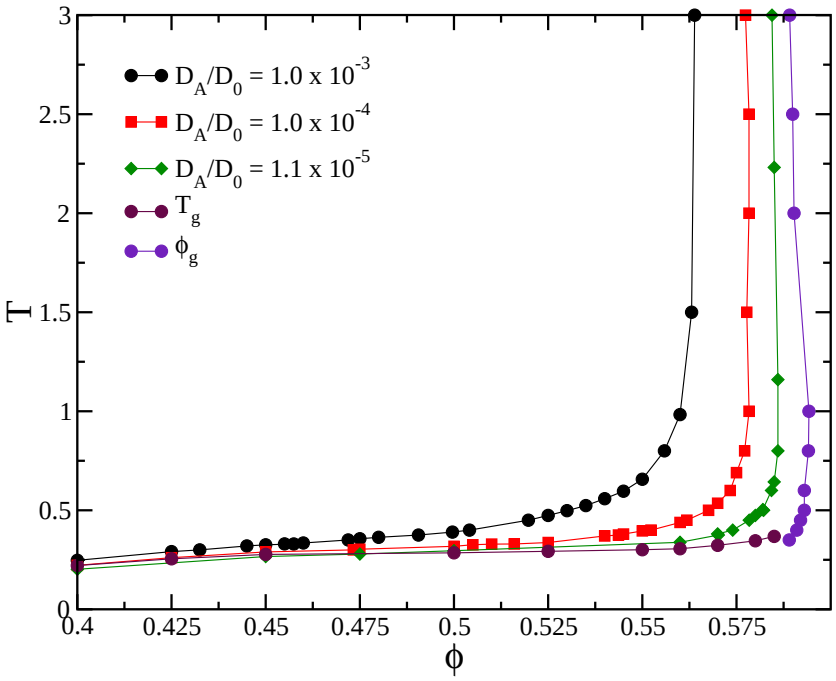

Figure 2.9: The extrapolated arrested ($D \to 0$) glass lines from the fits $D_A\ |\phi - \phi_g(T)|^{\gamma(T)}$ along isotherms and $D_A\ |T - T_g(\phi)|^{\gamma(\phi)}$ along isochores as shoen in Fig. 2.8. The arrested glass line shows a very good agreement with isodiffusivity lines confirming the presence of reentrance in T, while no reentrance in ϕ.

glass-glass transitions.

2.3.2 Verification of reentrance due to compression/expansion for different Δ

In order to verify the reentrance in (T, ϕ) plane due to compression/expansion, we did more simulations for different Δ. In Fig. 2.10, we plot the diffusion along a set of isotherms varying between $T = 1.0$ and 0.2. The behavior of D_A with ϕ is monotonic along all studied isotherms: from the dilute limit

D_A decreases monotonically at all T. For not too low T, the decrease becomes faster with increasing ϕ and is compatible with a power-law decay, as discussed below. We also verify the diffusivity for $\Delta = 0.2$ and 0.25 and do not observe any non-monotonic behavior. This indicates the absence of diffusion anomaly along isotherms which is a counter part of the reentrance due to compression.

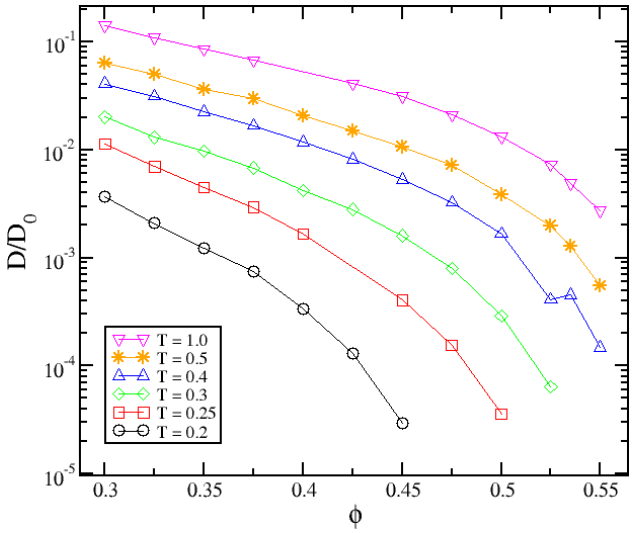

Figure 2.10: The behavior of self diffusion coefficient has been plotted with ϕ for $\Delta = 0.35$.

2.3.3 Comparison with old and new MCT results: role of the input structure factors and mapping to simulations

We now compare the MD simulation results for the ideal glass line with MCT predictions. While a mismatch of ϕ_g and T_g values is expected for the theoretical and numerical glass lines, the two should share the same shape, as

previously observed for a variety of glass-forming systems [17, 18, 27, 30, 62]. However, when referring to the RY-MCT calculations for $\Delta = 0.15$ [51], it is immediate to notice that while the numerical curve shows only one reentrance in T, the RY-MCT results display two of them, as shown in the inset of Fig. 2.11. No reentrance is conversely observed for PY-MCT[1]. Under this situation, we cannot perform a consistent mapping as previously done for SW systems [47], because the difference in the shape of the liquid-glass lines cannot be taken into account by a simple rescaling procedure. This matter thus deserves further investigation.

For understanding the difference between theory and MD results, at first we investigate the reliability of the different closures employed for producing the input $S(q)$ entering in MCT. In Fig. 2.11 $S(q)$ evaluated within RY and PY closures is shown together with that calculated directly from simulations of the monodisperse SS system for a representative state point. As expected, PY provides a rather poor estimate of S_q, since the height of its peaks and its amplitudes do not agree with those of the S_q evaluated from MD, while RY reproduces reasonably well the simulation results, as previously found for other repulsive potentials [27, 28, 32]. The good agreement between RY and MD $S(q)$ is found for all studied state points. However, this comparison is limited to the region of the phase diagram where the monodisperse system does not crystallize. The quality of the input structure factors is reflected in the better agreement of RY-MCT with the simulation iso-diffusivity lines. It is therefore natural from now on, to refer to RY-MCT results as the relevant theoretical predictions for the system.

[1] Courtesy of M. Sperl

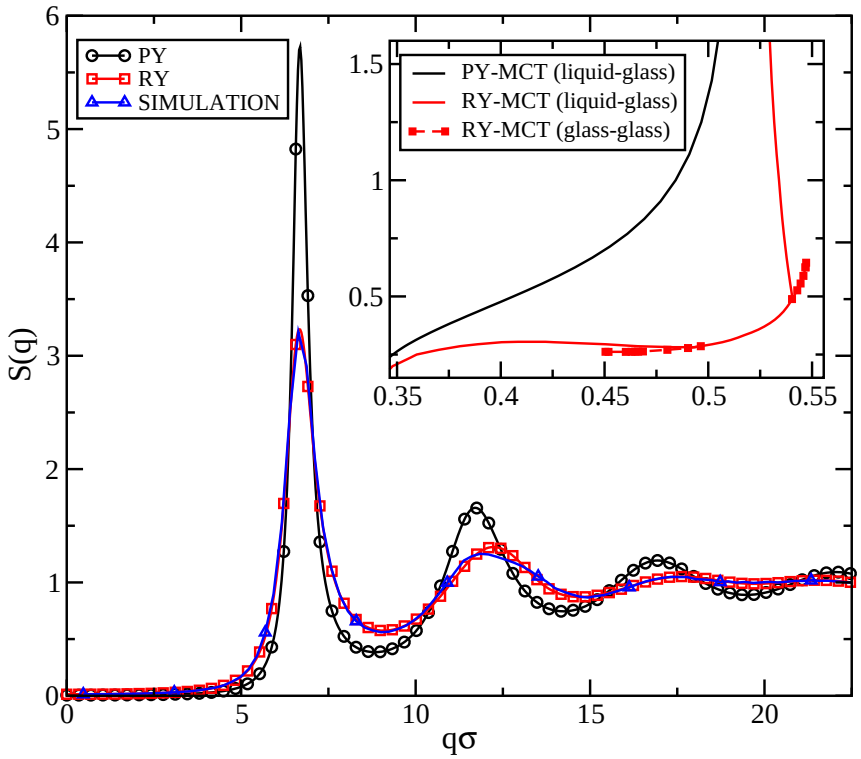

Figure 2.11: Static structure factors for a monodisperse SS system at $T = 0.5, \phi = 0.45$ calculated by MD simulations as well as solving the Ornstein-Zernike equation within Rogers-Young (RY) and Percus-Yevick (PY) closures. Inset: MCT results for the liquid-glass and glass-glass lines using PY and RY.

However, although the shape of the RY-MCT liquid-glass line is more similar to the MD results, with at least one reentrance recovered, there is still a discrepancy between RY-MCT and MD simulations. In fact, both from the analysis of D/D_0 and from the iso-diffusivity lines we could not detect the presence of a second reentrance (i.e. a diffusion anomaly) along ϕ (at fixed low-T).

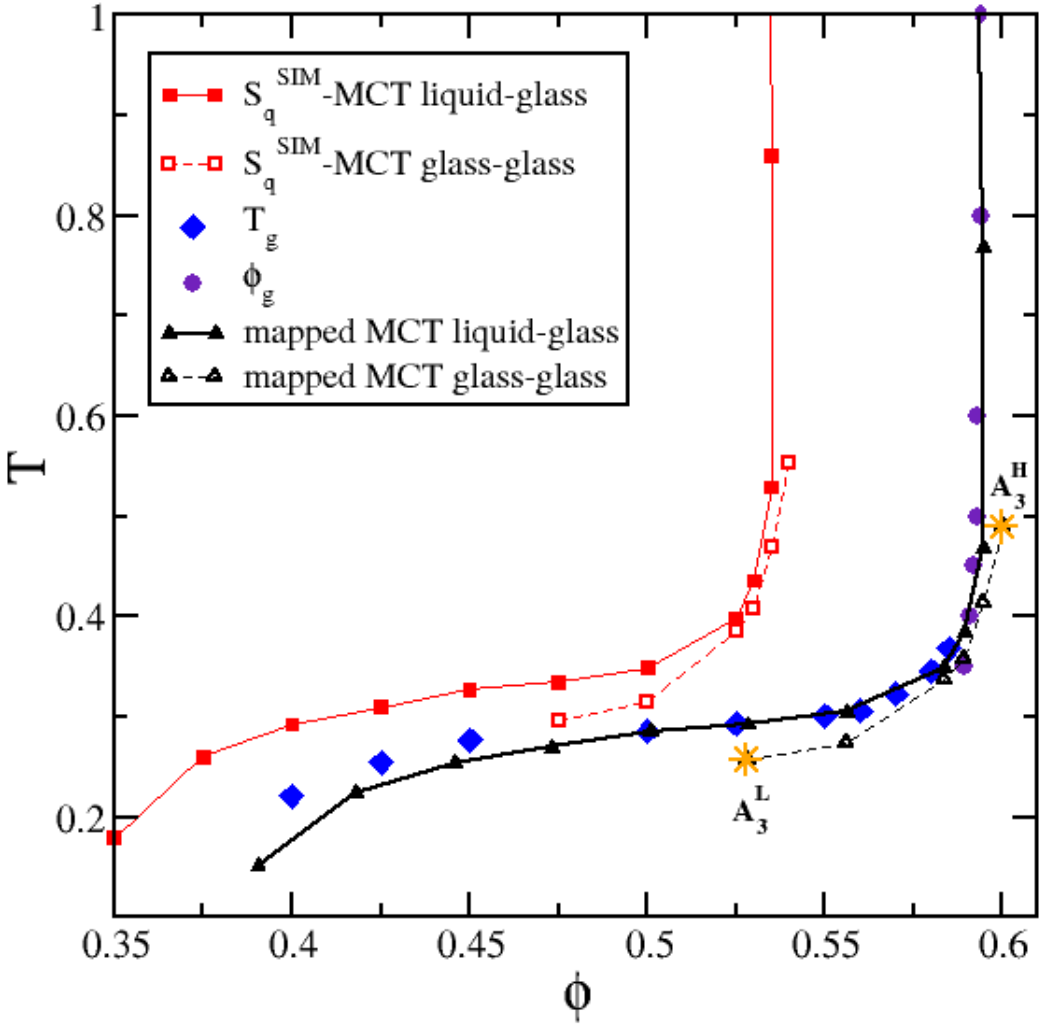

Figure 2.12: MCT results for the binary mixture under study using the static structure factors calculated from simulations as input, labeled as $S_q^{SIM} - MCT$ liquid glass (filled squares) and glass-glass (open squares). Arrest curve drawn from ϕ_g (filled circles) and T_g (filled diamonds) obtained from power-law fits of D_A as in Fig. 2.6. Mapped MCT lines onto the arrest curve: liquid-glass (filled triangles) and glass-glass (open triangles). Stars are the two predicted higher order singularities A_3^L and A_3^H.

Given this situation, we performed additional MCT calculations explicitly incorporating the binary nature of the system under investigation. To avoid to rely on a certain closure, we have used as inputs to the theory the partial structure factors evaluated from MD simulations $S_{ij}^{SIM}(q)$. Hence, we have solved the generalized version of long-time MCT equations (Eq. 1.3) for a binary mixture [23] on a discretised grid of 1000 wave vectors up to a cut-off value of $q\sigma_{BB} = 65$. This value is sufficient for the critical non-ergodicity parameters along the liquid-glass line to decay to zero. In this way, we determine the liquid-glass and (if any) the glass-glass transition, and associated non-ergodicity parameters.

The resulting liquid-glass line is reported in Fig. 2.12 together with the arrest line extrapolated from the fits of D_A. Despite the expected shift in the control parameters, it now appears that the new MCT results for the mixture are in full qualitative agreement with the simulation line, since the reentrance in ϕ is no longer present. We can now operate a bilinear transformation, as previously done [47, 48], to superimpose the MCT results onto the glass line obtained from simulations. The parameters are chosen via a best fit procedure, giving as a result

$$\begin{aligned} \phi &\rightarrow 1.1046\phi + 0.0038 \\ T &\rightarrow 0.9052T - 0.0111 \end{aligned} \tag{2.4}$$

and the mapped glass lines are shown in Fig. 2.12.

MCT calculations predict a 'disconnected' glass-glass line, a scenario that was also present in the one-component RY-MCT, albeit for lower values of

Δ [51]. Luckily, this glass-glass line lies just inside, but very close to the liquid-glass line so that signatures of the two A_3 endpoints are in principle detectable from simulations. When we study the dynamics far from this glass-glass line, it behaves as a normal liquid. On moving close enough to the glass-glass line in equilibrium phase the particle dynamics changes drastically near these higher order singularities. Through our mapping, we can now estimate the location of the two singularities, that will be referred from now on as A_3^L and A_3^H, respectively the one at lower and higher ϕ. We find $A_3^L = (\phi \sim 0.53, T \sim 0.26)$ and $A_3^H = (\phi \sim 0.60, T \sim 0.49)$. Both are rather close to the liquid glass transition, the distance being $\Delta T \sim 0.03$ along an isochore for A_3^L and $\Delta\phi \sim 0.06$ along an isotherm for A_3^H respectively.

2.3.4 Searching for higher-order singularities

In this section we investigate the presence of the higher-order singularities predicted by MCT in the numerical phase diagram. To this aim we concentrate on distinct paths in the phase diagram that allow us to approach closely the two A_3 points. We recall however, that both points are buried within the glass region, hence they are not directly accessible in equilibrium; moreover the behaviour of the observables that we examine are influenced also by the presence of the nearby liquid-glass transition. In the following we will only concentrate on species A, but we stress that the qualitative behaviour is identical for type B particles.

We start by discussing the presence of A_3^L: we examine the dynamical behaviour of the system along the isochore $\phi = 0.525$ with decreasing T.

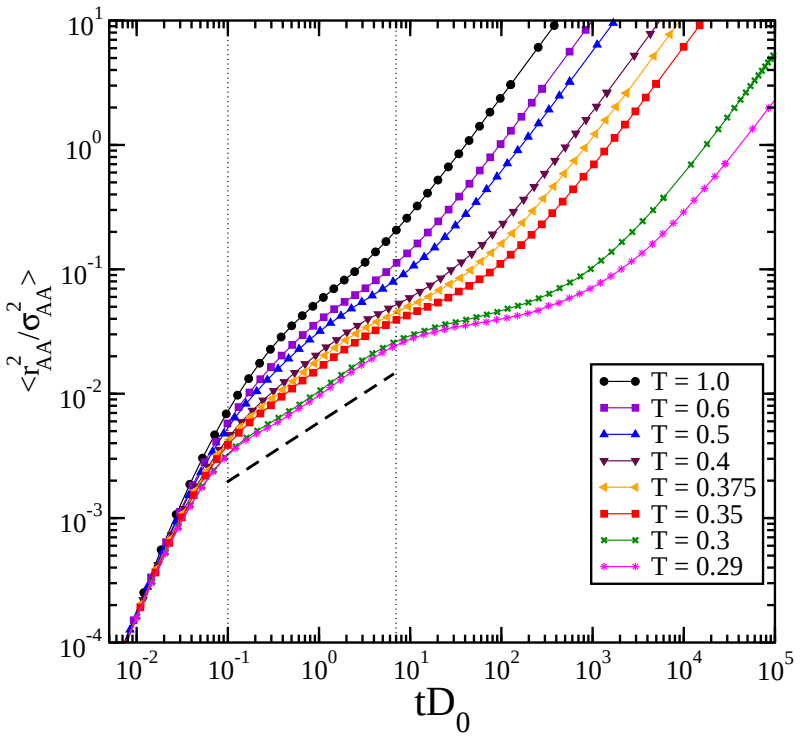

Figure 2.13: MSD for a particles as a function of scaled time tD_0 for $\phi = 0.525$ as a function of T, indicated in the labels. The two vertical dotted lines indicate as guides to the eye the regime of subdiffusive behaviour, which is highlighted by the dashed line ($\propto t^{0.5}$).

We recall that while the endpoint should be found at $T \sim 0.26$, the system becomes glassy according to MCT for $T \lesssim 0.28$ at this volume fraction.

Fig. 2.13 shows the MSD for A particles $\langle r^2_{AA} \rangle$ along this path. We observe that upon decreasing T the system shows a peculiar slowing down. Indeed, a characteristic subdiffusive behaviour at intermediate times ($0.1 \lesssim tD_0 \lesssim 10$) is observed for $T < 0.4$. Hence, we observe a sort of three-step behaviour of the MSD: after the ballistic transient, subdiffusion takes place for roughly two decades in time, where $\langle r^2 \rangle \sim t^\alpha$ with $\alpha \sim 0.5$. At long times the typical pattern of glass-forming systems takes place: a plateau later followed by

long-time diffusion. Indeed, when T is very low, the system is approaching the liquid-glass transition, that manifests itself in the MSD as the emergence of the plateau. This is observed for $T \leq 0.3$ and occurs at $tD_0 \sim 10^2$. The plateau height is found to be $\sim 0.04\sigma_{AA}^2$. Its square root, which provides a measure of the cage or localization length l_0 of the glass, turns out to be $\sim 0.2\sigma_{AA}$, roughly twice the typical HS cage length ($l_0^{HS} \sim 0.1\sigma$). Indeed, the packing fraction is significantly smaller than that of the HS ideal glass, due to the effect of the shoulder. While the long-time behaviour, and associated plateau, is controlled by the liquid-glass transition, the additional intermediate behaviour, which indicates the presence of a sub-diffusive regime, can be associated to the presence of the higher order singularity.

The presence of subdiffusivity is a hint of a closeby higher order singularity, but in order to provide a more convincing proof of its existence, we now look at the behaviour of the density auto-correlations functions. A distinctive feature is the presence of a pure logarithmic regime for a certain wave-vector q^*, where the second-order term of the asymptotic expansion in Eq. 1.8 vanishes. Below and above q^* the data should display a typical concave-to-convex transition. To visualize this behaviour one should be close enough to the A_3^L point, but far enough from the liquid-glass transition in order to avoid that the final two-step decay covers most of the time-window and preempts the observation of the logarithmic behaviour. We identify at this ϕ the optimal temperature obeying these requisites as $T = 0.375$, for which we show the collective normalized density auto-correlations functions $\Phi_q^{AA}(t)$ as a function of wave-vector in Fig. 2.14(a). Indeed, at this T we are

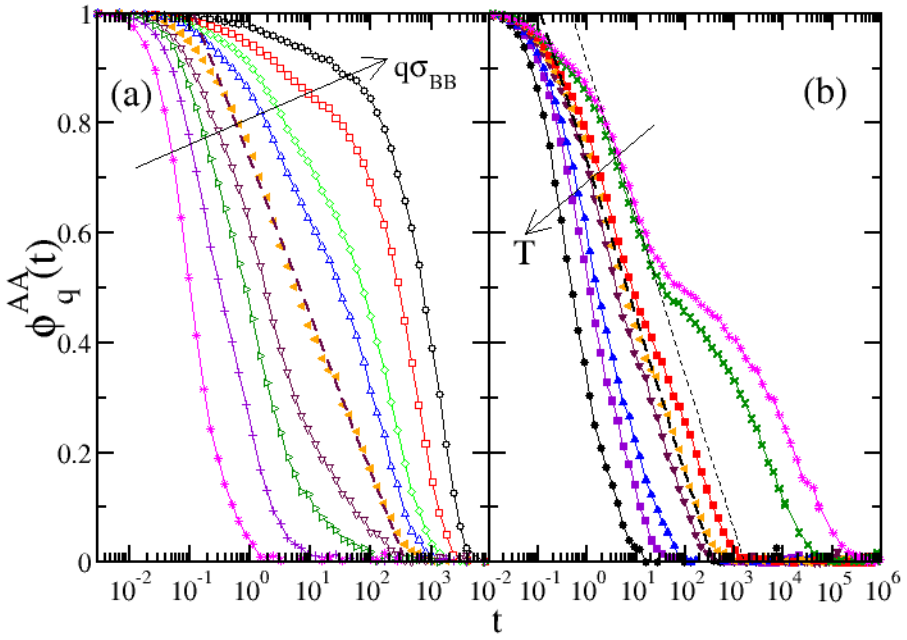

Figure 2.14: The density autocorrelation functions $\Phi_q^{AA}(t)$ for $\phi = 0.525$ as a function of time for (a) several wave vectors at $T = 0.375$. From top to bottom, $q\sigma_{AA} = 1.88, 2.81, 4.68, 5.63, 7.5, 10.32, 13.12, 17.82, 28.13$. A concave-convex shape transition is observed around $q^*\sigma_{AA} \approx 7.0$ where the decay of $\Phi_q^{AA}(t)$ is almost purely logarithmic; (b) several T at fixed wave vector $q = q^*$. From left to right, temperatures are $T = 1.0, 0.6, 0.5, 0.4, 0.375, 0.35, 0.3, 0.29$.

able to identify $q^*\sigma_{AA} \approx 7$ where the decay of the correlators is purely logarithmic. Across q^*, the concave-to-convex transition in the shape of $\Phi_q(t)$ with time is found. In Fig. 2.14(b), the T-dependence of the correlators at fixed $q = q^*$ is shown. It is clear that with further decreasing T the system approaches the liquid-glass transition, so that the signal of the logarithmic decay gets lost. Indeed, the range where the logarithmic dependence (dashed line) is valid shrinks upon reducing T. The evidence reported so far points to the existence of a higher order singularity in the vicinity of the explored path. While we cannot probe its exact location, since the system falls out of

equilibrium before this can be accessed, it seems to be located within, but not too far inside, the glassy region, compatibly with MCT predictions of a disconnected glass-glass line.

Next we investigate the presence of the second singularity A_3^H. To approach this singularity, we monitor the isotherm $T = 0.5$ and check the dynamical behaviour with increasing ϕ. We recall that the endpoint should be located at $\phi \sim 0.6$, while the system should become glassy around $\phi \sim 0.593$, as estimated by the power law fits of D_A. We repeat the same analysis as done for A_3^L.

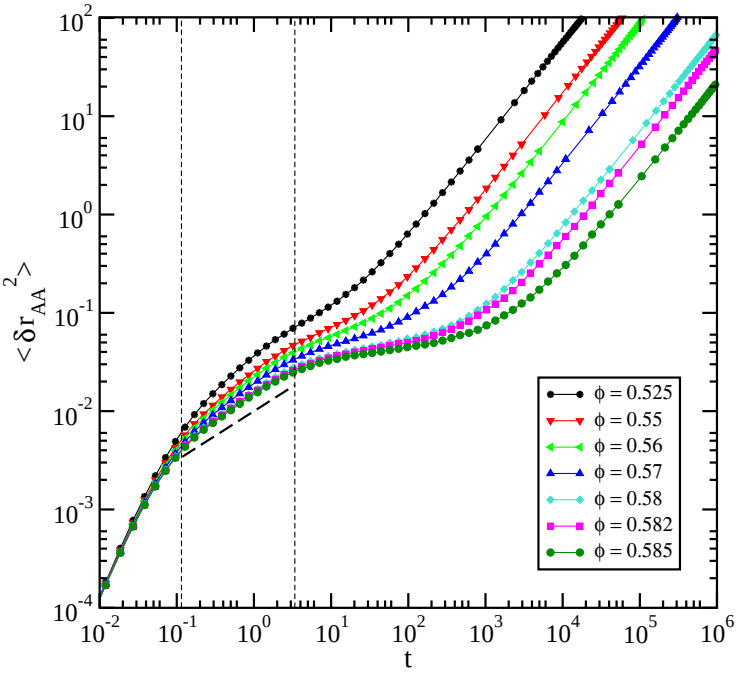

Figure 2.15: MSD for a particles as a function of scaled time tD_0 for $T = 0.5$ as a function of ϕ, indicated in the labels. The vertical dotted lines indicate as guides to the eye the regime of subdiffusive behaviour, which is highlighted by the dashed line ($\propto t^{0.5}$).

We trace the position of A_3^H by moving along isotherm $T = 0.5$ of the

phase diagram and understand the dynamics with increasing ϕ as shown. In Fig. 2.15, we plot the MSD for a set of ϕ varying between 0.425 and 0.585 for a fixed value of $T = 0.5$. Following the usual behavior, at low density ($\phi < 0.525$) the particle diffuses as a normal liquid. With increasing ϕ, an intermediate plateau region starts to appear and a clear subdiffusive region is formed at $\phi = 0.585$. The subdiffusivisity stays for two decades in magnitude for the intermediate time scale (tD_0) between 10^{-1} and 10^{1}. In long time limit the particle escape from the cage and diffuses linearly with time. The height of the plateau is $\sim 0.024\sigma_{AA}^2$ gives the localization length $l_0 \sim 0.15\sigma_{AA}$ which is close value of typical HS cage length ($l_0^{HS} \sim 0.1\sigma$).

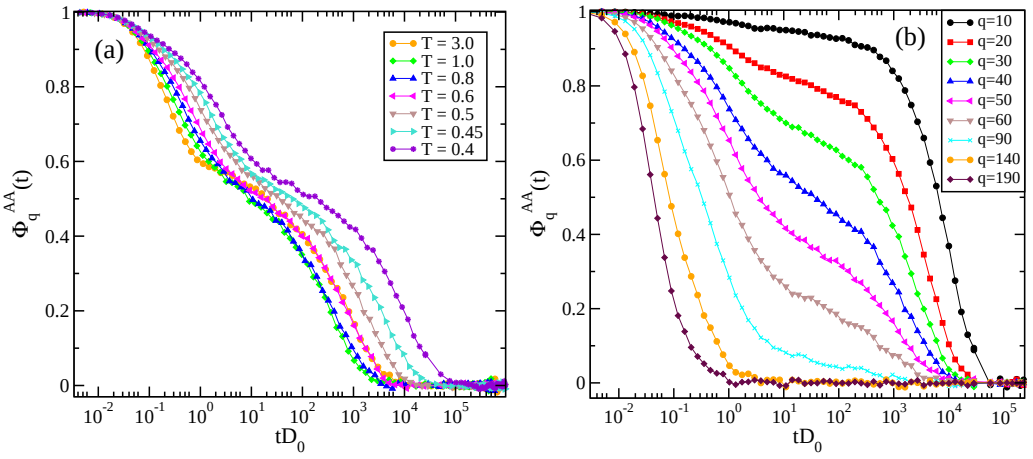

Figure 2.16: The figure shows (a) the density auto correlation functions for $q\sigma_{AA} \approx 7.75$ $\phi = 0.58$ with decreasing T. (b) The appearance of concave and convex shape for the state point $\phi = 0.58$ at $T = 0.5$.

In addition to the subdiffusive behavior in MSD we verify the logarithmic decay in density auto-correlations functions. We do the similar check as in case of A_3^L higher order singularity. From the previous analysis, we understood for a critical $q$vector q^*, whose above and below, the density

auto-correlation functions shows a transition from concave to convex shape. We choose the state point $\phi = 0.58$ for $T = 0.5$ and plotted $\Phi_q^{AA}(t)$ for a set of $q$vectors, where we could have a clear observation of transition from concave and convex shape. For the critical value of $q$vector $q^* \approx 7.75$, we do not see a pure logarithmic behavior as shown in Fig. 2.16 (b). The logarithmic time window is very short $(10^{-1}) \leqslant tD_0 \leqslant 10$, less than two orders of magnitude. In Fig. 2.16 (a), for $q^*\sigma_{AA} = 7.75$, the long time decay in density auto-correlation function changes at $\phi = 0.58$ on lowering the temperature T. At high T limit ($T \leqslant 0.8$), α-relaxation merge with each other. In the intermediate temperature between $T = 0.6$ and 0.5, the density auto-correlation function shows a logarithmic decay for a short time scale. On further lowering $T = 0.4$, the α relaxation shows a extremely decay.

As shown in Fig. 2.16(b), for high $\phi > 0.57$, the realization of logarithmic decay in $\Phi_q^{AA}(t)$ is in a very small interval of time scale less than 2 order of magnitude (between 10^0 and 10^{-2}). The decay in $\Phi_q^{AA}(t)$ does not show a clear picture of logarithmic behavior with increasing $q$vector. The two-step relaxation in the density density correlator brings an impression of higher order singularity. The interesting feature is reflected with three-step relaxation of density density correlator with increasing ϕ differently from usual the two-step relaxation [59].

Next, we report $\Phi_q^{AA}(t)$ at $T = 0.5$ for $q^*\sigma_{AA} = 7.75$ in Fig. 2.17 with increasing ϕ. At high packing fractions, on lowering the temperature, the three-step relaxation process becomes more prominent for intermediate wave vectors ($5.75 < q\sigma_{AA} < 13.6$) and the time scale increases by one decade. The logarithmic behavior in short time scale does not give a clear picture of

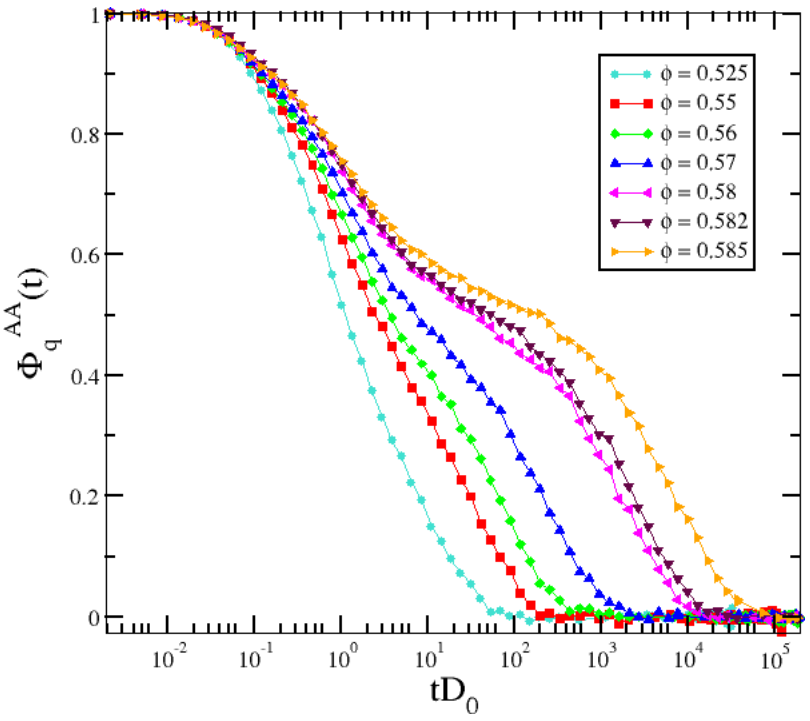

Figure 2.17: The behavior of density autocorrelation functions $\Phi_q^{AA}(t)$ with scaled time tD_0 has been shown at a fixed $T = 0.5$, with increasing packing fraction ϕ.

higher order singularity. All the analysis for A_3^H singularity does not give a clear picture of its presence. Indeed, also in this case, we observe subdiffusive regime and logarithmic dynamics centered around a similar value of q^*. Also in this case, the interference of the liquid-glass line does not allow us to probe the anomalous time window for a significant amount of time. To shed light on this point, simulations need to be performed for a system with a larger Δ where the glass-glass line merges with the liquid-glass line so that the anomalous dynamics can be approached in equilibrium.

The behaviour of the MSD, of $\Phi_q(t)$ with q not very close to the singularity, the estimate of q^*, and finally also the approach to the liquid-glass

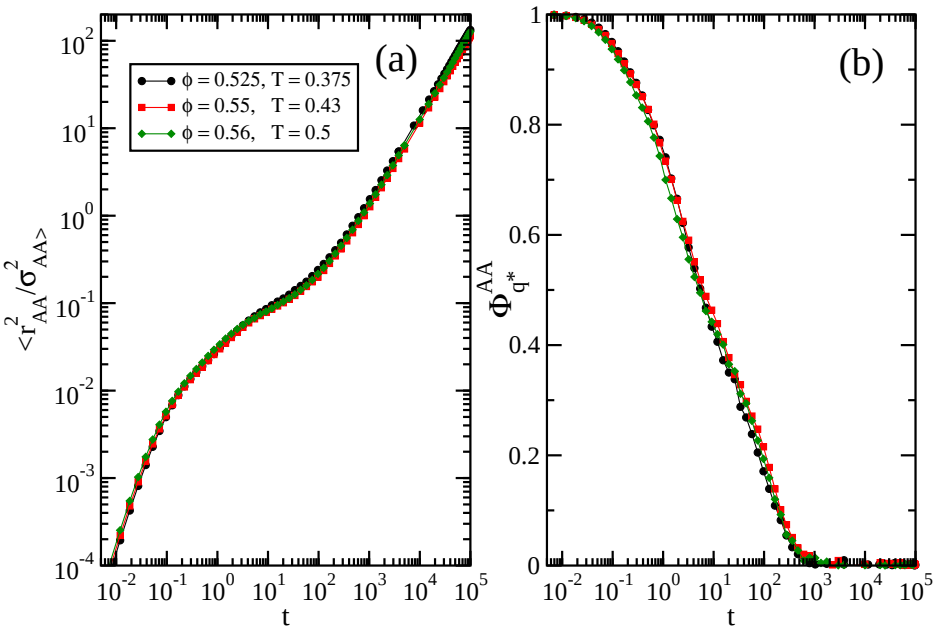

Figure 2.18: (a) MSD and (b) $\Phi_q(t)$ calculated for $q = q^*$ for three state points, indicated in the labels, which are located on the so-called line of invariant dynamics (see Fig. 2.12).

transition, all these features appear to be *indistinguishable* from the previous case. This is shown in Fig. 2.18 where the MSD and $\Phi_q(t)$ at the same $q^*\sigma_{AA} \sim 7.5$ are reported for state points not too far to the liquid glass transition, but pointing to approach the two singularities. This result seems to suggest that the correlators do not vary across the glass-glass transition or may be they change following a non-monotonic variation as suggested by the MCT results for the non-ergodicity parameters.

To discriminate between these two scenarios, we report in Fig. 2.18 also the corresponding dynamical functions for a state point with the same long-time dynamics (e.g. D/D_0) but close to the middle (rather than endpoints) of the putative glass-glass line. We find that also the MSD and $\Phi_q(t)$ for

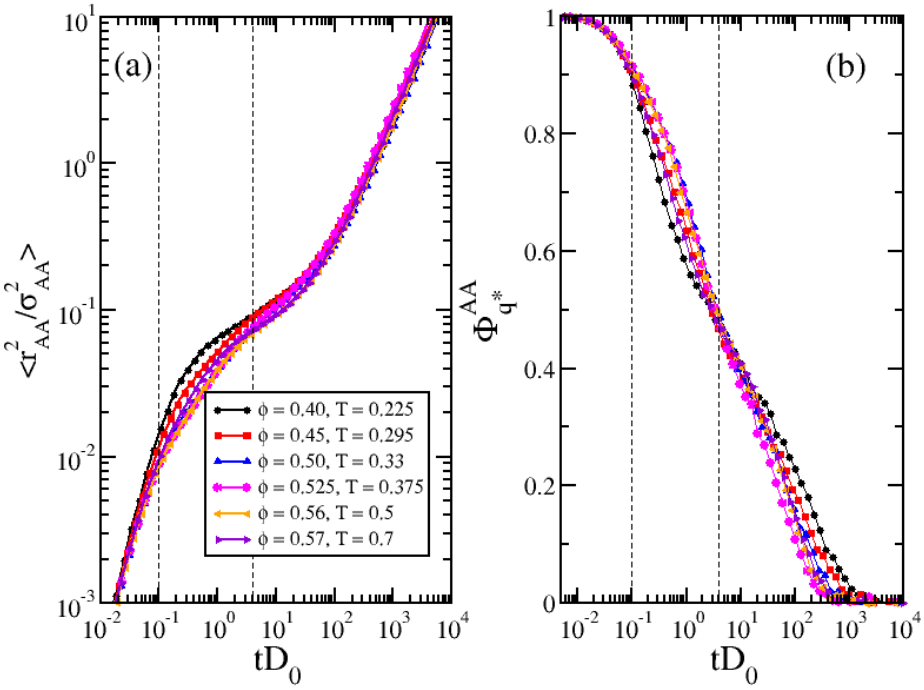

Figure 2.19: (a) MSD and (b) $\Phi_q(t)$ for $q = q^*$ for state points indicated in the labels, along an isodiffusivity line with $D/D_0 \sim 10^{-4}$ corresponding to the line of invariant dynamics (see Fig. 2.12). The vertical lines marks the boundary of the 'anomalous' time window, i.e. where subdiffusive behaviour is present close the singularities.

this state point actually coincide (within our numerical resolution) with the other two. This seems to exclude a non-monotonic variation of the non-ergodicity parameters associated to glass-glass line as predicted by the theory. Rather, and unexpectedly, we find that the influence of the glass-glass line on the dynamics, sufficiently far from any liquid-glass transition, does not depend on the particular position of the state points along the glass-glass transition and that a similar anomalous dynamics is observed independently of whether one approaches precisely the endpoints, i.e. the predicted higher

order singularities, or another point in between them along the glass-glass line.

We next investigate whether the two endpoints, not having any distinctive feature with respect to other points along the glass-glass line, do really exist. In other words we also want to explore where the glass-glass line terminates on both sides. A way to clarify this point is to look along the isodiffusivity line associated to the invariant dynamics discussed above and to compare MSD and $\Phi_q(t)$ even beyond the glass-glass line boundaries. The results of these comparisons are shown in Fig. 2.19. It can be clearly seen, within our numerical accuracy, that for ϕ outside the range of the glass-glass line boundaries we lose the invariant character of the dynamic observables, in particular in the 'anomalous' time window ($0.1 \lesssim tD_0 \lesssim 4$). Indeed, the subdiffusive behaviour gets curved (i.e. losing the power-law behaviour) as we go to either low or high ϕ. The deviations are more evident, as expected, when the system becomes more far from the glass-glass line. These results clearly point to a specific feature associated to the predicted glass-glass line, i.e. the invariant dynamics, which, to our knowledge, was not predicted or could be identified by MCT predictions. However, even if we do not find evidence of what should be an intrinsic characteristics of the higher-order singularities, i.e. an *enhanced* and *extended in time* logarithmic/subdiffusive dynamics, we do find that the two endpoints mark the boundaries of the glass-glass line. However, to *all* of this line seems to be associated the *same* and *equally extended in time* logarithmic/subdiffusive dynamics.

At present we cannot judge whether this effect is a limitation of our numerical accuracy, given to the significant distance to the glass-glass line

and to the interplay of the liquid-glass transition. To shed light on this point, simulations should be performed for a system with a larger Δ where the glass-glass line merges with the liquid-glass line and the anomalous dynamics can be approached in equilibrium. This investigation is beyond the scope of the present work.

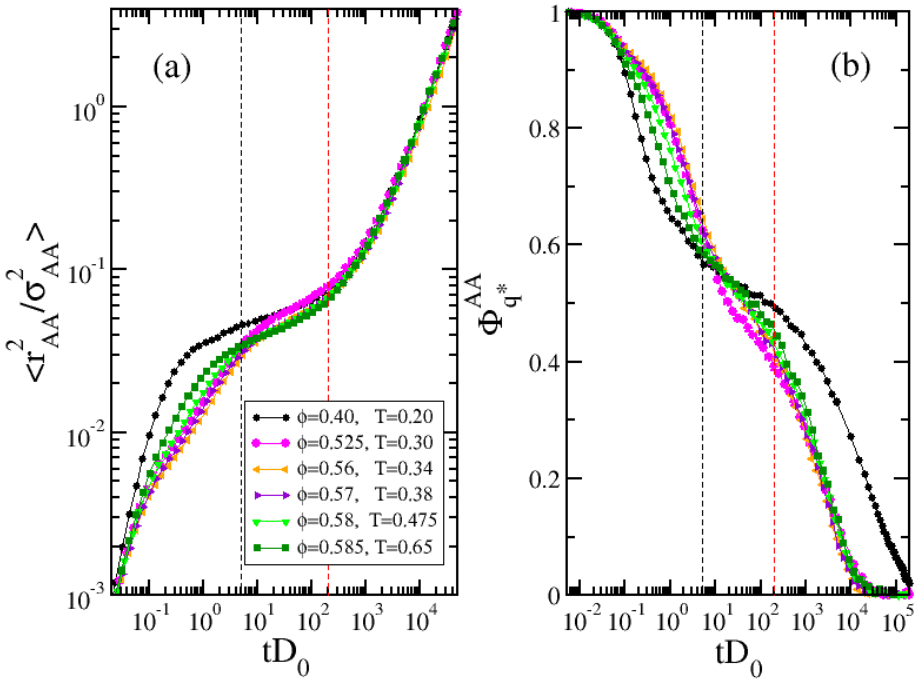

Figure 2.20: (a) MSD and (b) $\Phi_q(t)$ calculated for $q = q^*$ for state points indicated in the labels, having $D/D_0 \sim 4 \times 10^{-6}$. The vertical lines mark the boundaries between anomalous and standard two-step regimes.

Finally we try to approach the liquid-glass ideal line. To do this, we move again along an iso-diffusivity line to address the interference between two-step and logarithmic dynamics. We show in Fig. 2.20 the MSD and $\Phi_q(t)$ for very slow state points, for which $D/D_0 \sim 4 \times 10^{-6}$, in which we can detect both 'anomalous' (for $tD_0 \lesssim 5$) and standard two-step dynamics (for

$5 \lesssim tD_0 \lesssim 200$). Concerning the first regime, we substantially find confirmation of the previous observations where the two-step dynamics was not yet observed. A non-monotonic dependence of $\langle r^2 \rangle$ as well as $\Phi_q(t)$ is found in the anomalous time window. Again, a subdiffusive behaviour is visible only for packing fractions value close enough to the glass-glass line. Compared to the previous data more far from the liquid-glass transition, the extension of the subdiffusive window is minor (as it can be clearly seen focusing on a single isochore in Fig.s 2.13 and 2.14). We cannot judge at present whether this is a limitation of our numerical accuracy, given to the significant distance to the glass-glass line and to the interplay of the liquid-glass transition. To shed light on this point, simulations should be performed close to a even higher-order singularity, i.e. the A_4 rather than A_3 point, where the anomalous dynamics can be approached in equilibrium. This amounts to performing simulations (and MCT calculations) at a different value of Δ and is beyond the scope of the present work.

Focusing on the long-time dynamics, we observe that the plateau height of the MSD seems to decrease monotonically, while the height of the plateau in $\Phi_q(t)$ shows a non-monotonic trend. This will be discussed in more detail in the next paragraph where we will report the results for the non-ergodicity parameters from the simulations. Another dramatic effect is visible: the low ϕ data (e.g. $\phi = 0.40$) although belonging to the same iso-D/D_0 line show a huge increase in the α-relaxation time: a clear manifestation of the breakdown of the Stokes-Einstein relation. This is commonly observed in glass-forming systems, approaching the glass transition. The amount of deviation is often interpreted in terms of dynamic heterogeneity of the system.

We observe this effect being more pronounced at low/intermediate ϕ and low T, where the effect of *both* length scales is active, probably giving rise to a system which is more heterogeneous. A systematic investigation of these effects has been described in next Chapter.

2.3.5 Non-ergodicity parameters from MCT and simulations

In this section, we show the behaviour of the non-ergodicity parameters calculated within MCT and extracted from the fits of the density auto-correlation functi

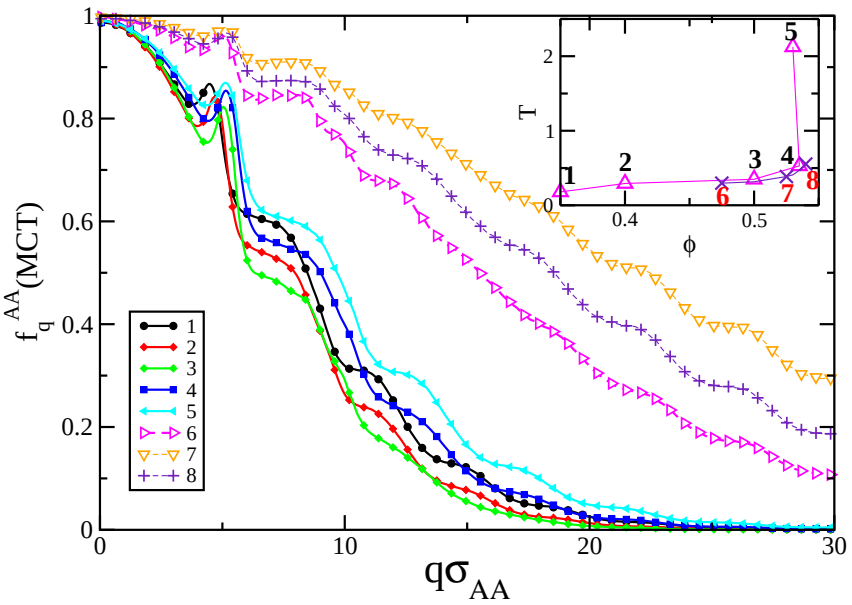

Figure 2.21: Critical non-ergodicity parameters for the A species calculated within MCT along the liquid-glass (curves labeled from 1 to 5) and along the glass-glass (curves labeled from 6 to 8) lines. The corresponding state points and their position on the MCT lines are reported in the inset: a non-monotonic behaviour with increasing ϕ is observed for both sets of data.

We start by showing in Fig. 2.21 the 'critical' non-ergodicity parameters $f_q^{AA}(MCT)$ for the A species along the liquid-glass and the glass-glass lines, calculated within MCT. The state points at which $f_q^{AA}(MCT)$ are evaluated are shown and numbered in the inset of Fig. 2.21. We find that along the liquid-glass line the theoretical $f_q^{AA}(MCT)$ follows two different types of behaviour: for $\phi \leq 0.50$, $f_q^{AA}(MCT)$ at first decreases, showing a shift of the peaks to larger wave vectors (from state point 1 to 3), while for $\phi > 0.50$ at all temperatures —below and above the reentrance— $f_q^{AA}(MCT)$ maintains its peaks and only grows around them in a continuous way (from state point 3 to 5). We note that the $f_q^{AA}(MCT)$ of the lowest and highest T (states 1 and 5) corresponds to two glasses made, respectively, by effective hard spheres of diameter $\sigma + \Delta$ and hard spheres of diameter σ. It follows that the two $f_q^{AA}(MCT)$ can be superimposed on top of each other by simply readjusting the diameters. In between these two limits, the system experiences the competition between the two length scales, which results in a non-trivial and non-monotonic behaviour of the non-ergodicity parameters. The crossover between the two regimes arises in a region that cannot be associated with any of the two higher order singularities.

Furthermore, we also show in Fig. 2.21 the evolution of $f_q^{AA}(MCT)$'s for the 'disconnected' glass, occurring upon crossing the glass-glass line. In this case the non-ergodicity parameters are much larger and longer-ranged in q, indicating more tightly-caged glasses, in analogy with previous observations of repulsive glasses for star polymer mixtures [30]. In the present case, the cage size is approximately one half of that of the first glass, as it can be estimated by the q-range of the non-ergodicity parameters. We observe a

non-monotonic behaviour when moving along the glass-glass line from low to high density, similarly to what observed for the liquid-glass line.

We now extract the non-ergodicity parameters by fitting the density auto-correlation functions close to the arrest line via the stretched exponential of Eq. (1.6). For simplicity, again we focus only on species A, since the results are formally identical for both species. We show in Fig. 2.22 the behaviour of f_q^{AA} along the liquid-glass line (for the state points labeled in the upper inset). We find a behaviour that is remarkably similar to the MCT predictions. Indeed, again we find that the non-ergodicity parameter shows a non-monotonic behaviour (at fixed q) with increasing ϕ. While at low ϕ and low T, f_q^{AA} is compatible with that of a HS with effective diameter $\sigma + \Delta$, it decreases at first with a shift of the peaks at larger q for intermediate densities. Then at a certain point, that we can roughly estimate as $\phi \approx 0.50$, the peaks do not move further in q while f_q^{AA} starts to increase in magnitude. This continues until it behaves as the f_q typical for HS of diameter σ. This interpretation is reinforced by the fact that we can perfectly scale the low-ϕ f_q^{AA} on top of the high ϕ-one by simply scaling it for the effective diameter (see lower inset). In addition, the behaviour of the stretching exponents obtained from the fits seems to indicate an increase of β^{AA} as the system moves along the liquid-glass line with increasing ϕ. Hence glasses found at lower T are considerably more stretched ($\beta^{AA} \lesssim 0.4$) than those found at higher ϕ.

Finally we could not estimate numerically the non-ergodicity parameters close the disconnected glass-glass transition, due to the fact that this is buried inside the glass phase. Hence, we do not have a numerical analogue of curves

(6-8) in Fig. 2.21.

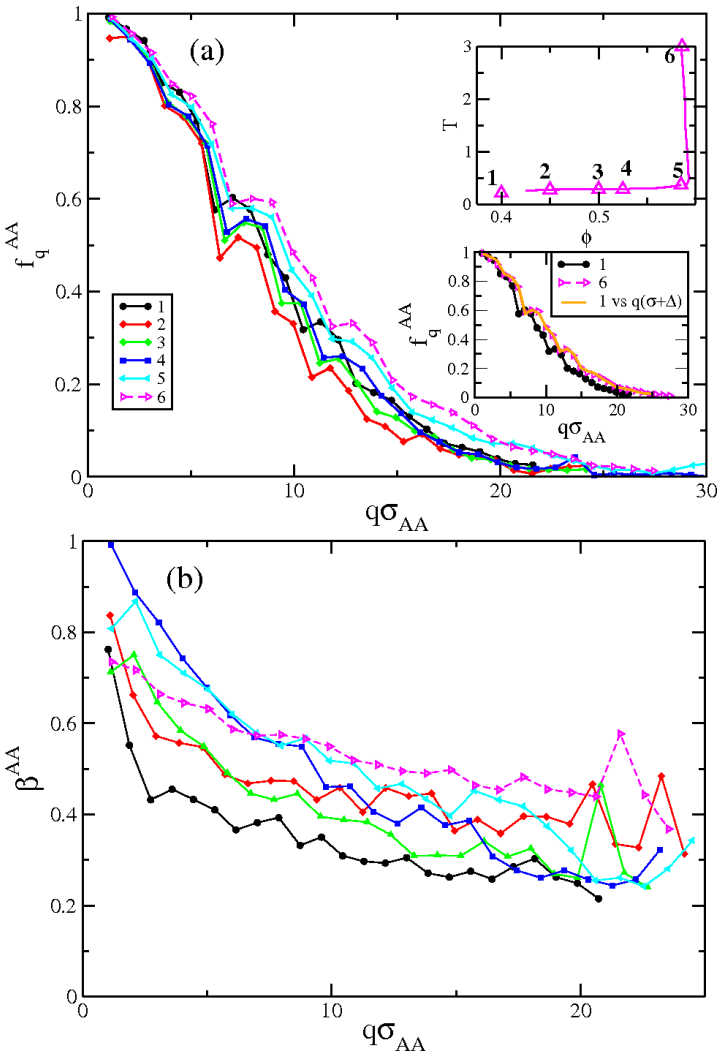

Figure 2.22: (a): Non-ergodicity parameters obtained from simulations, fitting the density auto-correlation functions with stretched exponential, for the state points reported in the upper inset. The behaviour along the liquid-glass line is strikingly similar to that of MCT predictions, reported in Fig. 2.21. Lower inset: f_q^{AA} for low ϕ (and low T) (state point 1) is identical to that of high ϕ (state point 6) upon a rescaling by the effective diameter $\sigma + \Delta$; (b) Stretching exponents β^{AA} obtained from the fits as a function of wave vector for the same state points considered in (a).

Chapter 3

Signature of Higher-order singularity driving new invariant dynamics in Square Shoulder System

3.1 Introduction

In Chapter 2, we investigated the dynamical phase diagram for $\Delta = 0.15$, where we observe two A_3 higher order singularities buried inside the glassy regime. We detect their position indirectly from the equilibrium phase. Now, we aim to approach the A_4 singularity in the liquid phase. Therefore we begin the simulation for $\Delta = 0.17$ and investigated the phase diagram. During all these analysis, we also found an unexpected invariant dynamics which has not been observed in any other systems before. In this Chapter, we will

discuss the results for $\Delta = 0.17$ and also give a detail description of the novel invariant dynamics and associated dynamical properties.

Recent work on the Square Well (SW) system revealed the existence of A_4 singularity in a three dimensional control parameter space [47]. The model system has particles interacting through a hard-core repulsion complemented by a short-range attractive well width with a few percent of the particles diameter. The MCT glass-transition scenarios have been worked out for the SW system [11] using Percus-Yevick (PY) approximation. There exists a characteristic well width Δ for the SW system which controls the position of higher order singularities in ϕ, Γ, Δ parameter plane, where $\Gamma = u_0/k_BT$.

In Sec. 1.2, we have given a brief description of higher order singularities. Close to the higher order singularity the density autocorrelation function suffers a bifurcation in the solution. In HS system, the system is driven by one control parameter ϕ, which brings A_2 point. The nonergodocity parameter $f_q = 0$ (see for more details in Sec. 1.2) is the only solution which is liquid state. In SW system, for a certain value of square well width Δ much smaller than the hard-core diameter, the MCT predicts a reentrant behavior of the liquid-glass line along with a glass-glass line which terminates with A_3 singularity in the temperature T and density ϕ phase diagram. The nonergodicity parameter $f_q > 0$ has two finite solutions f_1^G and f_2^G which characterize two different glasses. Moving around A_3 singularity, the values of f_q changes continuously. With a small increase in the well width Δ, the glass-line with A_3 point starts to shrink and makes A_4 singularity to appear in the liquid phase. A_4 singularity appears at a special point (ϕ^*, T^*, Δ^*) in the liquid phase. At A_4 singularity, f_q exhibits more than two solutions. Apparently,

at A_4, there is coalescence of three glassy solutions; f_1^G, f_2^G and f_3^G. When we pass through the glass-line, the value of nonergodicity parameter changes discontinuously. For $\Delta < \Delta^*$, the SW system always exhibits a glass-glass transition line with A_3 singularity as endpoints where as, for $\Delta > \Delta^*$, there is no cusp singularity. The morphology of these singularities is accompanied by logarithmic variations of density auto-correlation functions as a function of time and subdiffusive behavior of the MSD. MCT has also predicted the diffusion anomalies (diffusion maxima or minima) along the liquid-glass line.

In comparison to our simulation study for SS system, we observe a disconnected glass-glass transition line terminating with two A_3 higher order singularities for $\Delta = 0.15$, the similar case for theoretical observation at $\Delta = 0.13$. With increasing Δ, the glass-glass line moves and merges with the liquid-glass line which brings the A_4 singularity on the liquid-glass transition in equilibrium phase as predicted from theory. The theoretical calculations has been done for $\Delta = 0.17$. The phase diagram shows the reentrance with A_3 and A_4 singularities. So, we begin with simulations for $\Delta = 0.17$ aiming to locate the A_4 higher order singularity in liquid phase.

In this Chapter, we mostly concentrate on the numerical results for $\Delta = 0.17$. We have divided the Chapter in few sections and subsections, which will give a systematic view of the analysis and results we have obtained. In Sec. 3.2, we discuss the dynamics of the SS system in the phase diagram. This section has been divided into five subsections; In Sec. 3.2.1, we discuss the behavior of diffusivity with T and ϕ and extrapolated several isodiffusivity lines in the dynamical phase diagram. Sec. 3.2.2 describes the power-law fits and extracted glass line. In Sec. 3.2.3, we discuss about the MCT calculated

liquid-glass line and the mapping with glass line. In Sec. 3.2.4 and Sec. 3.2.5, we give a detailed analysis of higher order singularities and the behavior of nonergodicity parameters along the liquid-glass line. At the end, in Sec. 3.3, we describe the invariant dynamics followed by two subsections: Sec. 3.3.1,in which we discuss the variation of dynamical properties in a close approach to the liquid-glass line, whereby we identify an invariant dynamics behavour; Sec. 3.3.2, in which we verify the dynamical properties beyond the invariant line.

3.2 Results for $\Delta = 0.17$

We study a 50 : 50 mixture of $N = 2000$ particles of species A and B interacting via pairwise SS potential

$$V_{ij}(r) = \begin{cases} \infty, & r < \sigma_{ij} \\ u_0, & \sigma_{ij} \leq r < (1+\Delta)\sigma_{ij} \\ 0, & r \geq (1+\Delta)\sigma_{ij}, \end{cases} \tag{3.1}$$

where $i, j = A, B$, σ_{AA} and σ_{BB} are the particles diameters. We have used the same reduced units same as to $\Delta = 0.15$. We perform event-driven MD simulations of the system as a function of T and packing fraction ϕ. We use the same simulations techniques as for $\Delta = 0.15$ and performed in the canonical and microcanonical ensemble. A detail description about the simulation techniques will be found in Appendix A.

3.2.1 Diffusivity and isodiffusivity lines

We perform a systematic investigation of the dependency of diffusivity on temperature T and packing fraction ϕ. The normalized diffusivity D/D_0 is plotted with respect to ϕ in Fig. 3.1. We present the diffusivity data for temperature varying between 2.0 and 0.235 for a properly equilibrated system. Moving from high to low ϕ, for all the values of temperature T, the diffusivity increases monotonically. We do not observe any non-monotonic behavior of the diffusivity along isotherms.

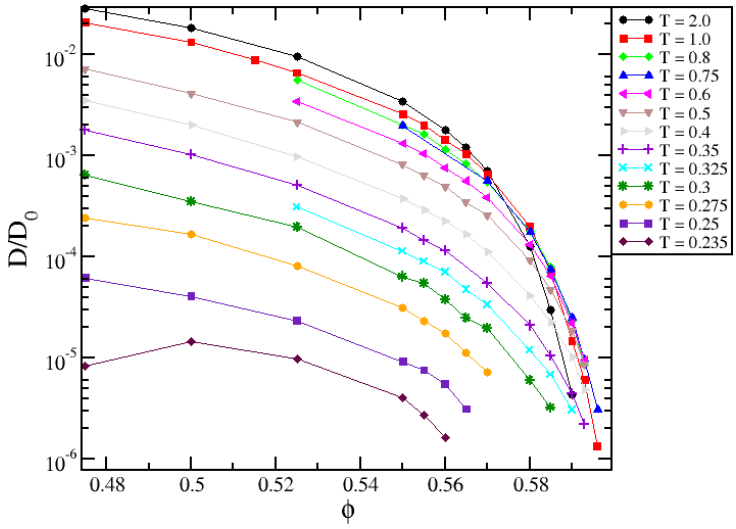

Figure 3.1: Normalized diffusion coefficient D_A/D_0 as a function of ϕ for several isotherms, as reported in the labels. At all investigated T data show a monotonic decrease with increasing ϕ, which clearly indicates the absence of diffusion anomaly associated to compression/expansion.

Fig. 3.2, shows the dependence of D/D_0 with T for different ϕ values varying between 0.45 and 0.596. The normalized diffusion coefficient D/D_0 shows a monotonic to the transition in the behavior of the diffusivity for $\phi \leqslant 0.57$. By moving along isochores, with increasing ϕ values, the diffusivity starts

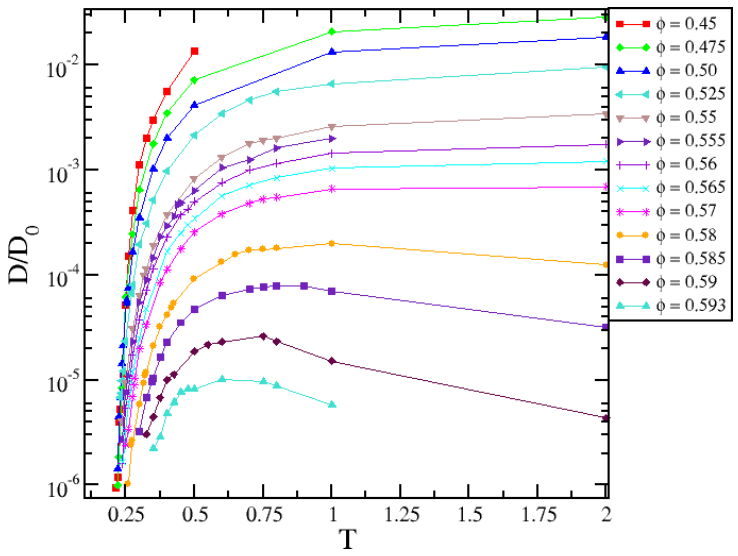

Figure 3.2: Normalized diffusion coefficient D_A/D_0 as a function of T for several isochores, as reported in the labels. The normalized diffusion coefficient shows a nonmonotonic behavior in terms of a peak along large iscohores. This indicates the presence of diffusion anomaly due to cooling.

to show a non-monotonic behavior with T. Such variation is highlighted by the presence of maximum in diffusivity at $T \sim 0.75$ for $\phi > 0.58$. A similar diffusivity maxima has already been discussed in Chapter 2 for $\Delta = 0.15$.

Using the data set of D/D_0 along isotherms (Fig. 3.1) and isochores (Fig. 3.2), we are able to build isodiffusivity lines and plot them in (ϕ, T) plane. The extracted normalized isodiffusivity curves are shown in Fig. 3.3.

The isodiffusivity lines are precursors of the ideal liquid-glass line. We measure the normalized isodiffusivity lines for three fixed values of normalized diffusion coefficient: $D_A/D_0 = 1.0\times10^{-3}, 1.0\times10^{-4}$ and 1.1×10^{-5}. Moreover, we verify the presence of the reentrances by selecting the lowest normalized isodiffusivity line $D_A/D_0 = 10^{-5}$. The reentrance is only observed along T due to cooling with the appearance of a non-monotonic behavior of D_A/D_0

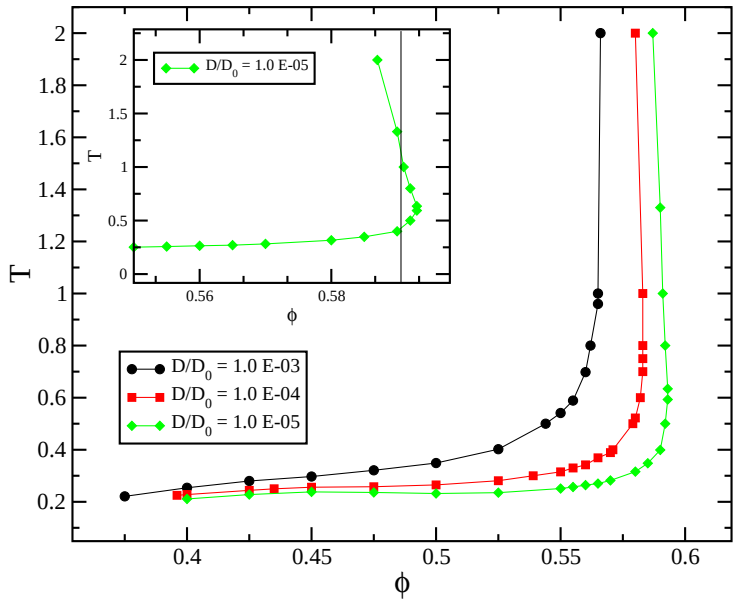

Figure 3.3: Isodiffusivity lines for $D_A/D_0 = 1.0 \times 10^{-3}, 1.0 \times 10^{-4}$ and 1.1×10^{-5}, extrapolated from the diffusivity plots in Fig. 3.1 and Fig. 3.2 along isotherms and isochores respectively. The reentrance is observed along T as displayed in the inset with a vertical line.

along isochores in Fig. 3.2.

3.2.2 Glass line

We are now interested in extrapolating the arrested line (i.e. the isodiffusivity line with $D_A/D_0 \to 0$) by performing a power-law fit of diffusivity along isochores and isotherms following the diffusivity equations Eq. (2.2) and Eq. (2.3). We fit our data for the temperatures varying between $T = 2.0$ and 0.3. We have not performed any fitting below $T = 0.3$ due to the deviation from power-law behavior. The power-law fits are shown in Fig. 3.4. We select the fitting range of diffusivity between 10^{-2} to 10^{-5} for $T \geqslant 0.75$ as shown in Fig. 3.4 (a). In the limit of diffusion $D_A \to 0$, we extracted the arrested

packing fraction ϕ_g along each isotherms. The resulting straight lines in Fig. 3.1 (b) show a systematic variation in diffusivity.

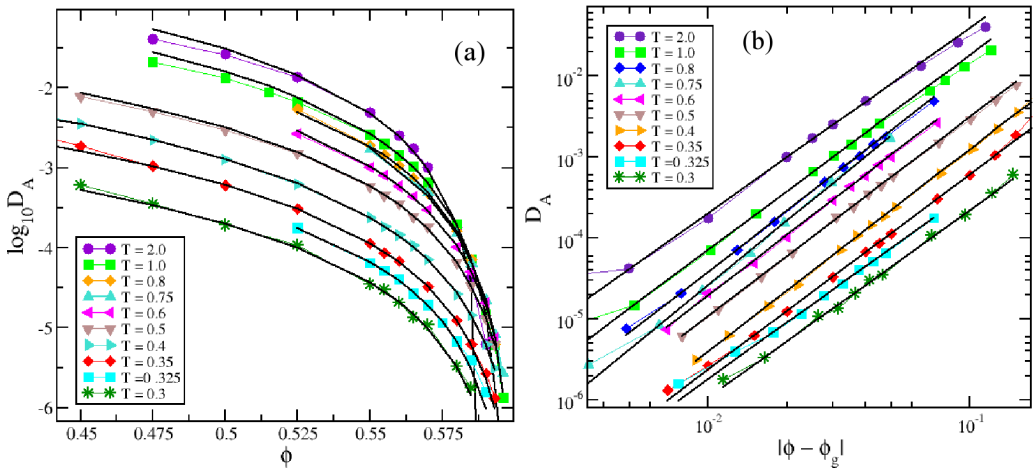

Figure 3.4: The power-law fit of diffusivity along isotherms for a set of temperatures $T = 2.0, 1.0, 0.8, 0.75, 0.6, 0.5, 0.4, 0.375, 0.35, 0.325$ and 0.3 and (a) extracted glass transition packing fraction ϕ_g in log scale shows a very good fitting (b) The diffusivity data put in log-log scale by rescaling x-axis with arrested packing fraction ϕ_g

The extracted value of ϕ_g and the corresponding exponent parameters γ are listed in Table 4.5. The value of exponent γ is roughly constant within error bars.

Similarly, we also extract the arrested temperature T_g by performing a power-law fit of D_A for each isochores varying between $\phi = 0.45$ and $\phi = 0.59$ as shown in Fig. 3.5 (a). When we put the diffusivity vs T plot in log-log scale, we always find a crossover for the isochores between 0.56 and 0.59.

We list the resulting values of T_g with their corresponding exponent parameter $\gamma(\phi)$ in Table 3.2. The value of γ shows a systematic increase with increasing ϕ and then starts to drop at $\phi = 0.55$. The variation in γ remains

T	$\gamma(T)$	ϕ_g
2.0	2.28	0.58
1.0	2.4	0.59
0.8	2.5	0.59
0.75	2.64	0.59
0.6	2.48	0.59
0.5	2.46	0.6
0.4	2.49	0.60
0.35	2.41	0.59
0.325	2.31	0.59
0.3	2.31	0.59

Table 3.1: Extrapolated values of $\gamma(T)$ and ϕ_g obtained from fitting data of Fig. 3.1 (a) with MCT predictions of Eq. (2.3), for the diffusion coefficient D_A. Error bars of the fit parameters typically amount to a few percent for the values of ϕ_g, while the γ exponents can vary systematically over different fit intervals, so they should be taken with caution.

same even we change the range of power-law fit.

The extracted ideal glass line is presented together with isodiffusivity lines in Fig. 3.6. The two branches of the glass line meet in the low T and high ϕ region of the phase diagram. On comparing the isodiffusivity lines with the extrapolated ideal glass line, the shape of the curves are in very good agreement with each other. This agreement confirms the reentrance along T. The observation of reentrant behavior due to cooling from our simulation study for $\Delta = 0.17$ is in agreement with the MCT results for $\Delta = 0.15$ [51]. When we change the range of the fitting, we could observe the subsequent variation in the exponent γ. Nonetheless, the values of ϕ_g and T_g extracted in the same way show only a little changes (of the order of a few percent), and hence they are robust. The overall shape of the ideal glass line remains same in the phase diagram.

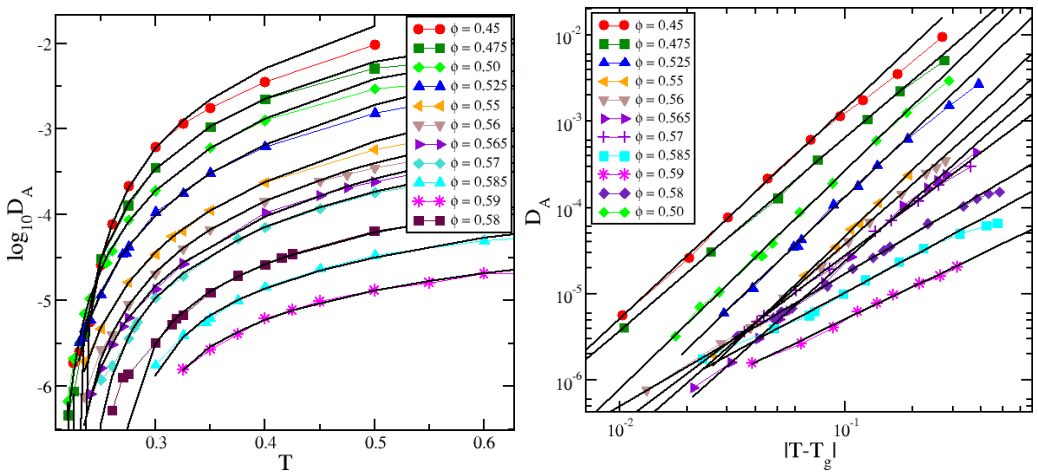

Figure 3.5: The power-law fit of diffusivity along isochores for a set of packing fractions $\phi = 0.45, 0.475, 0.50, 0.525, 0.55, 0.56, 0.565, 0.57, 0.58, 0.585$ and 0.59 and (a) extracted glass transition temperature T_g in log scale shows a very good fitting. (b) The diffusivity data put in log-log scale by rescaling x-axis with T_g

3.2.3 Mapping of MCT line and glass line

In our previous work for $\Delta = 0.15$, the revised MCT calculations using binary simulation predicted the liquid-glass along with the glass-glass line. The better understanding of the dynamical phase diagram is obtained from the comparison of simulation MCT liquid-glass line with glass line. MCT predictions suffer from a shift in the control parameter. Therefore, to locate the higher order singularities we perform a bilinear transformation in ϕ and T. Following the traditional way of mapping [47], we compare the MCT line with arrested line as we did for $\Delta = 0.15$. So, we do the MCT calculations for $\Delta = 0.17$ by giving as input the static structure factor S_q^{SIM} evaluated from numerical simulations. We solve the generalized version of long-time MCT equations (Eq. (1.3)) for a binary mixture [23] on a discretised grid of

ϕ	$\gamma(\phi)$	T_g
0.45	2.43	0.22
0.475	2.23	0.22
0.50	2.52	0.21
0.525	2.51	0.21
0.55	2.55	0.20
0.56	2.3	0.22
0.565	2.32	0.21
0.57	1.96	0.23
0.58	1.53	0.26
0.585	1.4	0.27
0.59	1.25	0.28

Table 3.2: Extrapolated values of $\gamma(\phi)$ and T_g obtained from fitting data of Fig. 3.2 (a) with MCT predictions of Eq. (2.2, for the diffusion coefficient D_A. Error bars of the fit parameters typically amount to a few percent for the values of T_g, while the γ exponents can vary systematically over different fit intervals, so they should be taken with caution.

1000 wave vectors up to a cut-off value of $q\sigma_{BB} = 65$. A detailed description of the simulation MCT calculation for liquid-glass line has been described in Chapter 2. We evaluate the critical non-ergodicity parameters along the liquid-glass line and the glass-glass line. Moreover, our calculations show the presence of an A_3 and A_4 singularities.

The MCT liquid-glass is reported together with the glass line (arrest line) evaluated from power-law fits in Fig. 3.7. The curve with red filled squares represents the MCT liquid-glass line and curve with red open squares represents the MCT glass-glass line joining two higher order singularities. This glass-glass line is not completely disconnected, whose one end is extended to lower T and ends in an A_3 singularity while the other end meets with the liquid-glass line at A_4 higher order singularity. The green filled triangle is

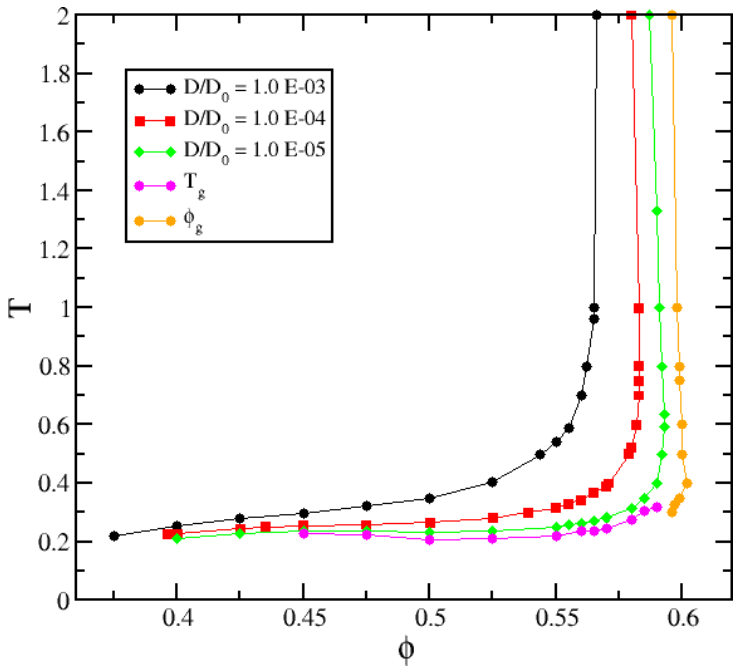

Figure 3.6: The extrapolated arrested ($D \to 0$) glass lines from the fits $D_A\ |\phi - \phi_g(T)|^{\gamma(T)}$ along isotherms and $D_A\ |T - T_g(\phi)|^{\gamma(\phi)}$ along isochores as shown in Figs. 3.1 and 3.2. The glass line shows a very good agreement with isodiffusivity lines confirming the presence of reentrance in T as well as in ϕ.

the A_3 singularity while the blue filled triangle corresponds to the A_4 singularity in high T region. The filled circles represent two branches of glass line. MCT always suffers for a small shift in the control parameters, but the shape of the resulting MCT liquid-glass line shows a qualitative agreement with the shape of the glass line. In order to make a one to one comparison, we superimpose the MCT liquid-glass together with the glass-glass line onto

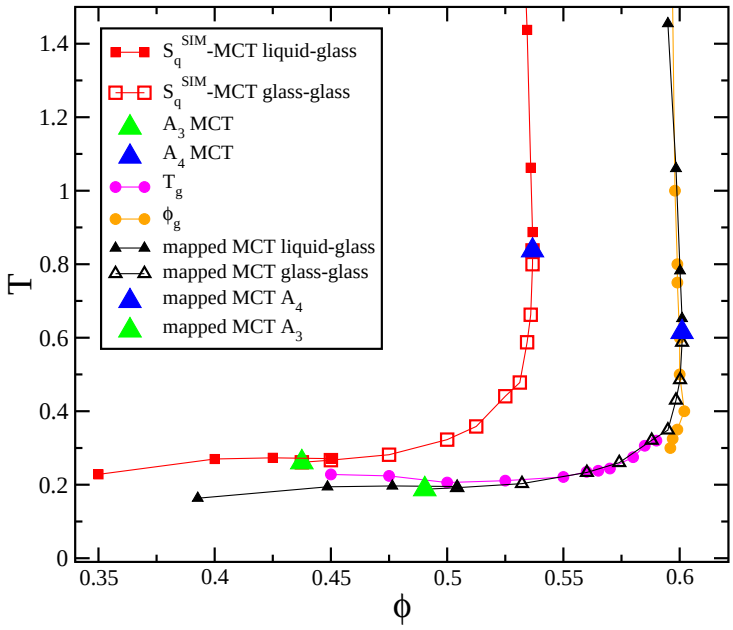

Figure 3.7: MCT results for the binary mixture under study using the static structure factors calculated from simulations as input, labeled as $S_q^{SIM} - MCT$ liquid glass (filled squares) and glass-glass (open squares). Arrest curve drawn from ϕ_g (filled circles) and T_g (filled diamonds) obtained from power-law fits of D_A as in Fig. 2.6. Mapped MCT lines onto the arrest curve: liquid-glass (filled triangles) and glass-glass (open triangles). Stars are the two predicted higher order singularities A_3^L and A_4.

the arrest line with the following bilinear transformation in ϕ and T

$$\begin{aligned} \phi &\rightarrow 1.115668\phi + 0.0135, \\ T &\rightarrow 0.741929T + 0.0061 \end{aligned} \tag{3.2}$$

The mapping shows a very good overlap at the meeting of two arrest lines and in the high temperature region i.e. repulsive driven HS glass as shown in Fig. 3.7. There is a small discrepancy in the low packing fraction limit i.e. the effective HS limit which is also observed in case of $\Delta = 0.15$. The

super position of the theoretical and numerical curves allows us to investigate the presence of the two higher order singularities which should be located at $A_3 = (\phi \sim 0.49, T \sim 0.187)$ and $A_4 = (\phi \sim 0.60, T \sim 0.615)$. A_4 is on the liquid-glass line while A_3 is very close to the liquid-glass transition with a distance $\Delta T \sim 0.02$ along an isochore.

3.2.4 Searching for Higher order singularities

The existence of higher order singularities is ascertained by means of the dynamical properties; subdiffusive behavior in MSD and logarithmic decay in density autocorrelation functions. These properties are well predicted from MCT and we have discussed about these properties in section 1.1.4. On approaching more closely to the higher order singularity, the density autocorrelation function shows more logarithmic behavior. One can trace the position of A_4 singularity in equilibrium phase as it lies in liquid phase; on the contrary the influence of A_3 can only be observed indirectly as it lies inside the glassy regime. From our simulation study, we start to locate the position of A_3 and A_4 higher order singularities by moving along a fixed isochore and isotherm respectively in the phase diagram.

In a close approach to the estimated position of A_3 singularity, we monitor the isochore $\phi = 0.50$ and plot MSD for a set of temperatures T varying between 0.4 and 0.225 as shown in Fig. 3.8. On lowering the temperature, the system starts to show slow dynamics and for $T < 0.3$, the system displays a characteristic subdiffusive behavior at the intermediate times which signals the presence of a higher order singularity as already observed for $\Delta = 0.15$.

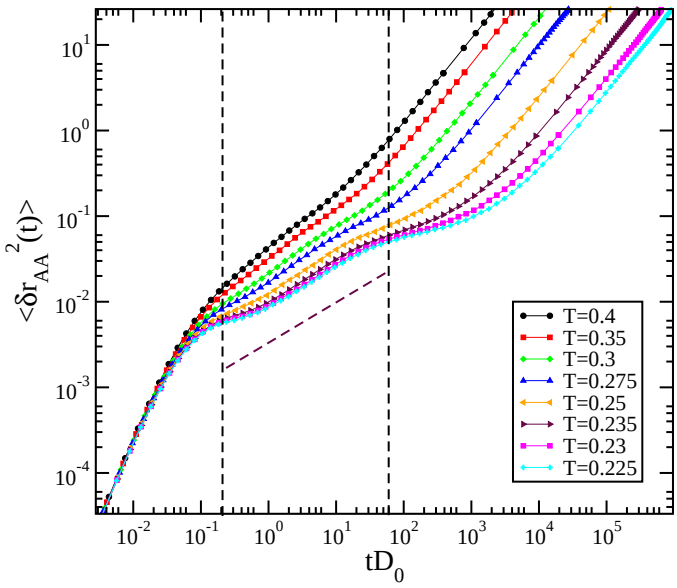

Figure 3.8: The data set of MSD at $\phi = 0.50$ for a set of temperatures $T = 0.4, 0.35, 0.3, 0.275, 0.25, 0.235, 0.23, 0.225$. There is a clear appearance of subdiffusive behavior marked with solid straight line with exponent $\alpha = 0.45$ at the intermediate time scale ($1 \leqslant tD_0 \leqslant 10^2$) on approaching the MCT predicted A_3 higher order singularity.

The subdiffusive region is more clear for $T = 0.235$. We observe a three-step behavior in MSD; the usual ballistic regime in the small time scale, then at intermediate time the particle gets caged by its neighboring particles and rattle inside the cage for a finite time. In this caged part, we could see the effect of two length scales in the SS system. After a finite time, the particle makes the path out of the cage and starts to show diffusive behavior as the system is in equilibrium. The subdiffusive behavior in MSD is marked with power-law fit with exponent $\alpha \sim 0.5$. This subdiffusivity is varying between $0.2 \leqslant tD_0 \leqslant 61.5$, with a plateau height of $0.06\sigma_{AA}^2$ that gives the localization length of $0.24\sigma_{AA}$. This localization length is very close to the value found for A_3 singularity for $\Delta = 0.15$. In order to give a more convincing proof to the

existence of A_3, we verify the logarithmic behavior in density-autocorrelation function.

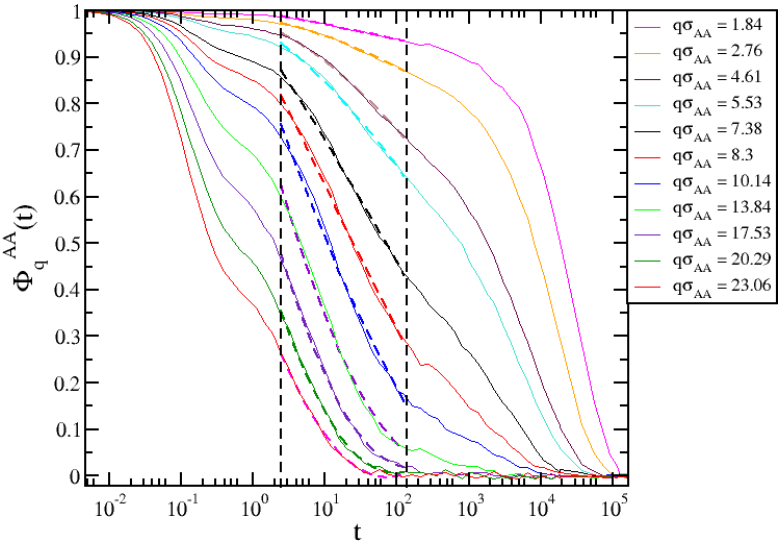

Figure 3.9: The density autocorrelation functions have been plotted for the state point $\phi = 0.50$ and $T = 0.235$ for several q vectors varying between 1.84 and 23.06. The fitting is followed by the asymptotic decay law given by Eq. (**??** at the intermediate time. The density auto correlation functions shows a logarithmic behavior in the fitting time window $4 \leqslant tD_0 \leqslant 10^2$ for $q\sigma_{AA} = 7.38, 8.3, 10.14$.

The fitting is done with general asymptotic decay law for the correlation function for a set of $q$vectors close to the higher order singularity as predicted from MCT

$$\Phi_q(t) \sim f_q + h_q^{(1)} ln(t/\tau) + h_q^{(2)} (ln(t/\tau))^2 \tag{3.3}$$

When the system approaches higher order singularity, $h_q^{(2)} \approx 0$ in Eq. ((3.3) for a specific value of $q$vector and a pure logarithmic behavior is observed in the density auto-correlation function for a critical value of $q$vector q^*. Above

and below this critical $q$vector q^*, the density correlation function creates a concave and convex shape. In order to observe all these behaviors, we fit the density autocorrelation functions to a quadratic polynomial in $\ln(t/\tau)$ for a set of $q$vectors $q\sigma_{AA} = 1.84, 2.76, 4.61, 5.53, 7.38, 8.3, 10.14, 13.84, 17.53, 20.29$ and 23.06. Fits are reported in Fig. 3.9 where the fitting time window extends about 2 decades. In Fig. 3.9, the density autocorrelation functions show a clear picture of logarithmic decay for $q\sigma_{AA} = 7.38$ in the time interval $10 \leqslant tD_0 \leqslant 10^2$ similar to those for MSD in Fig. 3.8. At this critical value of q^* the density autocorrelation functions show a transition from concave to convex shape. The range of logarithmic time window in density autocorrelation functions is similar to the time window of subdiffusive behavior in MSD.

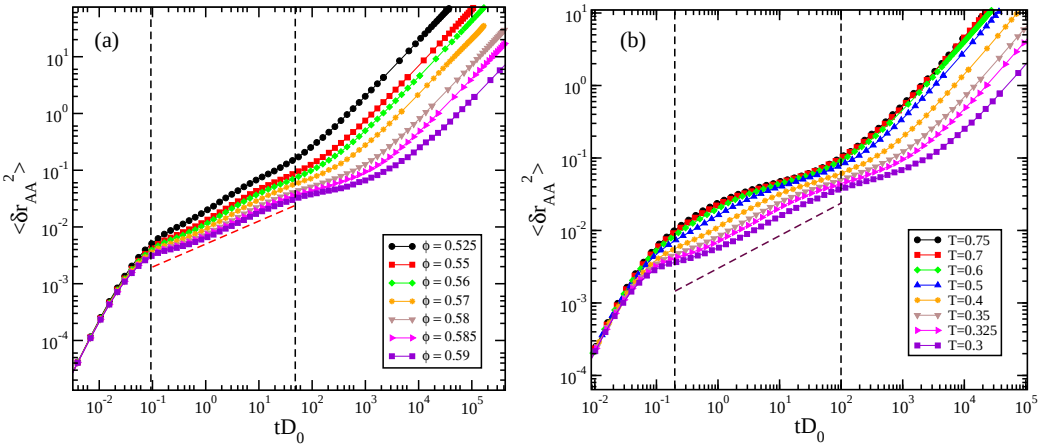

Figure 3.10: The presented data for MSD (a) along isotherm $T = 0.325$ with increasing ϕ shows a plateau of subdiffusivity at the intermediate time (tD_0) marked in thick (blue) line. (b) For $\phi = 0.585$, with decreasing T, the subdiffusivity becomes more prominent.

Next, we try to investigate the presence of A_4 singularity which is the only singularity accessible from liquid phase. The estimated position of A_4

singularity obtained within the scope of mapping of simulation MCT liquid-glass line with glass line in Fig. 3.7 is $A_4 = (\phi \sim 0.60, T \sim 0.615)$. In the limit of our simulation, we simulated the system up to $\phi = 0.60$ at the lowest $T = 0.4$. Initially, we monitor MSD along a set of isotherms close to A_4 and do not observe any subdiffusive behavior. When we go to the lowest $T = 0.325$, there is a clear visibility of subdiffusive behavior at $\phi = 0.585$ as shown in Fig. 3.10 (a). Then we follow the isochore $\phi = 0.585$ and plot MSD with lowering the temperature in Fig. 3.10 (b). We could see an appearance of subdiffusivity at $T = 0.325$ as we clarify from Fig. 3.10 (a).

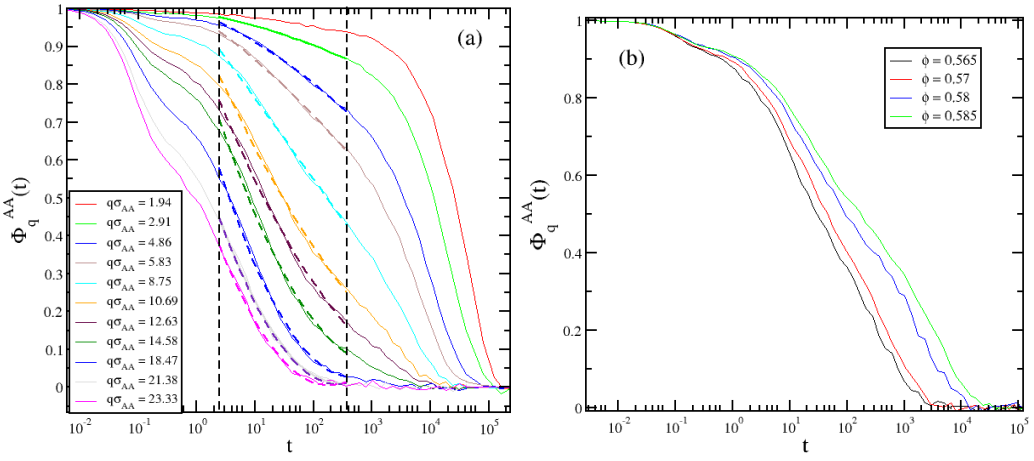

Figure 3.11: The density auto-correlation functions fitted with asymptotic decay law formula (a) at $\phi = 0.585, T = 0.325$ for a set of q vectors. The correlator has a logarithmic time window at $q\sigma_{AA} = 8.75$. (b) For the same critical vector $q\sigma_{AA} = 8.75$, we check more extended logarithmic time window at $T = 0.325$ with increasing ϕ.

We also verify the presence of A_4 singularity in terms of logarithmic behavior in density autocorrelation functions. We fit the general asymptotic decay law for the density autocorrelation function given in Eq. (3.3)

for a set of $q$vectors. We select the isochore $\phi = 0.585$ and do the fitting of density autocorrelation functions at $T = 0.325$ for a set of $q$vectors $q\sigma_{AA} = 0.19, 2.91, ..., 23.33$ as shown in Fig. 3.11(a). For the $q$vector $q\sigma_{AA} = 8.75$, the density autocorrelation function shows a logarithmic dependence at the intermediate time interval same as to MSD. Above and below this critical $q$vector $q^*_{\sigma_{AA}}$, the density autocorrelation function produces a concave and convex shape which is a clear indication of presence of higher order singularity. Along the same isotherm $T = 0.325$, we plot the density autocorrelation function for critical value of q^* in Fig. 3.11(b). We do not see a pure logarithmic decay with an extended period of time as expected close to A_4 higher order singularity. According to the mapping, the position of A_4 has been estimated at $T \sim 0.615$, where simulation data indicates at $T \sim 0.325$. We approach the A_4 singularity from different paths in the phase diagram and try to observe a pure logarithmic with an extension of time scale. The correlators, reported in Fig. 3.12, for a set of temperatures with increasing ϕ shows a full logarithmic behavior. Due to the competition between A_2 and A_4 singularities, a clear α relaxation does not take place for the state points along the studied path. We explore the path in (ϕ, T) plane and observe a pure logarithm behavior for the critical value of $q$vector $q^* \approx 7.75$ where the α relaxation does not occur. The fitting is done with general asymptotic decay law for the density correlation function following the Eq. (3.3) for a set of $q$vectors. The fitting is done in a fixed time interval so that the second term of Eq. (3.3) varnishes. We fixed the state points in ϕ and T and put them together in Fig. 3.12. The logarithmic time scale increases with increasing ϕ as we move close to A_4 singularity. We start

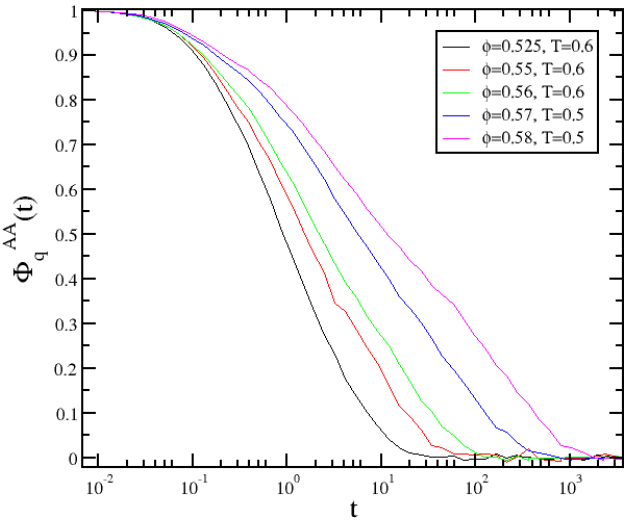

Figure 3.12: The density autocorrelation functions for state points exploring the path towards A_4 singularity for $\Delta = 0.17$. There is a visibility of logarithmic behavior for $\phi = 0.58, T = 0.5$.

to investigate the exact location of A_4 singularity in equilibrium phase by exploring the different values of Δ [22]. We carry out the simulation for Δ varying between 0.1625 and 0.1675 in an equal grid of 0.0025 for the state points at high packing fraction. In Fig. 3.13, we put all the state points together for different Δ to observe the pure logarithmic in anomalous time window.

We also do the several verifications for pure logarithmic feature for high ϕ value at different Δ. In Fig. 3.14, we have presented the density correlators for $\phi = 0.585$ and $T = 0.5$ on approaching A_4 for $\Delta = 0.1625, 0.165, 0.1675$ and 0.17. The correlator for $\phi = 0.585$ shows a more logarithmic at $\Delta = 0.17$ as compare to other studied values of Δ. Now, we are simulating the system close to the predicted state point for A_4 in high ϕ region.

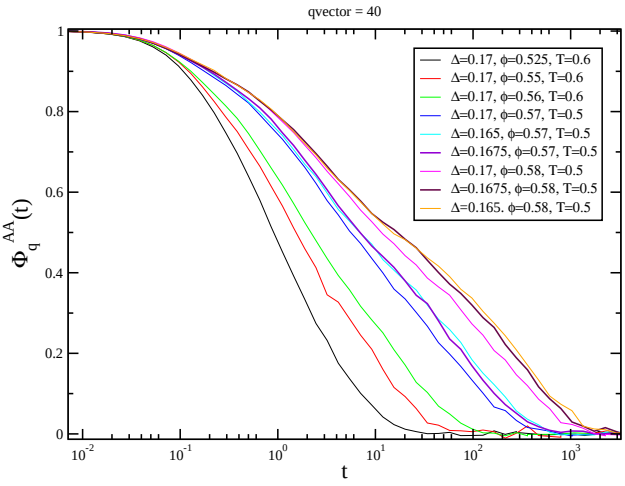

Figure 3.13: The density autocorrelation functions for $\Delta = 0.17, 0.1675, 0.165$. The solid dark line for $\Delta = 0.1675$ shows a pure logarithmic behavior for a large time scale with respect to other state points.

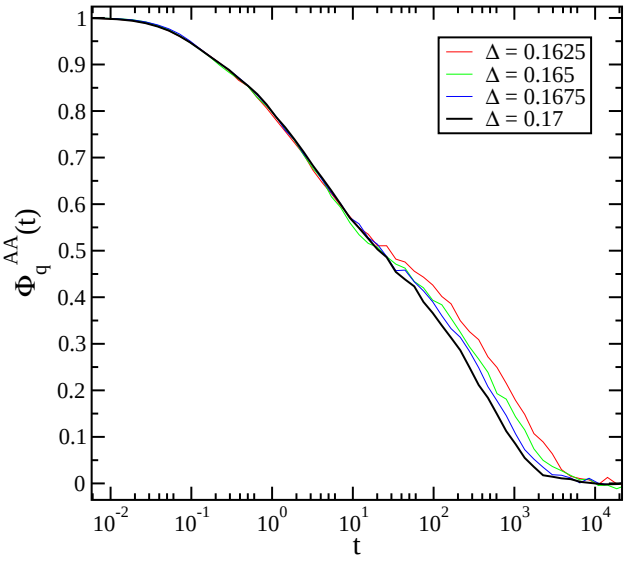

Figure 3.14: The density autocorrelation functions for $\Delta = 0.17, 0.1675, 0.165$for the state point $\phi = 0.585, T = 0.5$.

3.2.5 Non-ergodicity parameters

The behavior of the dynamical properties close to the singularities gives a clear understanding of their presence so far. There is still lacking of information to detect the exact position of A_4. We select an isodiffusivity line $D/D_0 = 9.5E-06$, where the system goes to arrested state and evaluated the non-ergodicity parameters. The fitting has been made with general asymptotic decay law Eq.(3.3) for the correlation function for the state points along the glass line joining two higher order singularities (curves 2-7) and extracted the non-ergodicity parameters. Similarly, we fit the long-time relaxation for a set of $q$vectors for the state points marked with 8 and 9 in with the stretched exponential

$$\Phi_q^{AA}(t) \sim f_q exp[-(t/\tau_q)^{\beta_q}] \tag{3.4}$$

for the state points marked with 8 and 9 in Fig. 3.15. The behavior of extracted non-ergodicity parameter f_q^{AA} is discussed very explicitly along the liquid-glass line. We denoted the state points with number to discuss easily the interesting region of the isodiffusivity line as shown in the inset of Fig. 3.15. We note that the f_q^{AA} at lowest T for the state $1(\phi = 0.40, T = 0.235)$ and at highest T for the state $9(\phi = 0.59, T = 1.0)$ corresponds to two type of repulsive glasses: effective HS glass (1) corresponds to effective hard sphere diameter $\sigma + \Delta$ and the HS glass (9) corresponds to hard sphere diameter σ respectively. When we rescale the effective HS glass with effective diameter $\sigma + \Delta$, they exactly fall on top of each other. The state points numbering with 2 and 7 represents the position of the higher order singularities A_3 and

A_4 respectively. As we could see, the behavior of f_q^{AA} at $\phi = 0.50$ and $\phi = 0.58$ are similar. The intermediate state points numbered from $3-6$ shows non-monotonous behavior in non-ergodicity parameter f_q^{AA} without any variation in the height of the peak. The state points marked with $3, 4, 5$ increases monotonically and then suddenly at 6, the height of f_q^{AA} drops down. This behavior of f_q^{AA} allow us to super impose the low-ϕ f_q^{AA} on top of the high-ϕ f_q^{AA} by simply scaling with the effective diameter.

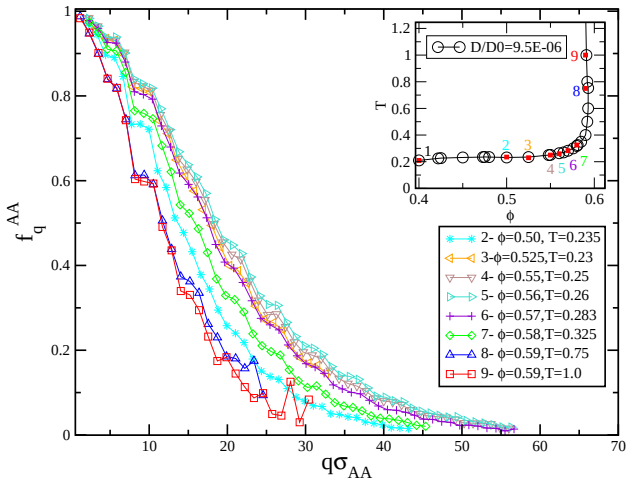

Figure 3.15: The non-ergodicity parameters extracted from the fitting of density auto-correlation functions along the isodiffusivity line $D/D_0 = 9.5E-06$ as shown in the inset. The state points are marked with numbers along the isodiffusivity line. The behavior of non-ergodicity parameter along the liquid-glass line shows a non-monotonous behavior.

From the fitting of density autocorrelation functions, we extract the fitting parameters for the coefficient $h_q^{(1)}$ and $h_q^{(2)}$ which are reported in Fig. 3.16 and 3.17. Following the typical variation in non-ergodicity parameters, we also observe the non-monotonic variation in the value of $h_q^{(1)}$ at the intermediate glassy regime. Initially, the curves for $2-5$ increases monotonically with

a small shift in the height of peaks with increasing q. The curve at $\phi = 0.57, T = 0.283$, starts to show a nonmonotonic behavior and height of the peak starts to drop. We scale the curve 2 on curve 6 with the effective diameter. In Fig. 3.17, the value of $h_q^{(2)}$ drops to zero and this gives the estimation of critical $q$vector q^*.

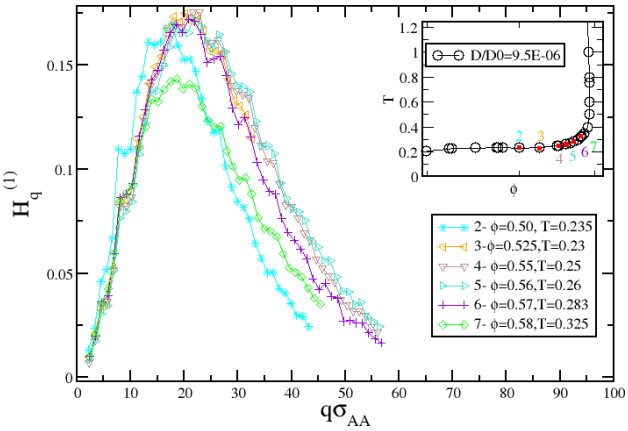

Figure 3.16: The figure shows the plot for $h_q^{(1)}$ for the state points along glass-glass line as shown in the inset.

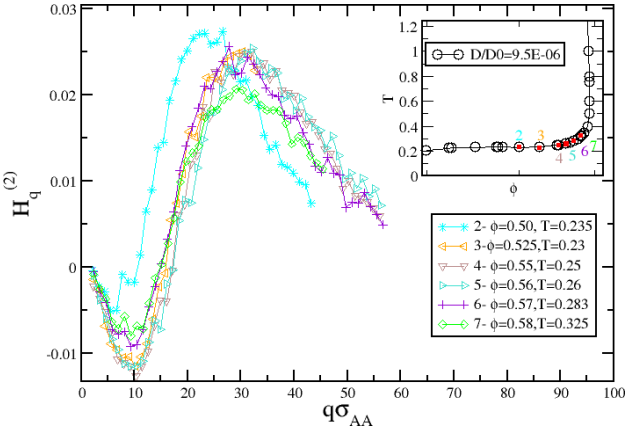

Figure 3.17: The figure shows the plot for $h_q^{(2)}$ for the state points along glass-glass line as shown in the inset.

3.3 Novel Invariant Dynamics

An extensive study for the presence of A_4 singularity gives an understanding of the dynamics of AA particles. During the analysis for higher order singularities, we encounter with peculiar properties in the dynamical quantities close to the intermediate region of the glass line in the phase diagram. The previous analysis for $\Delta = 0.15$ in Chapter 2, gives a notion that the dynamical features are indistinguishable close to the middle points (rather that endpoints) of the glass-glass line in the phase diagram. The similar observation for $\Delta = 0.17$, gives more clear picture of the dynamics on approaching the higher order singularities. So, we extend this analysis more and try to explore the endpoints of the glass-glass line. We also try to understand the dynamical features of the two end points with respect to other points along the glass transition line joining A_3 and A_4 higher order singularities. A way to clarify this point is to look along the isodiffusivity line associated to the invariant dynamics. We compare mean square displacement and density autocorrelation functions and verify the range of validity even beyond the glass line boundaries associated to the invariant dynamics. We investigate the dynamics along three isodiffusivity lines,$D/D_0 = 3.5 \times 10^{-4}, 5.5 \times 10^{-5}$ and 9.8×10^{-6} as shown in Fig. 3.18.

With a precise study of the dynamical properties, we are able to locate few invariant state points along each studied isonormalized diffusivity lines. We put these invariant state points in Fig. 3.18 marked with filled squares. We magnify the invariant region in inset of the figure. In the next section we discuss about the dynamical properties on a close approach to the liquid-glass

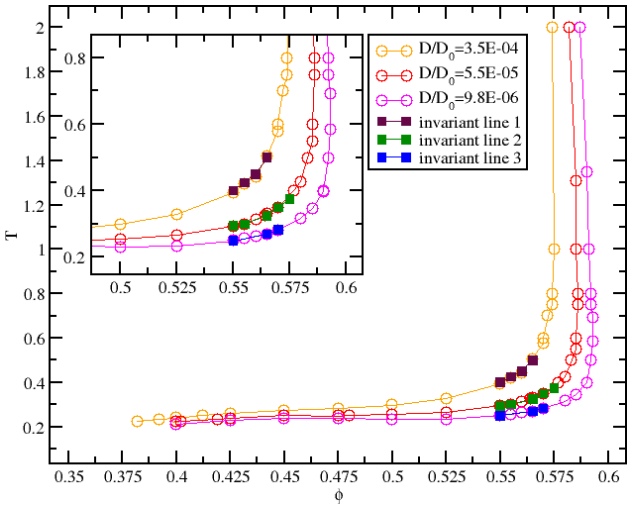

Figure 3.18: The invariant dynamics has been studied along three isodiffusivity lines $D/D_0 = 3.5 \times 10^{-4}, 5.5 \times 10^{-5}$ and 9.8×10^{-6}. The solid squares represent the invariant state points along the corresponding isodiffusivity lines.

line.

3.3.1 Dynamics along the invariant line

We begin our analysis for normalized isodiffusivity $D/D_0 = 3.5 \times 10^{-4}$ and plotted MSD for the state points $(0.55, 0.4), (0.555, 0.425), (0.56, 0.45)$ and $(0.565, 0.5)$ in Fig. 3.19 (a). The MSD exactly coincide for all the studied state points on scaling the time with factor $D_0 = \sigma_{BB}\sqrt{T/m}$. The invariant dynamics remain unchanged without any time scaling. We also verify the behavior of density autocorrelation functions for several q vectors for the above state points and observed the dynamic remain invariant for all the q vectors. In Fig. 3.19 (b), we have shown the density autocorrlation functions $\Phi_q^{AA}(t)$ for a set of selected $q$vectors.

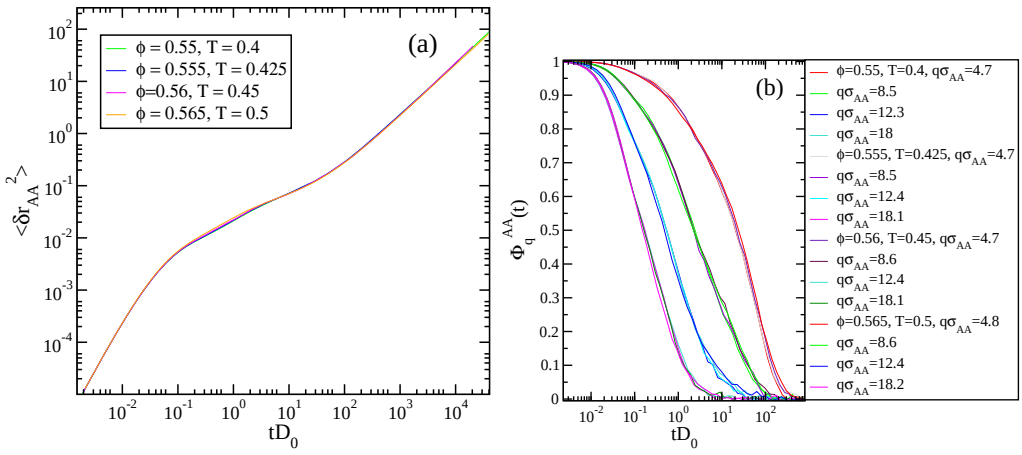

Figure 3.19: The locus of invariant state points along the isodiffusivity line $D/D_0 = 3.5 \times 10^{-4}$ shows an (a) exact overlap in MSD and (b) $\Phi_q^{AA}(t)$ for a set of $q$vectors.

We move close to the liquid-glass line and track the dynamics along the isodiffusivity line $D/D_0 = 5.5 \times 10^{-5}$. In Fig. 3.20, we have shown MSD and $\Phi_q^{AA}(t)$. We observe the similar behavior which indicates the invariant dynamics.

Finally, we make a close approach to the liquid-glass ideal line by studying dynamics along the isodiffusivity line $D/D_0 = 9.8 \times 10^{-6}$. We shows the behavior of MSD and density auto correlation functions for slow state points in Fig. 3.21. The dynamics remains unchanged and are in good agreement with previous analysis for invariant dynamics. In this case, the invariant line shorter compare to other two or may be we do not have enough state points. During the above analysis we find that the influence of glass line associated to the higher order singularities on dynamics, sufficiently far from any liquid-glass transition, does not depend on the particular position of the state points along the glass transition and that a similar anomalous dynamics

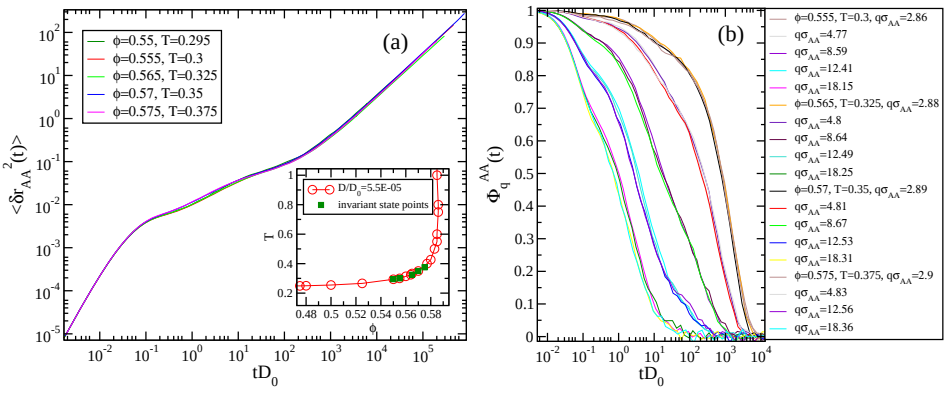

Figure 3.20: The locus of invariant state points the along isodiffusivity line $D/D_0 = 5.5 \times 10^{-5}$ shows an (a) exact overlap in MSD and (b) $\Phi_q^{AA}(t)$ for a set of $q$vectors.

is observed independently of whether one approaches precisely the endpoints, i.e. the predicted higher order singularities, or another point in between then along the glass line.

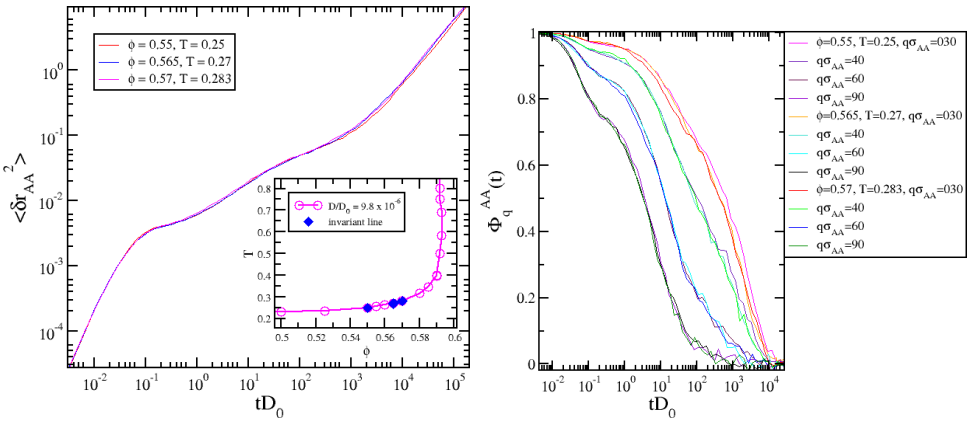

Figure 3.21: The locus of invariant state points the along isodiffusivity line $D/D_0 = 9.8 \times 10^{-6}$ shows an (a) exact overlap in MSD and (b) $\Phi_q^{AA}(t)$ for a set of $q$vectors.

3.3.2 Dynamics beyond the invariant line

We next investigate the dynamical properties beyond the invariant line and compare with the state points along the glass line associated to the higher order singularities. We would like to see, where the line of invariant terminates on both sides. For this we compare MSD and $\Phi_q^{AA}(t)$ for the state points even beyond the invariant one along the liquid-glass line. We selected the isodiffusivity line $D/D_0 = 5.5 \times 10^{-5}$ in order to observe the validity of the invariant dynamics. The state points denoted with blue stars in the inset of Fig. 3.22, beyond the invariant line. We verify the MSD and $\Phi_q^{AA}(t)$ for the state points say: non-invariant state points. We could see in Fig. 3.22, at the intermediate time scale ($0.1 \leqslant tD_0 \leqslant 10^2$), MSD doesn't overlap as we observed for invariant state points. In high density ($\phi = 0.585$) and temperature ($T = 1.0$) region the MSD starts to show the curvature at the intermediate time scale. The long time limit of MSD does not overlap for the non-invariant state points.

In order to have a more clear picture of the non-invariant dynamics we also study the density auto correlation functions for the same non-invariant state points. The density auto correlation functions for a set of $q$vectors in Fig. 3.23. The solid magenta curve is the density autocorrelation function for an invariant state point is a guideline to the eye. When we compare $\Phi_q^{AA}(t)$ of non-invariant points with invariant state point, we could see a clear discrepancy at β relaxation. The density autocorrelation function starts to bend instead of overlapping with each other. The deviations of MSD and density autocorrelation functions from the invariant dynamics clearly

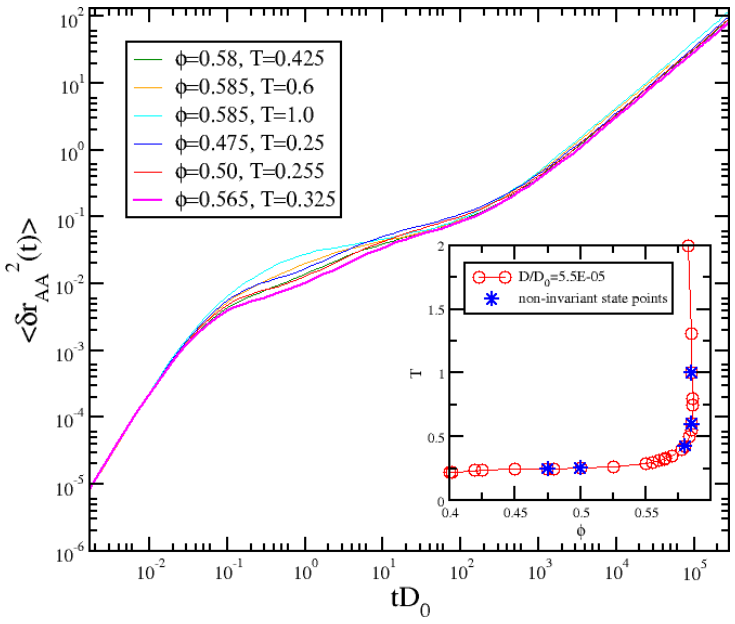

Figure 3.22: The dynamics studied for the state points beyond the invariant state points along the isodiffusivity line $D/D_0 = 5.5 \times 10^{-5}$. MSD shows a clear bending in the subdiffusivity region indicates the termination of invariant dynamics.

indicates the peculiar invariant dynamics associated to the glass line joining the higher order singularities, even if it does not predict the exact location of the singularities.

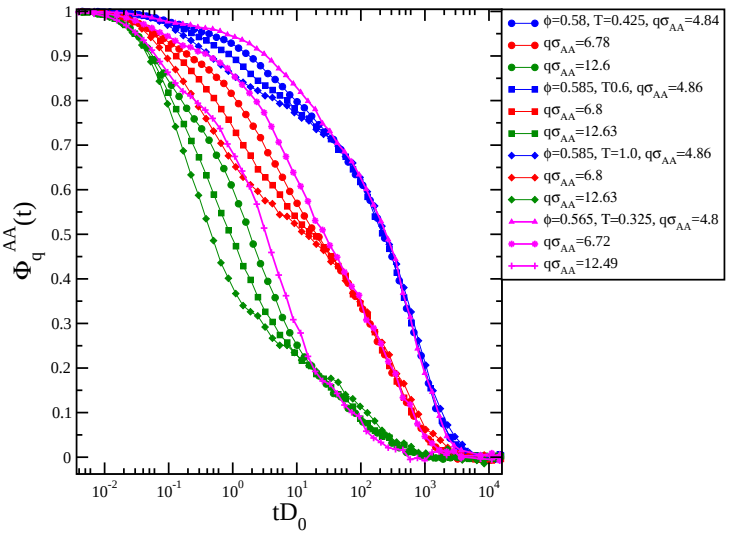

Figure 3.23: The dynamics studied for the state points beyond the invariant state points along the isodiffusivity line $D/D_0 = 5.5 \times 10^{-5}$. $\Phi_q^{AA}(t)$ shows a bending in the anomalous time window and does not overlap.

Chapter 4

Low Density glassy dynamics: fragile to strong behavior

4.1 Introduction

An important concept of glassy physics is fragility. According to Angell-classification [1], in glass forming liquids, the viscosity shows two phenomenological behavior as a function of temperature, as temperatures decreases towards the glass transition. One is known as Arrhenius relaxation law where viscosity as well as relaxation times grow exponentially with lowering of temperatures as

$$\eta \;=\; \eta_0 \; e^{A/T} \tag{4.1}$$

where A is the activation energy. Systems exhibiting Arrhenius behavior are designated as strong glass former [1]. The second one is the Vogel-Fulcher-Tammann-Hesse law (or simply VFT), expressed as

$$\eta = \eta_0 \, e^{\beta/(T-T_0)} \tag{4.2}$$

The η diverges even faster than the Arrhenius one, sometimes called super-Arrhenius. Systems whose viscosity follows the VFT law are designated as fragile glass former.

Dynamics of colloidal systems are often studied through diusivity. In equilibrium phase, the diusivity is related to the viscosity by the Stokes-Einstein relation as

$$D = k_B T/(6\pi r\eta) \tag{4.3}$$

where, D/T is inversely proportional to the viscosity η.

Sometimes the system shows a fragile behavior and becoming stronger at a certain packing fraction ϕ. There is a contribution to fragility from the kinetic term determined by the stretching exponent β_q. This stretching exponent is extracted from long time limit of $\alpha-$relaxation of the density autocorrelation functions following the stretched exponential

$$\Phi_q(t) = A_q \, exp[-(t/\tau_q)^{\beta_q}] \tag{4.4}$$

where, τ_q is the relaxation time and β_q is the stretching exponent. The stretching exponent obtained from the fitting of stretch exponential gives

the dependency of the fragility in the viscous liquids. A value of $\beta_q = 1$ gives simple exponential relaxation; lower values of β_q yield increasingly nonexponential relaxation. The higher value of β_q leads to strong glass.

Recently a model system with spherical pair-wise additive along with directional interactions has been studied by using a binary mixture of non-additive hard spheres [31]. While large spheres mimic the colloidal particles, small spheres act as bonds between the large ones. The interaction is attractive only between small and large particles and it is modeled via a short range square well potential. To control the valency, the hardcore interaction between small particles is chosen significantly larger than their actual size. In this system, the phase separation is suppressed by using a limited valency. At low T bonding is the dominant mechanism of structural arrest. An extensive simulation study of the system shows an Arrhenius behavior. For a square well (SW) model [41] there is a breakdown of Stokes-Einstein (SE) relation for attractive glass at low T and also for repulsive glass in high T. In our model system instead of any attraction, we add the repulsive interaction to the hard sphere; Square Shoulder (SS). Without the presence of any attraction, we found the super-Arrhenius behavior and breakdown of SE relation due to the competition between two repulsive length scales. We made a detail investigation in the low packing fraction ϕ and low temperature T limit and discuss the complete phase diagram.

In Chapter 3, we discussed the phase diagram of SS system in (ϕ, T) plane. A detail numerical simulation study for SS system shows the anomalous diffusion and reentrant behavior due to cooling for a fixed interaction range $\Delta = 0.15$ that has been predicted by MCT [51]. In order to explore the low

packing fraction region of the phase diagram, we carried out the simulations for a $50-50$ binary mixture of SS spheres for $\Delta = 0.15$. One aspect of this study is peculiar: it shows that at low ϕ we can approach the glass transition down to very low temperatures, without intervening crystallization or phase separation. This was previously achieved only in systems with directional attraction as we have discussed above [31]. The dynamics at low T was found to be dominated by bonding processes, showing an Arrhenius dependence. Here on the contrary, bonding is not present and the dynamics seems to always retain the fragile character of HS systems. The absence of phase separation at low T and ϕ for the present system thus offers the unexplored possibility to investigate the glass transition at $T \to 0$ for $\phi \to \phi_g[\sigma/(\sigma+\Delta)]^3$. In this Chapter, we make a detail investigation of dynamics in the low density region for $T \to 0$ and explore the phase behavior of SS system in low density regime.

The contents of this chapter is organized as follows: In Sec. 4.2, we will give a small description about the system and molecular dynamics (MD) simulations we perform. Then, in Sec. 4.3, we will discuss about the associated dynamical properties. It is subdivided into subsections: in Sec. 4.3.1, we will discuss the behavior of diffusivity along isochores and isotherms and associated isodiffusivity lines; in Sec. 4.3.2, we explore the dynamical phase diagram in low ϕ and T region. Together with all these studies, we present a detailed discussion about the strong glass former in Sec. 4.4. Finally, in Sec.4.5 we discuss the breakdown of Stokes-Einstein relation in Square Shoulder (SS) system.

4.2 Results

We continue with the simulation for a 50-50 binary mixture of 2000 particles using Event-driven Molecular Dynamics simulations where particles interact with a pairwise (SS) potential. Following the same simulation techniques for $\Delta = 0.15$ as explained in Chapter 2, we equilibrate the system in NVT and NVE ensembles. A systematic study of the diffusivity has been made for the packing fraction ranging between 0.30 and 0.425 for the temperature limit $T \to 0$. In the entire simulations we only concentrate on the large A type particles, because of the similarity between the two species. For each packing fraction, we continue the simulations until we approach a dynamical arrest and equilibration becomes prohibitively long. We evaluate the self diffusion coefficient D from the long time limit of mean square displacement following the Einstein relation,

$$D = \lim_{t\to\infty} \frac{< r^2(t) >}{6t} \tag{4.5}$$

4.3 Dynamical Properties

4.3.1 Self-diffusion coefficient and isodiffusivity lines

During the entire simulation, the system is in fluid state for the packing fraction $0.30 \leqslant \phi \leqslant 0.385$ even at $T \to 0$. We presented this strange behavior of the particle in Fig. 4.1(a) in terms of MSD. The particle diffuses faster at all values of T as a normal liquid. When we increase the packing fraction $\phi = 0.385$, we could see in Fig. 4.1(b), at high T, the particle diffuses faster

and then starts to diffuse more faster with decreasing T. At high $T > 0.1$, the particle diffuses very fast as we could see in Fig. 4.1(b). When we move along T and decrease further to lower value of $T < 0.01$, the particle shows a very peculiar dynamics. Initially, particle obeys a ballistic behavior. At intermediate time $0.01 \leqslant t \leq 10^3$, the particle gets caged by its neighboring particles and rattle inside the cage for a subsequent period of time. At large time scale due to some activated processes, there will be space created by small particles. Due to these activated processes the particle moves out of the cage and starts to diffuse linearly with time.

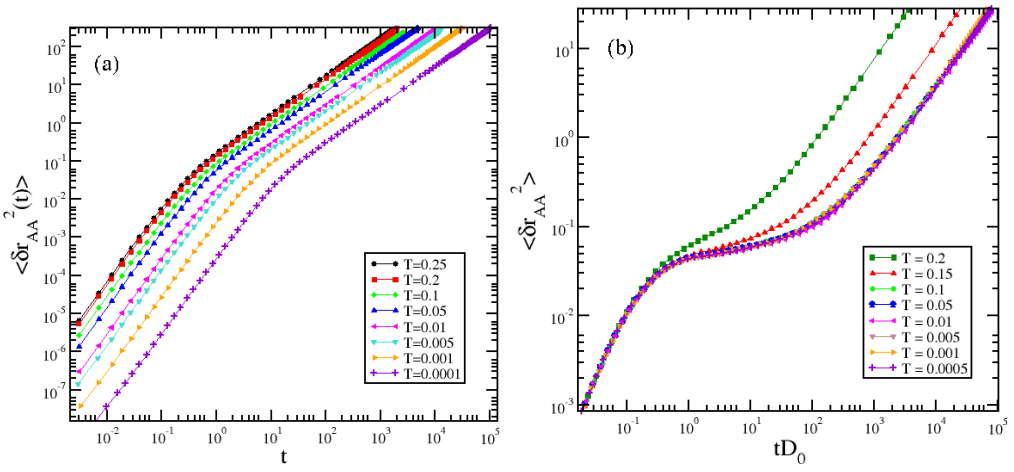

Figure 4.1: MSD along the isochore (a) $\phi = 0.30$ shows a normal behavior of liquid at $T \to 0$, while (b) along isochore $\phi = 0.38$ produces a long plateau for $T \to 0$ and becomes diffusive in long limit of time scaled with $D_0 = \sigma\sqrt{T/m}$.

We made a systematic investigation of diffusivity with temperature T for the packing fraction ranging between 0.30 and 0.425. We start by looking at high $\phi \geqslant 0.40$, where the diffusivity shows a monotonic variation with decreasing T along each isochore. For $\phi \leqslant 0.40$, there is a bending which becomes more clear along isochores $\phi \leqslant 0.395$ at a certain value of T. The

kink in the diffusivity is observed at different values of T along each isochore. On further lowering the temperature, we encounter with a sharp drop in the diffusivity as shown in Fig. 4.2. This bending becomes more clear with decreasing ϕ and disappears at $\phi = 0.30$ below which the system behaves as normal liquid.

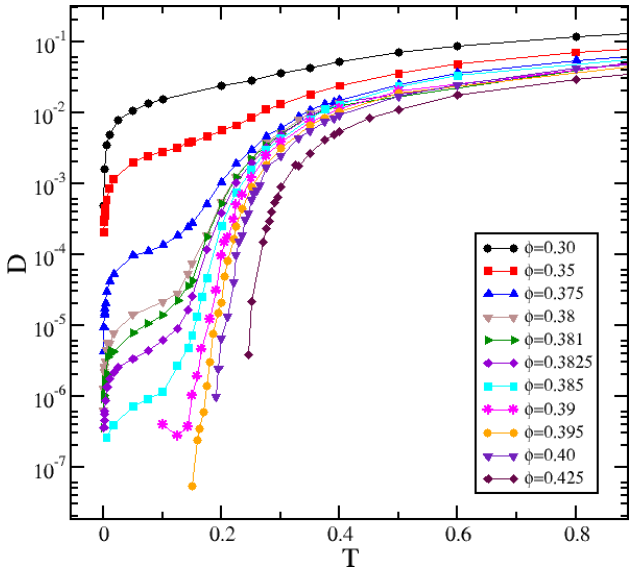

Figure 4.2: The diffusion coefficient D is plotted with T along a set of isochores. The diffusivity shows a curvature on lowering the temperature and then drops to a constant value in the limit of $T \to 0$.

We observe that for certain value of ϕ the diffusivity shows an Arrhenius dependence at low T. Fig. 4.3 (a) shows the diffuision D as a function of $1/T$. In log scale the diffusivity shows an arrhenius dependence in ϕ. In our simulation, the best isochores showing Arrhenius behavior are $\phi = 0.39$ and 0.395. We did the Arrhenius fitting using the relation $D = C\ exp[-(E_A/K_BT)]$, where E_A is the activation energy.

In the range of Arrhenius fitting, we extracted the activation energy and

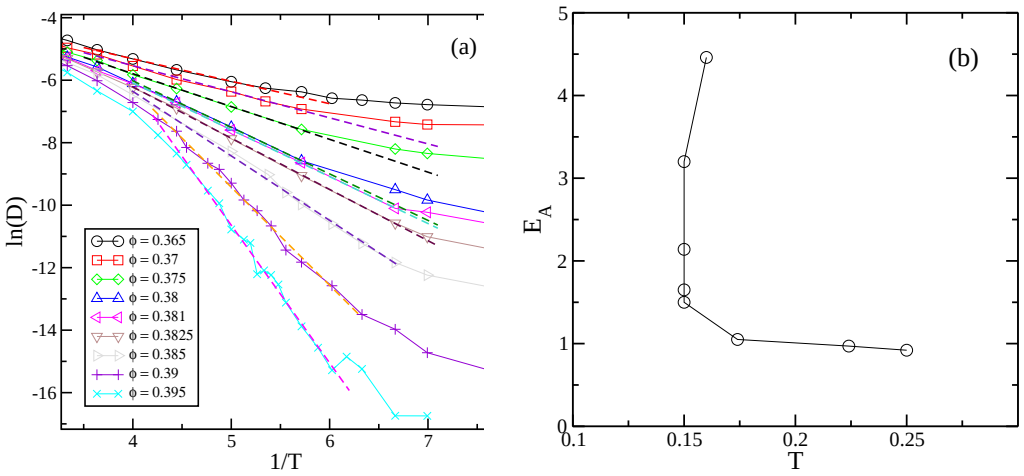

Figure 4.3: (a) Arrhenius plot of the diffusion coefficient along the studied isochores. The dashed lines represent the fitting along each isochores. (b) The value of activation energy E_A extracted from the Arrhenius fitting.

it increases systematically with increasing ϕ. The list of activation energy E_A extracted from Arrhenius fitting has been plotted in Fig. 4.3 (b).

In order to have a better understanding of the phase diagram we plotted the isodiffusivity lines extracted from the diffusivity plot of Fig. 4.2 for $D \to 0$. We cover three different normalized isodiffusivity lines, $D/D_0 = 10^{-3}, 10^{-4}$ and 1.7×10^{-5} in Fig. 4.4. As we have discussed in Chapter 3 and Chapter 4, these lines estimates the shape of the arrested line. In the previous study for $\Delta = 0.15$, we proposed the phase diagram with reentrance due to cooling along the isodiffusivity line and is confirmed both from simulations and new MCT calculations. Now we are concentrating on the same phase diagram in the low density part. The isodiffusivity line show an interesting behavior. In the phase diagram, we could see a sharp fall in temperature along the isodiffusivity line, $D/D_0 = 1.7 \times 10^{-5}$ and $T \to 0$ for $\phi \sim 0.3825$ as shown in Fig. 4.4. There is always a deviation at $\phi = 0.395$ along each isodiffusivity

lines.

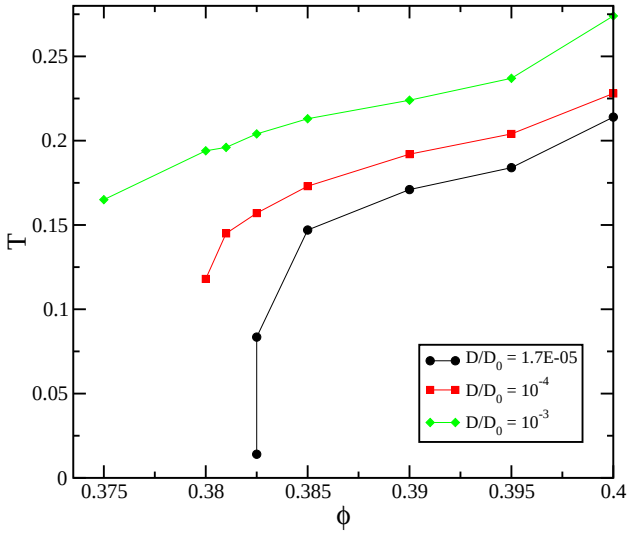

Figure 4.4: The iso-normalized diffusivity lines are plotted for $D/D_0 = 10^{-3}$ (solid green), 10^{-4} (solid red) and 1.7×10^{-5} (solid black).

To verify the shape of the isodiffusivity lines , we extract the arrested glass line from power-law fits along isotherms only. We do the power-law fit along a set of isotherms varying between 0.2 and 0.001 as shown in Fig. 4.5. We extract the transition value ϕ_g by performing the power-law fit of diffusivity $D \sim |\phi - \phi_g(T)|^{\gamma(T)}$ along isotherms and corresponding power-law exponent γ. The fitting has been made for a fixed range of diffusivity in order to observe a systematic variation in γ. The range of fitting changes for $\phi \leqslant 0.425$ as the system starts to show an arrhenius dependence of diffusivity in Fig. 4.3. So, we set different range for fitting for the low density regime.

In Table 1, we put together the extracted ϕ_g and the corresponding $\gamma(T)$. The value of γ increases with decreasing T and at $T = 0.01$ it starts to decrease. We could see a systematic decrease in ϕ_g value with decreasing

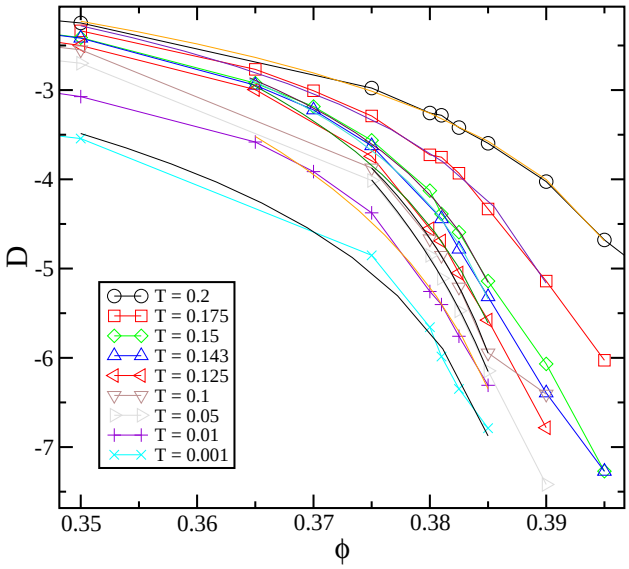

Figure 4.5: Diffusion coefficient dependence on ϕ for various studied isotherms. The power-law fits are done with the diffusion equation $D_A \sim |\phi - \phi_g(T)|^{\gamma(T)}$ along isotherms.

T. When the temperature $T \to 0$, the arrested ϕ_g becomes constant. The arrested line obtained from ϕ_g in the low density region of the phase diagram preserves the same shape as observed along the isodiffusivity line, $D/D_0 = 1.7 \times 10^{-5}$. There are large error bars in the fits especially in the calculated values for γ, but nonetheless the fits give a good estimate of $\phi_g(t)$, which drops rather vertically to low T at around $\phi \approx 0.395$.

T	$\gamma(T)$	ϕ_g
0.2	2.69	0.40
0.175	2.94	0.39
0.15	3.17	0.38
0.143	3.44	0.38
0.125	4.24	0.39
0.1	4.75	0.39
0.05	6.65	0.39
0.01	4.74	0.39

Table 4.1: Extracted value of ϕ_g from the diffusivity plot of Fig. 4.5 following the formula $D \sim |\phi - \phi_g(T)|^{\gamma(T)}$.

4.3.2 Phase diagram

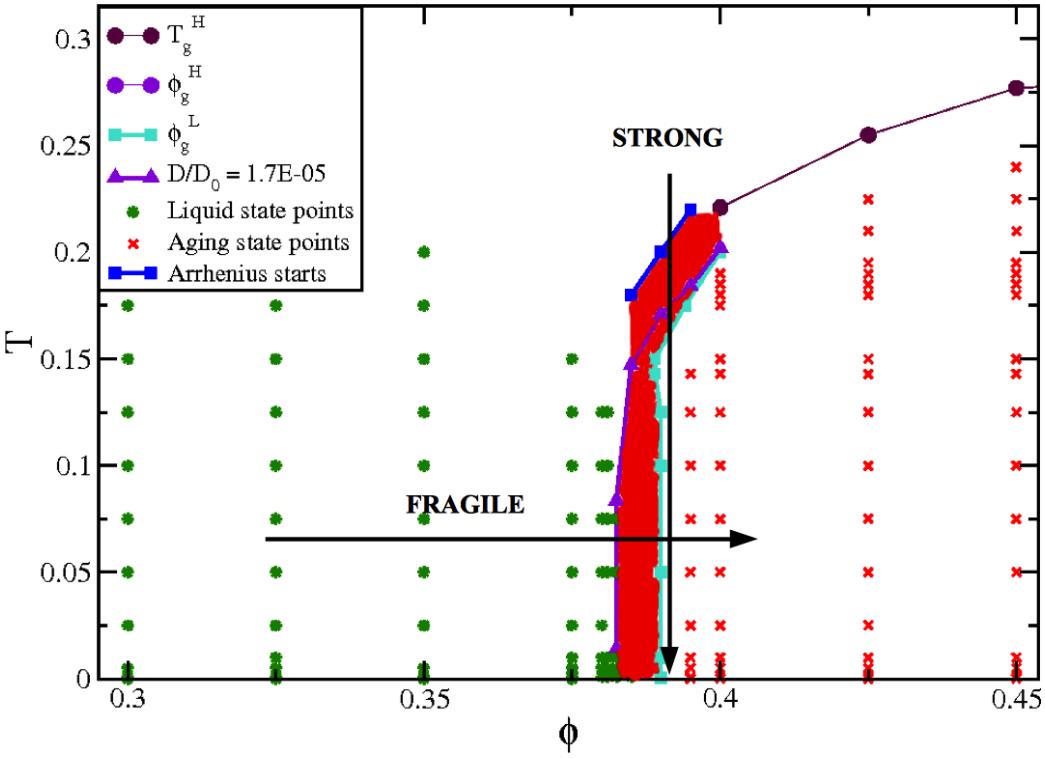

Figure 4.6: The phase diagram of SS system for low ϕ and low T in (ϕ, T) plane.

Now, we compare the simulation results obtained from the power-law fit and Arrhenius time window in the phase diagram of Fig. 4.6. We plot the arrested glass line represented with filled circles obtained from power-law fits in the high density regime for $\Delta = 0.15$. These lines are represented with T_g^H and ϕ_g^H. The open squares represent the arrested ϕ_g^L obtained from power-law fits of diffusivity for several isotherms in the low packing fraction regime. The curve with filled triangles represents the lowest isodiffusivity line, $D/D_0 = 1.7 \times 10^{-5}$ which has been extrapolated from diffusivity plot of T dependence

in Fig. 4.2. We have also put the liquid state points (green star) for $\phi \leqslant 0.385$ where the system remains in liquid phase for $T \rightarrow 0$. Since, the system shows Arrhenius dependence, we selected the most arrhenius isochores and mark the region where the Arrhenius begins along each isochore (blue open square). The red stars represent the aging state points for the system fall out of equilibrium. The interesting behavior observed in the phase diagram is the fragile behavior of system with the interruption of strong behavior. In the low density region of the phase diagram ($\phi \leqslant 0.385$) shows a fragile behavior for $T \rightarrow 0$. There is a small channel of strong behavior observed for the packing fraction range between $\phi = 0.39$ and 0.395.

4.4 Do we have a strong glass former?

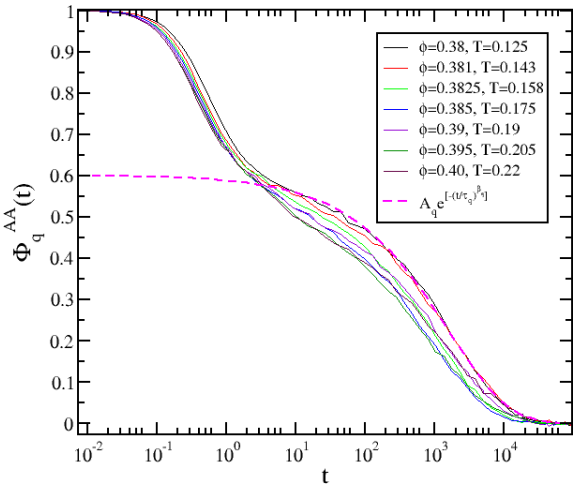

Figure 4.7: The density autocorrelation functions along the isodiffusivity lines $D/D_0 = 10^{-4}, 1.7 \times 10^{-5}$ for $q\sigma_{AA} \approx 5.56$, the first peak of partial structure factor.

In the beginning of the Chapter, we give a small introduction to the properties of strong glass former. In our study for low density region of the phase diagram, the system shows a fragile behavior and becoming stronger at a certain packing fraction ϕ. We verify this strong behavior of glassy system by extracting the stretching exponent β_q from Eq. (4.4). The stretching exponent obtained from the fitting of stretch exponential gives the dependency of the fragility in the viscous liquids. The value of β_q defines the behavior of strong glass former. A value of $\beta_q = 1$ gives simple exponential relaxation; lower values of β yield increasingly nonexponential relaxation. A higher value of β_q is characteristic of strong glass behavior. Initially, we start to understand the behavior of β_q along isodiffusivity line $D/D_0 = 10^{-4}$ and 1.7×10^{-5}.

We do the fitting with stretched exponential (Eq. (4.4)) and extracted relaxation time τ_q and corresponding stretching exponent β_q along the isodiffusivity lines $D/D_0 = 10^{-4}, 1.7 \times 10^{-5}$. In Fig. 4.7, we plot the density autocorrelation functions for critical value of $q$vector obtained from first peak of partial structure factor, along the isodiffusivity line $D/D_0 = 10^{-4}$.

ϕ	T	β_q
0.38	0.143	0.53
0.381	0.143	0.51
0.3825	0.15	0.49
0.385	0.175	0.46
0.39	0.195	0.49
0.395	0.205	0.45
0.40	0.22	0.45

Table 4.2: The value of tau β_q extracted with stretched exponential fitting of $\Phi_q(t)$ for the closest simulated state points to the isodiffusivity line $D/D_0 = 10^{-4}$.

We monitor isodiffusivity line $D/D_0 = 10^{-4}$ and put extracted β_q in Table. 4.2. We note that the relaxation time τ_q increases monotonically and then decreases with increasing ϕ and T. We do not observe any significant variation in β_q. Moving closer to the liquid-glass line, we verify the behavior of β_q along isodiffusivity line $D/D_0 = 1.7 \times 10^{-5}$ and we do not find any significant change in β_q again. From the above analysis, the isochores $\phi = 0.39, 0.395$, shows a good Arrhenius dependence and we start to explore more along these isochores with decreasing T. We plot the density autocorrelation functions for isochores 0.39 and 0.395 for low T.

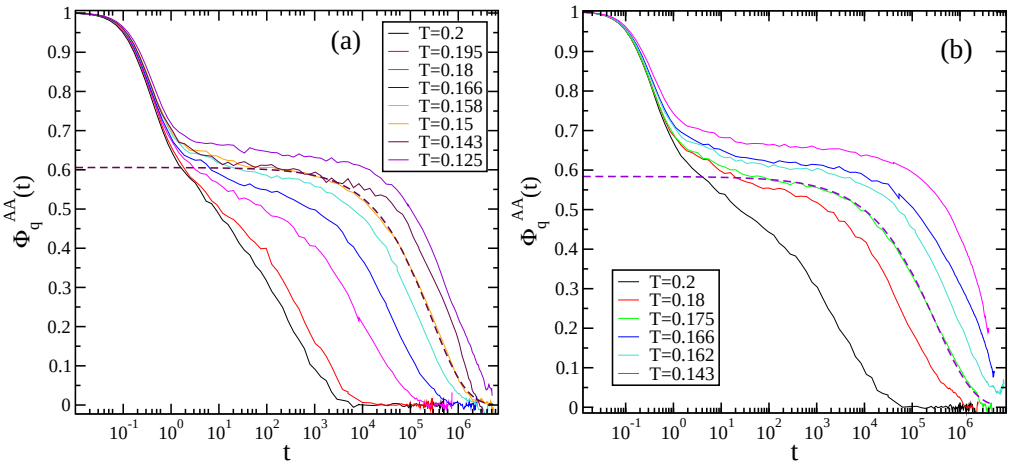

Figure 4.8: The density autocorrelation functions for (a) isochore, $\phi = 0.39$, and (b) isochore $\phi = 0.395$ with decreasing T.

The increase in the value of $\beta_q \to 1$, the diffusion should be more Arrhenius. In order to approach the highest value of β, we evaluated the stretching exponent β_q along isochores 0.39 and 0.395 with decreasing T. We do the fitting with stretched exponential, but simulations are still running because the full decay to zero of $\Phi_q(t)$ is needed before a robust value of β can be

drawn. We plot the dependency of β on temperature in Fig. 4.9. In high T region the value of β remains constant. On lowering the temperature T, the value of β increases.

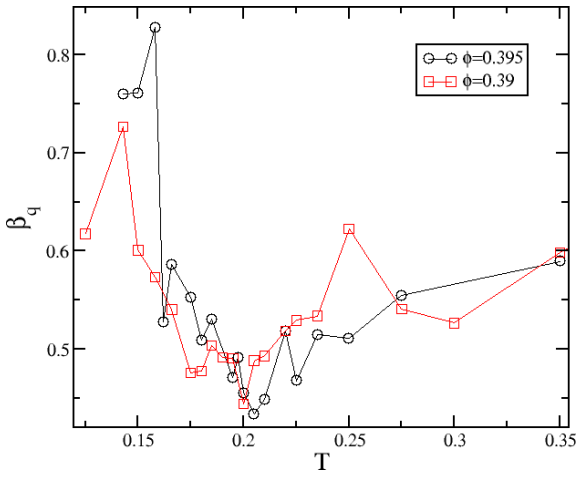

Figure 4.9: The behavior of β_q is plotted with dependence of temperature T.

4.5 Breakdown of Stokes-Einstein relations

Typical homogeneous equilibrium liquids, far above their glass transition temperature (T_g), obey the Stokes-Einstein (SE) equation, $D\eta$ =constant, where D is the diffusion coefficient and η the reduced shear viscosity[$\eta = \eta_s/T$, where η_s is the shear viscosity]. Recent experiments [56] and simulations [2] on supercooled liquids have shown that the structural relaxation time τ obeys proportionality, $\tau \propto \eta$ so that both $D\tau$ and $D\eta$ are essentially constant well above T_g. However, both of these relations "breakdown dramatically" in the immediate vicinity of T_g [6, 9, 15, 45, 52]. It is commonly accepted that this effect results from"dynamic heterogeneity" in supercooled liquids.

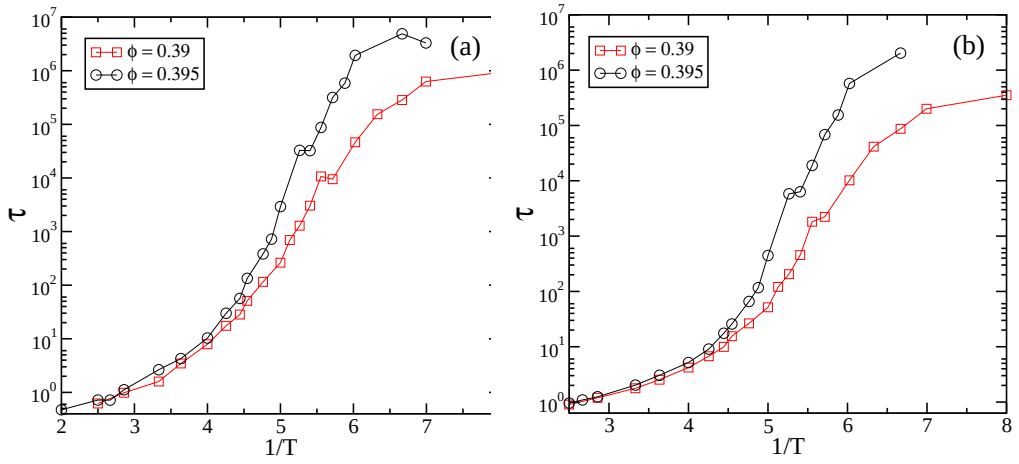

Figure 4.10: Extracted τ along isochores $\phi = 0.39$ and 0.395 from $\Phi_q(t)$ defined by (a) stretched exponential, and (b) $\Phi_q^{AA}(t) = 1/e$.

A detail study of Arrhenius behavior in Sec. 4.3.1, provides two stable isochores $\phi = 0.39$ and 0.395. We start examining the SE relation for the binary hard-sphere with repulsion. The validity of SE relation can be checked

with the temperature dependence of relaxation time τ. The relaxation time τ has been extracted from the $\alpha-$relaxation of density autocorrelation function $\Phi_q(t)$ with the fitting of stretched exponential in Eq. (4.4). We study the behavior of τ with temperature dependence in Fig. 4.10. The decay in τ is described by an Arrhenius law in the low T region in Fig. 4.10 (a). We also verify the same behavior of τ by fitting with $\Phi_q^{AA}(t) = 1/e$. The decay in τ follows the same Arrhenius law along each isochores.

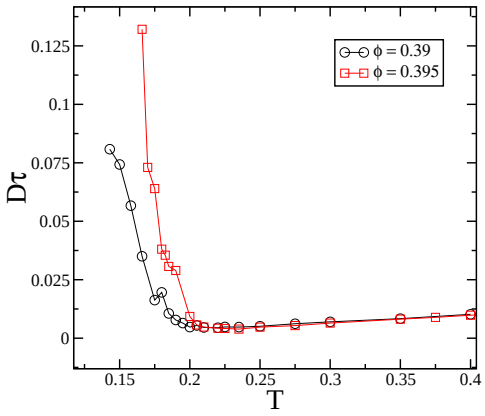

Figure 4.11: The figure shows the breakdown of Stokes-Einstein relation defined with the divergence of $D\tau$ at low temperature T.

To determine in which region of the phase diagram the SE relation is valid, we show the behavior of scaled diffusivity $D\tau$ with temperature $T \leqslant 0.2$ in Fig. 4.11. AT high temperature $T > 0.2$, the diffusion remains constant obeying SE relations $D\tau = constant$, even on increasing the packing fraction. When the temperature is lowered, $D\tau$ is enhanced and starts to diverge from SE relations. The growth in $D\tau$ at low T reflects the shoulder effect on the motion of the particle. The earlier study for the breakdown of the SE relations for the model system of water [prl, vol97, 055901 (2006)], has

shown the deviation from SE relations driven by the transnational and rotational diffusion. In the present study, we understood that simple isotropic interaction can enhance the diffusivity and violates the SE relation.

Conclusions

In this work we have reported an extensive investigation of the SS model by doing simulations and theory. Despite the simplicity of the model, its dynamical behavior close to the glass transition had largely remained unexplored, while its thermodynamic phase diagram showing the presence of many crystal phases has been addressed in a number of publications [36, 38, 63]. The recent predictions by MCT of multiple glass transitions for the SS model [51] is the motivation for the present work. Given the amount of effort requested to elucidate the various aspects of both liquid-glass transition and glass-glass lines, we have focused on two different values of the width of the SS model to address the dependence on Δ of the results presented here.

In Chapter 2, our investigation focused on searching for the so-called diffusion anomalies, i.e. a local maximum in the self-diffusion coefficient, both upon compressing the system and upon cooling it, as predicted by MCT for $\Delta = 0.15$. We performed the simulations down to a T-range at the limit of today computational capabilities and we did not detect the presence of an anomaly upon compression/expansion in contrast to theoretical results, as well as with other studies of core-softened potentials [19, 27, 39, 43]. However, none of these previous studies involved a potential with sharply-defined

length scales such as the SS, so that this might be the reason why a different behaviour is observed. Also, it remains to be established whether such different models share the intriguing glassy properties of the one-component SS model, as detailed MCT studies have not been performed.

The role of the SS width is also crucial within MCT, because it controls the position of the glass-glass line and its endpoints with respect to the liquid-glass line. The present case was predicted to show two glass-glass lines merging from the liquid-glass one by RY-MCT for the monodisperse SS [51]. However, when we have repeated the MCT calculations for the binary mixture investigated by MD simulations, which avoided the onset of crystallization, we found a different topology. Namely, a disconnected glass-glass transition lying all inside the glassy region with two endpoints, i.e. a scenario that RY-MCT attributed to lower values of Δ. Such a shift in the control parameters is expected when comparing with MCT, although for the SW model there was a remarkable good agreement between theory and simulations at the same Δ [47]. Also no reentrance in ϕ was detected within the binary MCT calculations, in agreement with the simulation results. The disconnected glass-glass topology seems to be confirmed by simulations, which have shown the presence of a regime of logarithmic decay of the correlators and of subdiffusive increase of the MSD, in agreement with the predictions close to a higher order singularity. Also the presence of the glass-glass line and its special endpoints, called A_3^L and A_3^H, is compatible with the presented results.

We have also found evidence that the non-ergodicity parameters along the liquid-glass line vary in a non-monotonic fashion, in very good agreement

with the theory. We have shown that the glass found at low/intermediate ϕ (e.g. $\phi = 0.40$) and low T is identical to that found at high ϕ (and almost T-independent) when a scaling of the effective diameter is performed to take into account the effect of the shoulder width. Thus the system clearly displays two *identical* glasses, both of HS type, driven solely by excluded volume, and differing between themselves only by a change of length scale. However, the interplay between these two glasses is highly non-trivial, giving rise to anomalous behaviour in the dynamics, although not in the form of a local maximum in the diffusion coefficient, but in the form of clear subdiffusive regime in the MSD and logarithmic dynamics of the density correlators. This is enhanced at a length scale that is compatible with that always associated as the main responsible for the hard-sphere transition, i.e. the nearest-neighbour length. It is a remarkable finding that this simple physics is capable of producing such non-trivial and unexpected dynamical behaviour.

In order to approach the higher order singularity in equilibrium phase and to rule out the presence of a diffusivity maximum in density we have also carried out extensive simulations for $\Delta = 0.17$ which were discussed in Chapter 3. By following the same simulation techniques as we have done in Chapter 2, we studied the behavior of diffusivity along isochores and isotherms and propose the dynamical phase diagram for $\Delta = 0.17$. In the phase diagram, we found a glass-glass line connecting A_3 singularity lying inside the glassy regime and the A_4 singularity lying on the liquid-glass line. The glass-glass line along with the liquid-glass line is evaluated from the binary MCT calculations. We map the MCT liquid-glass line onto the arrested line obtained from power-law fits along isochores and isotherms. The estimated position

of A_3 and A_4 singularities obtained from mapping is confirmed with logarithmic behavior in density autocorrelation function and subdiffusive increase in MSD. MCT predicts a pure logarithmic in density autocorrelation function close to A_4 singularity. Following the same behavior, we are now investigating the exact location of A_4 singularity in equilibrium phase by exploring different values of Δ.

One of the novel results of this work is the identification of a locus of invariant dynamics, at a certain distance from the glass-glass transition where the influence of the liquid-glass boundary does not yet interferes with that of the glass-glass one. These findings will need to be complemented by the MCT solutions for the full-time equations (Eq. 1.1) in order to judge their regime of validity. Currently, we have established a collaboration with Dr. Matthias Sperl in Koln to investigate this matter theoretically. From our numerical analysis, we found that this invariant dynamics breaks at the certain point close to the glass-glass line. The MCT results for the glass-glass non-ergodicity parameter suggest a non-monotonic variation, which imply that the invariance is broken. An extensive numerical study for $\Delta = 0.17$ has revealed that the simple competition between two repulsive length scales brings a new invariant dynamics along the putative glass-glass line which has not been observed in any other systems. Our work shows that in order to explore unexpected dynamics, it is not needed to rely on two different physical ingredients, such as attraction and repulsion, but competing isotropic repulsions are sufficient.

Last, but not the least, we have concentrated on the dynamics of the system at low ϕ, where we can approach the glass transition down to very

low temperatures, without intervening crystallization or phase separation. The temperature dependence of diffusivity sh"ows an Arrhenius behavior at low T and remains constant with increasing T. This behavior of the system describes the presence of some "activated dynamics (but generated by a purely repulsive potential) which makes the system more diffusive at $T \to 0$. We explore the low ϕ and T region of the phase diagram for $\Delta = 0.15$, where we identify a crossover from fragile to strong behavior at low T. The above analysis suggests that the SS system retains strong-like character in the small region of the phase diagram (see Fig.4.3.2). Also a significant violation of SE relation is observed in analogy to other glass-forming systems.

In our work, we are able to explore the entire dynamical phase diagram of the SS system by means of numerical simulations. We are also able to explore a new invariant dynamics which could possibly be observed in other systems with two competing repulsive length scales.

List of publications

1. *Unveiling the complex glassy dynamics of square shoulder systems: simulations and theory*

   Gayatri Das, Nicoletta Gnan, Francesco Sciortino and Emanuela Zaccarelli,

   J. Chem. Phys., 138, 134501 (2013).

2. *Breakdown of the Stokes-Einstein relation in Square Shoulder systems with an evidence of strong glass former* (manuscript under preparation)

   Gayatri Das and Emanuela Zaccarelli

3. *Competition between two repulsive length scales driving a new invariant dynamics: theory and simulations* (manuscript under preparation)

   Gayatri Das, Nicoletta Gnan, Emanuela Zaccarelli, Francesco Sciortino and Matthias Sperl

Appendix A

Molecular Dynamics simulations

Molecular dynamics (MD) simulations have been used to study thermodynamic as well as dynamic properties of material (characterized by an interaction potential). The simulation considered as a close approach to experimental studies at the level of theoretical approach. The first MD simulation used for hard sphere fluid/solid [M. P. Allen, G. T. Evans, D. Frenkel, and B. M. Mulder, Hard convex body fluids, Advances in Chemical Physics 86 (1993), 1-166]. For soft particles, one needs to integrate a system of ordinary differential equations given by Newton's law of motion. Several algorithms have been developed to solve the Newton's equations of motion. However, for hard sphere, integrating the equation of motion is a difficult task as the particles follow the sequence of binary collisions, or collisions of the particles with hard walls of a container if any. So, it is necessary to predict and process a sequence of discrete events with time. The algorithm for hard particles

therefore are called event-driven. In event-driven MD one has to schedule the sequence of events predicted to happen in future. The schedule of events is updated if necessary and the same process is repeated.

Using the event-driven MD simulation techniques, we prepare an initial configuration randomly generated for the desired packing fraction. The position of the particle is chosen from an uniform random number generator and the particle velocities are extracted from a Maxwell-Boltzmann distribution corresponding to the desired T. The periodic boundary conditions have been applied along x, y and z directions to make infinite periodic boxes where each particle can interact with its nearest neighboring particles. Due to the replicas of the simulation box a particle that leaves the simulation box through a particular bounding face immediately reenters the box through the opposite face. Using successive steps, we generate a random configuration where two particles at least separated by a distance of 1σ. After generating the configuration, we add a finite repulsion 15% of the particle size to the HS system.

Simulations are performed in the canonical and microcanonical ensembles. MD simulations follow three main steps: (1) Initialization of the system, (2) Evolution of the system towards equilibrium and (3) Calculation of equilibrium properties. The system is equilibrated by performing Event-Driven MD simulations in the canonical ensemble with appropriate rescaling of particle velocities. During the evolution of system, a number of particles are selected to undergo a collision process with the heat bath. The use of step potential introduces the following set of collisions in the system:

1. collision between the hard cores

2. two atoms either entering or leaving their mutual potential

3. two atoms bounce as the potential boundary is reached

As we discussed above, in order to predict the future events after collision, one has to prepare an *Event calendar*. Depending on the events, the calendar has been organized to schedule the future collisions and the necessary changes are incorporated. During the simulation, each particle is at the point in time when the last event involving it happened. Each particle predicts its upcoming event and when it is expected to happen. The positions and momenta of the particles involved in this event are updated, the particles' next event predicted, the event queue updated, and the simulation continued with the next event. In the early stages of the simulation it is natural for the temperature to move away from the value at which it was set. We avoid the thermal hindrance by rescaling of particle velocities. In thermal equilibration, we measure average kinetic energy and pressure. Once the equilibration is reached for each investigated state points, NVE simulations are performed for times ranging from $t = 10^2$ for the highly diffusive state points, to $t = 10^6$ for the most viscous state points. For all the simulations t is measured in units of $\sigma_{BB}(m/u_0)^{1/2}$. In this ensemble, the system has been described with a fixed number of particles N, a fixed volume V, and a fixed energy E. The longer equilibration makes the system fluctuate around the mean pressure P and fixed temperature T as compared to canonical ensemble. The equilibration is verified by measuring the energy, pressure and temperature fluctuation around the fixed value. For each studied configuration, we measured the self diffusion coefficient D in the long time limit of mean square

displacement (MSD). We also looked at the time dependent density auto correlation function to compare with mode coupling theory (MCT) predictions. In this chapter, we discuss some basic concepts of dynamical quantities.

Bibliography

[1] Angell, C. A. 1988 Structural instability and relaxation in liquid and glassy phases near the fragile liquid limit *J. Non-Cryst. Solids* **102**, 205–221.

[2] Barrat, J. L., Roux, J. N. & Hansen, J. P. 1990 Diffusion, viscosity and structural slowing down in soft sphere alloys near the kinetic glass transition *Chem. Phys.* **149**, 197.

[3] Baxter, R. J. 1968 Ornsteinzernike relation for a disordered fluid *J. Chem. Phys.* **49**, 2770.

[4] Baxter, R. J. 1970 Ornsteinzernike relation and percusyevick approximation for fluid mixtures *J. Chem. Phys.* **52**, 4559.

[5] Bergenholtz, J. & Fuchs, M. 1999 Nonergodicity transitions in colloidal suspensions with attractive interactions *Phys. Rev. E* **59**, 5706–5715.

[6] Berthier, L., Chandler, D. & Garrahan, J. P. 2005 Thermodynamics of coarse-grained models of supercooled liquids *Europhys. Lett.* **69**, 329.

[7] Böhmer, R., Ngai, K. L., Angell, C. A. & Plazek, D. J. 1993 Nonexponential relaxations in strong and fragile glass formers *J. Chem. Phys.* **99**, 4201–4209.

[8] Caccamo, C. 1996 Integral equation theory description of phase equilibria in classical fluids *Phys. Reports* **274**, 1–105.

[9] Cummins, H. Z. 2005 Dynamics of supercooled liquids: excess wings, peaks, and rotationtranslation coupling *Condens. Matter* **17**, 1457.

[10] Das, G., Gnan, N., Sciortino, F. & Zaccarelli, E. 2013 Unveiling the complex glassy dynamics of square shoulder systems: Simulations and theory *J. Chem. Phys.* **138**, 134501.

[11] Dawson, K. A., Foffi, G., Fuchs, M., Götze, W., Sciortino, F., Sperl, M., Tartaglia, P., Voigtmann, T. & Zaccarelli, E. 2001 Higher-order glass-transition singularities in colloidal systems with attractive interactions *Phys. Rev. E* **63**, 011401.

[12] Dawson, K. A., Foffi, G., McCullagh, G. D., Sciortino, F., Tartaglia, P. & Zaccarelli, E. 2002 Ideal glass in attractive systems with different potentials *J. Phys.: Condens. Matter* **14**, 2223–2235.

[13] Duran, J. *Sands and Powders and Grains: An Introduction to the Physics of Granular Materials* Springer, New York, 1999.

[14] Eckert, T. & Bartsch, E. 2002 Re-entrant glass transition in a colloidal-polymer mixture with depletion attractions *Phys. Rev. Lett.* **89**, 125701.

[15] Ediger, M. D. 2000 Spatially heterogeneous dynamics in supercooled liquids *Annu. Rev. Phys. Chem.* **51**, 99.

[16] Fabbian, L., Götze, W., Sciortino, F., Tartaglia, P. & Thiery, F. 1999 Ideal glass-glass transitions and logarithmic decay of correlations in a simple system *Phys. Rev. E* **59(2)**, 1347–1350.

[17] Foffi, G., Dawson, K. A., Buldyrev, S. V., Sciortino, F., Zaccarelli, E. & Tartaglia, P. 2002 Evidence for an unusual dynamical-arrest scenario in short-ranged colloidal systems *Phys. Rev. E* **65**, 050802.

[18] Foffi, G., Sciortino, F., Tartaglia, P., Zaccarelli, E., Lo Verso, F., Reatto, L., Dawson, K. A. & Likos, C. N. 2003 Structural arrest in dense star-polymer solutions *Phys. Rev. Lett.* **90**, 238301.

[19] Fomin, Y. D., Tsiok, E. N. & Ryzhov, V. N. 2011 Core-softened system with attraction: Trajectory dependence of anomalous behavior *J. Chem. Phys.* **135**, 124512.

[20] Gallo, P. & Sciortino, F. 2012 Ising Universality Class for the Liquid-Liquid Critical Point of a One Component Fluid: A Finite-Size Scaling Test *Phys. Rev. Lett.* **109**, 177801.

[21] Götze, W. *Liquids, Freezing and the Glass Transition* North-Holland Amsterdam, 1991 287–503.

[22] Götze, W. & Sperl, M. 2002 *Phys. Rev. E* **66**, 011405.

[23] Götze, W. & Voigtmann, T. 2003 Effect of composition changes on the structural relaxation of a binary mixture *Phys. Rev. E* **67**, 021502.

[24] Hansen, J. P. & McDonald, I. R. *Theory of simple liquids* 3rd edn. Academic Press, New York, 2006.

[25] Horbach, J. 2008 Molecular dynamics computer simulation of amorphous silica under high pressure *J. Phys. Condens. Matter* **20**, 244118.

[26] Jagla, E. A. 1999 Core-softened potentials and the anomalous properties of water *J. Chem. Phys.* **111**, 8980.

[27] Kumar, P., Buldyrev, S. V., Sciortino, F., Zaccarelli, E. & Stanley, H. E. 2005 Static and dynamic anomalies in a repulsive spherical ramp liquid: Theory and simulation *Phys. Rev. E.* **72**, 021501.

[28] Lang, A., Kahl, G., Likos, C. N., Löwen, H. & Watzlawek, M. 1999 Structure and thermodynamics of square-well and square-shoulder fluids *J. Phys. Condens. Matter* **11**, 10143.

[29] Likos, C. N., Löwen, H., Watzlawek, M., Abbas, B., Juchnischke, O., Allgaier, J. & Richter, D. 1998 Star polymers viewed as ultrasoft colloidal particles *Phys. Rev. Lett.* **80(20)**, 4450–4453.

[30] Mayer, C., Sciortino, F., Likos, C. N., Tartaglia, P., Loewen, H. & Zaccarelli, E. 2009 Multiple glass transition in star polymer mixtures: Insights from theory and simulations *Macromolecules* **42**, 423–434.

[31] Mayer, C., Sciortino, F., Tartaglia, P. & Zaccarelli, E. 2010 A spherical model with directional interactions: II. Dynamics and landscape properties *J. Phys. Condens. Matter* **22**, 104110.

[32] Mayer, C., Stiakakis, E., Zaccarelli, E., Likos, C. N., Sciortino, F., Tartaglia, P., Löwen, H. & Vlassopoulos, D. 2007 Rheological transitions in asymmetric colloidal star mixtures *Rheol. Acta* **46**, 611.

[33] Mayer, C., Zaccarelli, E., Stiakakis, E., Likos, C. N., Sciortino, F., Munam, A., Gauthier, M., Hadjichristidis, N., Iatrou, H., Tartaglia, P., Loewen, H. & Vlassopoulos, D. 2008 Asymmetric caging in soft colloidal mixtures *Nat. Mater.* **7**, 780–784.

[34] Netz, P. A., Starr, F. W., Stanley, H. E. & Barbosa, M. C. 2001 Static and dynamic properties of stretched water *J. Chem. Phys.* **115**, 344.

[35] Osterman, N., Babic, D., Poberaj, I., Dobnikar, J. & Ziherl, P. 2007 Observation of Condensed Phases of Quasiplanar Core-Softened Colloids *Phys. Rev. Lett.* **99**, 248301.

[36] Pauschenwein, G. J. & Kahl, G. 2008 Zero temperature phase diagram of the square-shoulder system *J. Chem. Phys.* **129**, 174107.

[37] Pham, K. N., Puertas, A. M., Bergenholtz, J., Egelhaaf, S. U., Moussa¨id, A., Pusey, P. N., Schofield, A. B., Cates, M. E., Fuchs, M. & Poon, W. C. K. 2002 Multiple glassy states in a simple model system *Science* **296**, 104–106.

[38] Prestipino, S., Saija, F. & Malescio, G. 2009 The zero-temperature phase diagram of soft-repulsive particle fluids *Soft Matter* **5**, 2795.

[39] Prestipino, S., Saija, F. & Malescio, G. 2010 Anomalous phase behavior in a model fluid with only one type of local structure *J. Chem. Phys.* **133**, 144504.

[40] Puertas, A. M., Fuchs, M. & Cates, M. E. 2002 Comparative simulation study of colloidal gels and glasses *Phys. Rev. Lett.* **88**, 098301.

[41] Puertas, A. M., Michele, C. D., Sciortino, F., Tartaglia, P. & Zaccarelli, E. 2007 Viscoelasticity and stokes-einstein relation in repulsive and attractive colloidal glasses *J. Chem. Phys.* **127**, 31133157.

[42] Pusey, P. N. & van Megen, W. 1987 Observation of a glass transition in suspensions of spherical colloidal particles *Phys. Rev. Lett.* **59(18)**, 2083–2086.

[43] Saija, F., Prestipino, S. & Malescio, G. 2009 Anomalous phase behavior of a soft-repulsive potential with a strictly monotonic force *Phys. Rev. E.* **80**, 031502.

[44] Saunders, B. R. & Vincent, B. 1999 Advances in colloid and interface science **80**.

[45] Schweizer, K. S. & Saltzman, E. J. 2004 Activated hopping, barrier fluctuations, and heterogeneity in glassy suspensions and liquids *J. Phys. Chem. B* **108**, 19729.

[46] Sciortino, F. 2002 Disordered materials: One liquid, two glasses *Nature Materials* **1**, 145–168.

[47] Sciortino, F., Tartaglia, P. & Zaccarelli, E. 2003 Evidence of a higher-order singularity in dense short-ranged attractive colloids *Phys. Rev. Lett.* **91**, 268301.

[48] Sperl, M. 2003 *Phys. Rev. E* **68**, 031405.

[49] Sperl, M. 2010 *Prog. Theor. Phys. Supp.* **184**, 209–219.

[50] Sperl, M. 2010 Higher-order singularities without glass-glass transitions *Prog. Theor. Phys.* **184**, 211–221.

[51] Sperl, M., Zaccarelli, E., Sciortino, F., Kumar, P. & Stanley, H. E. 2010 Disconnected Glass-Glass Transitions and Diffusion Anomalies in a Model with Two Repulsive Length Scales *Phys. Rev. Lett.* **104**, 145701.

[52] Swallen, S. F., Bonvallet, P. A., McMahon, R. J. & Ediger, M. D. 2003 Self-diffusion of tris-naphthylbenzene near the glass transition temperature *Phys. Rev. Lett.* **90**, 015901.

[53] van Megen, W. & Underwood, S. M. 1993 Glass transition in colloidal hard spheres: Mode-coupling theory analysis *Phys. Rev. Lett.* **70**, 2766–2769.

[54] Voigtmann, T. 2011 Multiple glasses in asymmetric binary hard spheres *Europhys. Lett.* **96**, 36006.

[55] Xu, L., Buldyrev, S. V., Angell, C. A. & Stanley, H. E. 2006 Thermodynamics and dynamics of the two-scale spherically symmetric Jagla ramp model of anomalous liquids *Phys. Rev. E.* **74**, 031108.

[56] Yamamoto, R. & Onuki, A. 1998 Dynamics of highly supercooled liquids: Heterogeneity, rheology, and diffusion *Phys. Rev. E.* **58**, 3515.

[57] Young, D. A. & Alder, B. J. 1977 Melting-Curve Extrema from a Repulsive "Step" Potential *Phys. Rev. Lett.* **38**, 1213.

[58] Zaccarelli, E. 2007 Colloidal gels: Equilibrium and non-equilibrium routes *J. Phys.: Condens. Matter* **19**, 323101.

[59] Zaccarelli, E., Foffi, G., Dawson, K. A., Buldyrev, S. V., Sciortino, F. & Tartaglia, P. 2002 Confirmation of anomalous dynamical arrest in attractive colloids: A molecular dynamics study *Phys. Rev. E* **66**, 041402.

[60] Zaccarelli, E. & Poon, W. C. K. 2009 Colloidal glasses and gels: The interplay of bonding and caging *Proc. Natl. Acad. Sci. U.S.A.* **106(36)**, 15203–15208.

[61] Zaccarelli, E., Saika-Voivod, I., Buldyrev, S. V., Moreno, A. J., Tartaglia, P. & Sciortino, F. 2006 Gel to glass transition in simulation of a valence-limited colloidal system *J. Chem. Phys.* **124**, 124908.

[62] Zaccarelli, E., Valeriani, C., Sanz, E., Poon, W. C. K., Cates, M. E. & Pusey, P. N. 2009 Crystallization of hard-sphere glasses *Phys. Rev. Lett.* **103**, 135704.

[63] Ziherl, P. & Kamien, R. D. 2001 Maximizing entropy by minimizing area: Towards a new principle of self-organization *J. Chem. Phys. B* **105**, 42.